Studying the Importin-regulation of Contractile Proteins in Cytokinesis

Nhat Phi Pham

A Thesis

In the Department

of

Biology

Presented in Partial Fulfilment of the Requirements

For the Degree of

Doctor of Philosophy (Biology) at

Concordia University

Montreal, Quebec, Canada

July 2025

© Nhat Phi Pham, 2025

CONCORDIA UNIVERSITY

School of Graduate Studies

This is to certify that the thesis prepared

By: Nhat Phi Pham

Entitled: Studying the Importin-regulation of Contractile Proteins in Cytokinesis

and submitted in partial fulfilment of the requirements for the degree of

Doctor of Philosophy (Biology)

complies with the regulations of the University and meets the accepted standards with respect to its originality and quality.

Signed by the final Examining Committee:

_____ Chair

Dr. Grant Brown

_____ External Examiner

Dr. Ryan Petrie

_____ External Examiner

Dr. Brandon Helfield

_____ Examiner

Dr. Elena Kuzmin

_____ Examiner

Dr. Gilles Hickson

_____ Thesis Supervisor

Dr. Alisa Piekny

Approved by _____

Dr. Robert Weladji, Graduate Program Director

August 28th, 2025 _____

Dr. Pascale Sicotte, Dean, Faculty of Arts and Science

Abstract

Studying the Importin-regulation of Contractile Proteins in Cytokinesis

Nhat Phi Pham, Ph.D.

Concordia University, 2025

Cytokinesis is the physical separation of a dividing cell into two daughters. Multiple pathways regulate cytokinesis to spatiotemporally couple the segregation of chromosomes and the constriction of the contractile ring. RhoA, the master regulator of cytokinesis, is activated at the equatorial cortex by its activator Ect2. This interaction requires Ect2 interacting with the centralspindlin complex, although how the Ect2-centralspindlin complex is recruited to the membrane is unclear. After ingression, Ect2 signal at the midbody decreases, and Ect2 is presumably re-localized to the nucleus, but this has not been studied. It is also unclear whether decreasing Rhoa activity is required after ingression for abscission. In this work, we show that the polybasic cluster region (PBC) contains a nuclear localization signal (NLS) that binds to importins, that this NLS is required for cytokinesis. Mutating this NLS can abolish Ect2 recruitment at the membrane. We propose that importin-binding facilitates the recruitment of Ect2 at the cortex, potentially by favouring a conformation with higher affinity for lipids. We also show that the nuclear re-sequestration of Ect2 is required for the stability of the intercellular bridge and abscission. Mutating the central NLS, which mediates nuclear import, causes sustained RhoA activity at the intercellular bridge. We propose that nuclear sequestration may regulate other contractile proteins to promote midbody maturation and abscission. Finally, to identify other contractile proteins regulated by importins, we perform a TurboID assay and identify 10 potentially novel interactors of importin-β1 in mitosis, with potential roles in cytokinesis.

Acknowledgements

I would first like to thank Alisa Piekny for taking me into her lab all those years ago. Thank you for trusting me, and for giving me the freedom to answer fascinating questions about cell biology. I had an incredible time in the Piekny lab and at Concordia.

I would also like to thank my committee members. Thank you to Dr. Elena Kuzmin, for your encouragement to test our phenotype in other cell lines, and to Dr. Gilles Hickson, for great group meetings and for the idea to tag our mutant with the SV40NLS. I would also like to thank Dr. Ryan Petrie and Dr. Brandon Helfield for taking the time to evaluate my thesis, especially during grant season. Also thank you to Dr. Bill Zerges for his warmth, candor, and much needed feedback throughout the years.

This work could not have been completed without the amazing team at Concordia. First, microscope and computer wizard Chris Law, who brought the Swept (the princess) back to life more times than I can count. Thank you to Sonia Ruiz, Robert Carson, and Mila for making sure we had everything we need, from equipment to reagents.

I want to take a moment to thank the Old Guard. When I joined the lab, I was the baby, and I am now the last of this generation. Thank you to Imge and Mathieu, who made science so much fun. Thank you to Kevin, for all those talks on the drive home. Thank you to Su Pin for your patience and well of knowledge.

I have had the pleasure to mentor many students during my degree, and I may forget some. Thank you to Jason, Ariel, Ramisha, Mandana, Olivia, Claudia, Kosar, Lou, and Mathieu.

As I move on, I am incredibly hopeful for the future of our lab and our work. The Piekny lab is an amazing team. Thank you to Natasha for her leadership, to Alex for all the dog pictures (and hallah bread!), to Ioanna for her relentless positivity, and to Juliette for fun book chats, and to Cécilia for thoughtful discussion. Thank you as well to Adryanne for her contagious energy, and

to Lancia for teaching us about space. Last but not least, thank you to Gabrielle, who is twice the student I was in half the time. Thank you to our lab mascot, Karl, for keeping our heads above the water.

Special thanks to Natasha, Gabrielle and Juliette for their help on the work in these chapters, and for the eventual manuscripts.

Thank you to the extended Piekny lab family as well. Thank you to Melanie (obviously!), and to Gabe, for all the memes and good times.

Thank you as well to Christina, Amélie and Casey. Christina, we did it!

Finally, thank you to the Squad Fam: Rigel, Vee, Matthew (plus Ariane, baby James and Sophie!), and Meghana. You guys can stop reading now.

Dedications

I dedicate this thesis to the two most important people in my life.

Thank you to my mom, Diem Tien Pham. Mom, as you'll agree, I think I did enough schooling for the two of us. Love you, and thank you for your patience, and for being the best mother I could ask for.

Melanie, thank you for your love and support. It drove me forward during the more challenging times of this degree. I love you.

Contribution of Authors

Chapter 2: The PBC of Ect2 controls membrane localization

This project was supervised by Alisa Piekny. Nhat Pham designed experiments and performed the majority of the cloning experiments. Nhat Pham performed microscopy for Figure 9, Figure S1, and for the microscopy used for the binucleate cell counts in Figure 6 and Figure S2. Natasha Letourneau performed microscopy for Figure 5, 7, 8, and supplemental Figure S1. Gabrielle Schick performed pull-down assays of Figure 5 and 8, and the binucleate cell counts of Figure 6. The cortical linescan analysis was performed by Natasha Letourneau and Jason Carnevale. Cartoon figures in Figure 8D were made by Natasha Letourneau, and other cartoon figures were made by Nhat Pham. The CellProfiler segmentation pipeline was made by Nhat Pham.

Chapter 3: The nuclear localization of Ect2 is required for cytokinesis

This project was supervised by Alisa Piekny. Nhat Pham and Joseph Del Corpo designed experiments. Nhat Pham performed microscopy for Figure 11, 12B, 13-17 and S4. Joseph Del Corpo performed the fixed cell rescue assays in Figure 12E-F and S3. The pull-down assays in Figure 12C-D were performed by Gabrielle Schick. The endogenous cell lines used in Figure 11, 15 and S4 were engineered by Mathieu Husser. The microscopy and analysis were performed by Nhat Pham. Cartoon figures were made by Nhat Pham.

Chapter 4: Identifying potential targets of the Ran-importin pathway In cytokinesis

This project was supervised by Alisa Piekny. Nhat Pham and Su Pin Koh designed experiments. Su Pin Koh performed the cell experiments for Figure 19. Nhat Pham performed the protein sample preparation and downstream analysis for Figure 19, S9, S10, and Table 9 and 10. Pull-

down assays in Figure 20 were performed by Nhat Pham and Mandana Shams. Localization experiments in Figure 22 and S10 were performed by Nhat Pham and Olivia Drummond. The shRNA-knockdown experiment in Figure 21 was performed by Nhat Pham and Ramisha Rahman.

Table of Contents

List of Figures

List of Tables

List of Supplemental Figures

List of Abbreviations

ABI2	Abelson interactor 2
ANXA1	Annexin A1
ANXA2	Annexin A2
APC	Anaphase Promoting Complex
BFDR	Bayesian False Discovery Rate
BIOGRID	Biological General Repository for Interaction Datasets
BioID	Proximity-based biotinylation assay (also TurboID)
BRCT	BRCA1 C-terminal
C2	Protein kinase C conserved lipid binding region 2
Cdc42	Cell division control protein 42
Cdk1	Cyclin-dependent kinase 1
cDNA	Complementary DNA
CEP55	Centrosomal protein 55
CKAP5	Cytoskeleton associated protein 5
CLIP170	Cytoplasmic linker protein 170
C-term	C-terminus or carboxyl-terminus
Cyk4	Cytokinesis defect 4 [or MgcRacGAP (Male germ cell RacGAP (RacGTPase activating protein)) rho-family GAP in humans; RacGAP50C in *Drosophila*]
DAPI	4’,6-diamidino-2’-phenylindole dihydrochloride
DAVID	Database for Annotation, Visualization and Integrated Discovery
DH	Dbl (diffuse B-cell lymphoma) homology
DIAPH3	Diaphanous-related formin 3
DKC1	Dyskerin pseudouridine synthase 1
DMEM	Dulbecco’s Modified Eagle Medium (DMEM)
DNA	Deoxyribunucleic acids
DOCK7	Dedicator of Cytokinesis 7

DTT	D-Dithiothreitol
ECL	Enhanced chemiluminescence
Ect2	Epithelial cell transforming 2
ERK	Extracellular signaling-regulated kinase
ESCRT-III	Endosomal sorting complexes required for transport-III
FAK	Focal adhesion kinase
FL	Full length
FRAP	Fluorescence recovery after photobleaching
FRET	Förster resonance energy transfer
GAP	GTPase activating protein
GBD	GTPase binding domain (also RBD)
GDP	Guanosine diphosphate
GEF	Guanosine nucleotide exchange factor
GFP	Green fluorescent protein
GST	Glutathione S-transferase
GTP	Guanosine triphosphate
GTPase	Guanosine triphosphatase
HEK293	Human embryonic kidney 293
HeLa	Henrietta Lacks (uterine cells derived from)
His	Poly-histidine tag
HRP	Horseradish peroxidase
IBB domain	Importin- β binding domain
Imp-β	Importin-β nuclear transport receptors
iPSC	Induced pluripotent stem cells
IQGAP1	I(soleucine) Q(glutamine) motif containing GTPase activating protein 1
KPNB1	Karyopherin-β1 or importin-β1
LLPS	Liquid-liquid phase separation
M.W.	Molecular weight
MAPK	Mitogen-activated protein kinase
MCAK	Mitotic centromere-associated kinase

MP-GAP	Mitotic-phase GTPase activating protein
mCherry	Monomeric cherry fluorescent protein
MKLP1	Mitotic kinesin like protein 1
mNeonGreen	monomeric Neon Green
MS	Mass spectrometry
mScarlet-I	monomeric Scarlet-I
MT	Microtubules
Myc	Polypeptide affinity protein tag derived from cMyc
n.s.	Not significant
NES	Nuclear Export Signal
NLS	Nuclear Localization Signal
NMR	Nuclear magnetic resonance
NSCLC	Non-small-cell lung carcinoma
N-term	N-terminus or NH2-terminus
OCRL	Oculocerebrorenal syndrome of Lowe
PBC	Polybasic cluster
Pebble	*Drosophila* homolog of Ect2
PH	Pleckstrin homology
$PI(4,5)P_2$	Phosphatidylinositol 4,5-bisphosphate
$PI(3,4,5)P_3$	Phosphatidylinositol (3,4,5)-trisphosphate
PKCε	Protein kinase C epsilon
PKCι	Protein kinase C iota
Plk1	Polo-like kinase 1
PMSF	Phenylmethylsulfonyl fluoride
PP1-Sds22	Protein phosphatase 1 and its regulatory subunit Sds22
Ptk1	*Potorous tridactylus* kidney 1
Rac	Ras-related C3 botulinum toxin substrate protein
	RacGAP50C in *Drosophila*]
RacGAP	Rac GTPase activating protein
Ran	Ras-related nuclear protein GTPase

RanGAP	Ran GTPase activating protein
RBD	Rho-binding domain
RCC1	Regulator of chromosome condensation 1
RhoA	Ras homolog family member A
RNA	Ribonucleic Acid
RNAi	Ribonucleic Acid interference
ROCK	Rho-associated protein kinase
ROI	Region of interest
SAC	Spindle Assembly Checkpoint
SAF	Spindle assembly factor
SAINT-Express	Significance of Interactome-Express
SD	Standard deviation
SEM	Standard error of the mean
SEPT6	Septin 6
SEPT9	Septin 9
shRNA	short-hairpin RNA
SHTN1	Shootin1
siRNA	Small interfering ribonucleic acid
STC	S-trityl-L-cysteine
SUMO1	Small ubiquitin-related modifier 1
SUMO5	Small ubiquitin-related modifier 5
TBS-T	Tris-buffered saline-Triton (also Tween)
TEK	Threonine, Glutamate, Lysine
WASF2	Wiskott-Aldrich syndrome protein family member 2
WAVE	Wiskott-Aldrich syndrome protein Verprolin-homologous protein
YWHAE	14-3-3 epsilon
YWHAZ	14-3-3 zeta

Chapter 1: Introduction

Section 1.3 is adapted from: Koh, S.P., Pham, N.P., Piekny, A. "Seeing is believing: tools to study the role of Rho GTPases during cytokinesis." Small GTPases vol. 13,1 (2022): 211-224. doi:10.1080/21541248.2021.1957384

1.1 Overview

During mitosis, chromosome segregation is coupled with cytokinesis, the physical separation of the cell membrane. Cytokinesis occurs over several hours, beginning in anaphase when the chromosomes detach from one another, and ending when the daughter cells are physically separated. This process is driven by the formation and constriction of a contractile ring between the segregating chromosomes. After ingression, the ring matures into a small structure termed the midbody inside an intercellular bridge that connects the two daughter cells into G_1 phase; this midbody mediates abscission, the cutting of the bridge and the end of cytokinesis. Multiple pathways tightly regulate cytokinesis to ensure the spatiotemporal coupling of ring ingression and chromosome segregation. A novel mechanism is the regulation of contractile proteins by chromatin-associated cues through the Ran-importin pathway. This chromosome-based system regulates nucleocytoplasmic transport in interphase cells, and is repurposed for the assembly of the mitotic spindle during mitosis. Our lab and other groups have demonstrated that the Ran-importin pathway regulates the positioning of contractile proteins at the cortex for ingression. Building on this work, we show that this pathway also regulates abscission, the last step of cytokinesis.

1.2 The cell cycle and cell division

Cell division in animal cells involves extensive reorganization of the cytoskeleton. As cells exit interphase and enter prometaphase, they round up as the microtubules become more dynamic, the nuclear envelope breaks down and the chromosomes condense. Subsequently in metaphase, a bipolar spindle forms with attachments to the kinetochores of the sister chromatids, which become aligned in the middle of the cell (Figure 1). Mitotic exit triggers cells to enter anaphase, during which the chromosomes are segregated to either pole. It is at this step that cytokinesis begins the process of cleaving the cell into two daughters. Cytokinesis occurs due to the assembly and ingression of a contractile ring made of actin and myosin filaments. An array of antiparallel microtubules called the central spindle forms between the segregating chromosomes and recruits cytokinesis regulators to the equatorial cortex. As the cells progress through telophase, the nuclear envelope reforms around the nuclei of the two daughter cells, and DNA is decondensed. In addition, the contractile ring ingresses, then matures into a dense structure called the midbody, which forms at the centre of an intracellular bridge that connects the nascent daughter cells. This bridge is cut via abscission to physically release the two daughters. Various pathways ensure the spatiotemporal coupling of cytokinesis with chromosome segregation in anaphase to prevent aneuploidy.

The temporal regulation of mitotic entry and cytokinesis is controlled by cell cycle regulators. In interphase, which spans G_1, S and G_2 phases, cells prepare for mitosis by replicating DNA, organelles and proteins. The activity of distinct cyclin and cyclin-dependent kinase (Cdk) complexes regulate entry into the next stage of the cell cycle and is irreversible. Cdk-cyclins coordinate cell cycle events by phosphorylating hundreds of proteins to positively or negatively regulate their function. The transition between G_2/M is marked by the rise in activity of

Cdk1 and its cyclin partners. Notably, phosphorylation by Cdk1 controls multiple mitotic events including nuclear envelope breakdown, mitotic spindle formation and chromosome condensation (Peter et al., 1990; Prosser and Pelletier, 2017; Jeong et al., 2022). Critically, Cdk1 activity must decrease for mitotic exit and cytokinesis. During metaphase, the spindle assembly checkpoint (SAC) remains active until all chromosomes have formed proper attachments to the spindle via their respective kinetochores. Correct attachment silences the SAC, which relieves inhibition of the anaphase promoting complex (APC), leading to the degradation of cyclin B and inactivation of Cdk1 for mitotic exit. Cdk1 dephosphorylation is required for assembly of the central spindle and activation of the RhoA GEF, Ect2 to form the contractile ring in the equatorial plane. The spatial regulation of cytokinesis involves several mechanisms, which include cues from spindle microtubules, cortical proteins and chromatin. These mechanisms will be expanded upon in the following sections.

1.3 Cytokinesis in mammalian cells

1.3.1 Assembly of the contractile ring

As the master regulator of cytokinesis, RhoA plays a central role in the regulation of cytokinesis (Figure 2). Upon its activation, RhoA regulates contractile ring assembly at the equatorial cortex (Basant and Glotzer, 2018; Chircop, 2014; Green et al., 2012; Leite et al., 2019). Active RhoA is generated by Ect2, a guanine nucleotide exchange factor (GEF), which requires the formation of a complex with Cyk4/MgcRacGAP to be active in anaphase (Figures 2-4; Somers and Saint, 2003; Yüce et al., 2005; Nishimura and Yonemura, 2006). Activation of RhoA is uniformly dampened at the cortex by Mitotic phase-GTPase activating protein (MP-GAP), which

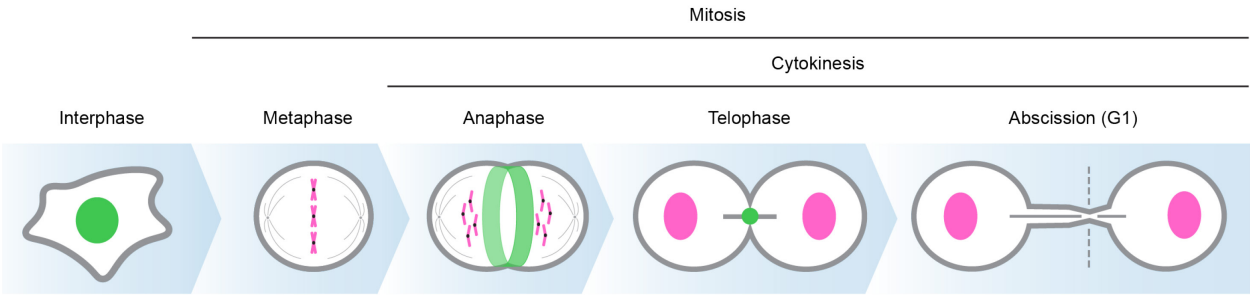

Figure 1. Cartoon schematic of a cell undergoing mitosis and cytokinesis, from metaphase to abscission.

In metaphase, the chromosomes align at the metaphase plate and the mitotic spindle microtubules attach to kinetochores on sister chromatids. In anaphase, the chromosomes are segregated, and the contractile ring forms, pinching the cell into two at the equator. In telophase, after ingression, the nuclear envelope reforms around chromosomes, and cells are connected by an intercellular bridge until abscission. The contractile ring matures into the midbody. Abscission cuts the intercellular bridge and physically separates the daughter cells.

presumably is over-ridden by a higher concentration of Ect2 in the equatorial plane (Figure 3; Zanin et al., 2013). Active RhoA binds to and activates effectors including diaphanous-related formins to promote the nucleation of long, unbranched F-actin, and Rho-dependent kinase (ROCK) to phosphorylate myosin light chain for the assembly of non-muscle myosin filaments (Figure 4; Kosako et al., 2000; Rose et al., 2005). This core RhoA module is conserved among metazoans (Glotzer, 2017). In human cells, Cyk4 or Ect2 depletion causes early cytokinesis defects due to failed contractile ring formation and insufficient levels of active RhoA in the equatorial plane (Yüce et al., 2005; Frenette et al., 2012; Nishimura and Yonemura, 2006). A major question in the field is how a tight zone of active RhoA is maintained for ring assembly and ingression.

1.3.2 Pathways regulating cytokinesis

1.3.2.1 Spindle-dependent pathways

During mitosis, the mitotic spindle ensures that ring assembly and ingression occurs at the cell equator (Figures 2-3). The mitotic spindle is composed of astral microtubules, emanating from the centrosomes at the poles, and the central spindle, an array of microtubules forming between segregating chromosomes. In anaphase, the central spindle forms from microtubules of the metaphase spindle and newly nucleated microtubules (Uehara and Goshima, 2010; Kamasaki et al., 2013). The assembly of the central spindle requires the activity of several protein complexes that regulate bundling (Green et al., 2012). One of these complexes is centralspindlin, which is a heterotetramer of MgcRacGAP/Cyk4 and MKLP1 (Mishima et al., 2002). It is through this complex that the central spindle stimulates cytokinesis. Cyk4 recruits the GEF Ect2 to the spindle midzone, then directs Ect2 to the overlying cortex to activate RhoA (Yüce et al., 2005; Kamijo et al., 2006).

The requirement for Cyk4-binding to target Ect2 to the equatorial cortex is well-studied, and has been demonstrated in mammalian cells, as well as Drosophila and echinoderm embryos (Somers and Saint, 2003; Bement et al., 2005; Yüce et al., 2005). Cells where this interaction was impaired by depleting Cyk4 or mutation fail to ingress (Bement et al., 2005; Yüce et al., 2005). However, this model has been refined in more recent years. Ect2 contains several lipid-binding domains in its C-terminus that are required for its activity, and centralspindlin also associated with the membrane via the C1 domain of Cyk4 which is required for its function in regulating Ect2 (Frenette et al., 2012; Glotzer, 2013; Su et al., 2011; Lekomtsev et al., 2012). Subsequent studies found that membrane localization and not central spindle recruitment of Ect2 is required for its activity (Kotýnková et al., 2016). Cyk4 also requires phosphorylation by Plk1 for Ect2-binding (Figures 1; Petronczki et al., 2007; Wolfe et al., 2009; Gómez-Cavazos et al., 2020). However, the Plk1-regulation of Ect2-centralspindlin could involve additional mechanisms. Plk1 activity negatively regulates microtubule-bundling which would release Ect2-centralspindlin complexes for transition to the overlying membrane where they are regulated by Aurora B kinase (Figures 1; Basant et al., 2015; Adriaans et al., 2019). Thus, the central spindle could help direct complexes to the equatorial plane, but is not required for their activation per se.

Astral microtubules negatively regulate contractile proteins at the poles (Figure 3). In *C. elegans* embryos, perturbing asters by laser ablation caused ectopic ingression, and delaying aster separation caused ingression delay and ectopic accumulation of anillin and myosin-II at the cortex (Bringmann and Hyman, 2005; Lewellyn et al., 2010). Using gamma-tubulin depleted *C. elegans* embryos, a study showed that contacts between microtubules of the resulting monopolar spindle could clear myosin at the cortex (Werner et al., 2007). In human cells, depletion of astral microtubules increases the breadth of RhoA and myosin at the cell equator, whereas extending

A

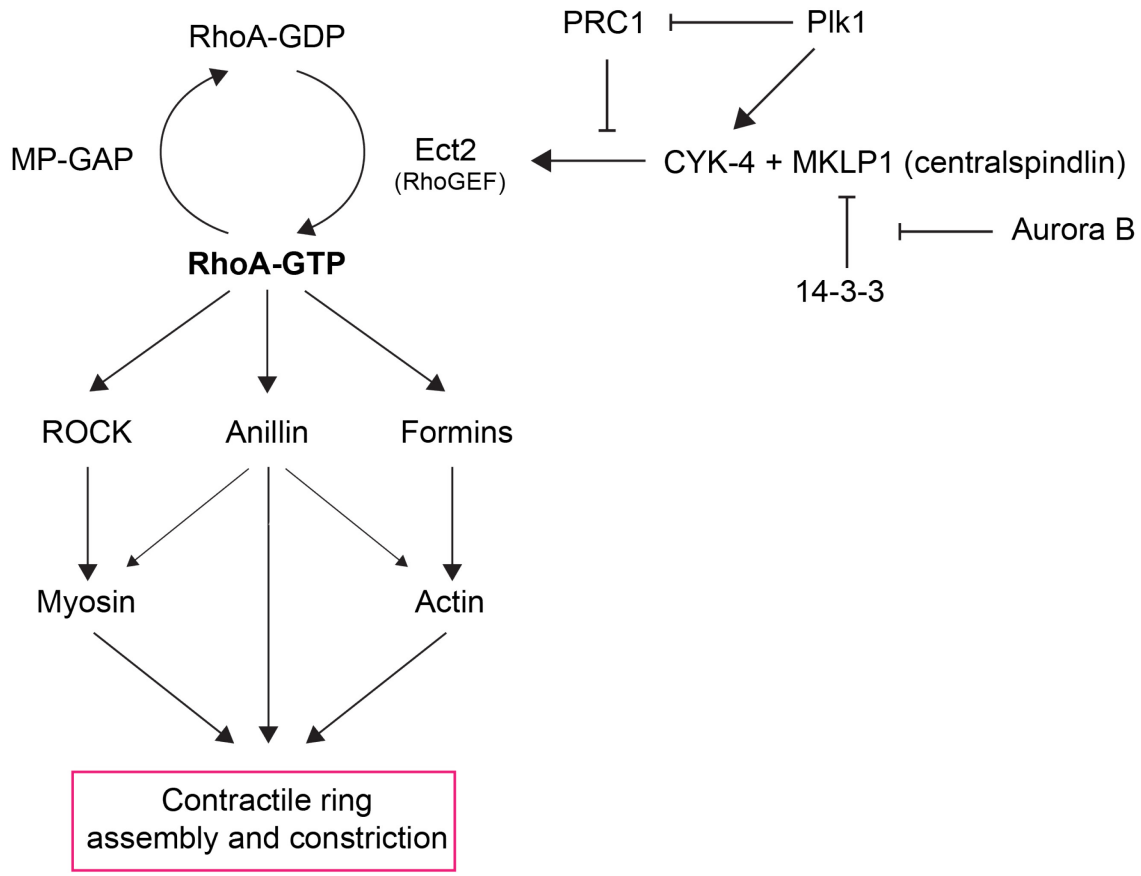
RhoA-GDP
PRC1
Plk1
MP-GAP
Ect2
(RhoGEF)
CYK-4 + MKLP1 (centralspindlin)
Aurora B
RhoA-GTP
14-3-3
ROCK
Anillin
Formins
Myosin
Actin
Contractile ring
assembly and constriction

B

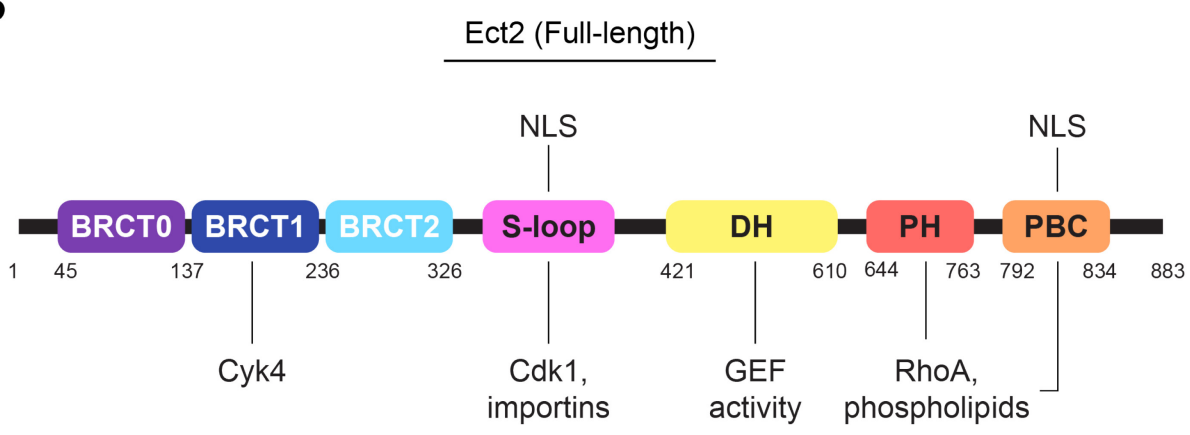
Ect2 (Full-length)
NLS
NLS
BRCT0
BRCT1
BRCT2
S-loop
DH
PH
PBC
1
45
137
236
326
421
610
644
763
792
834
883
Cyk4
Cdk1,
importins
GEF
activity
RhoA,
phospholipids

Figure 2. Rho GTPase signalling pathways that regulate cytokinesis.

(A) RhoA is required for cytokinesis and is considered the master regulator of contractile ring assembly. Active RhoA is generated in the equatorial plane during anaphase by the GEF Ect2, which exchanges GDP for GTP. Outside of this region, MP-GAP inactivates RhoA via stimulating GTP hydrolysis. Ect2 requires binding to the centralspindlin complex (a tetramer of Cyk4 and MKLP1) for its activity. Binding to RhoA also relieves the autoinhibition of Ect2. At the cortex, MKLP1 is inhibited by 14-3-3, which is relieved by Aurora B kinase phosphorylation. Plk1 phosphorylation of Cyk4 is also required for Ect2-binding, and to prevent PRC1 from sequestering centralspindlin on the spindle. In the equatorial plane, active RhoA forms a contractile ring through its effectors formin and ROCK, which control actin polymerization and myosin activation, respectively. Another RhoA effector, anillin, crosslinks the ring to the overlying membrane to control ring position, and stabilizes RhoA at the membrane. (B) Cartoon diagram of Ect2 with its BRCT domains, S-loop, DH, PH and PBC region. Binding partners for cytokinesis are labeled under the domains. In metaphase, the BRCTs are proposed to inhibit the DH due to phosphorylation of the S-loop by Cdk1. Cyk4 binds to the BRCTs to activate Ect2 in anaphase, when Cdk1 activity is decreased. Subsequently, Ect2 localizes to the membrane via its PH, and possibly PBC, and activates RhoA through its DH domain. Ect2 has a NLS in its central S-loop region which mediates nuclear import, and a predicted NLS in its PBC region.

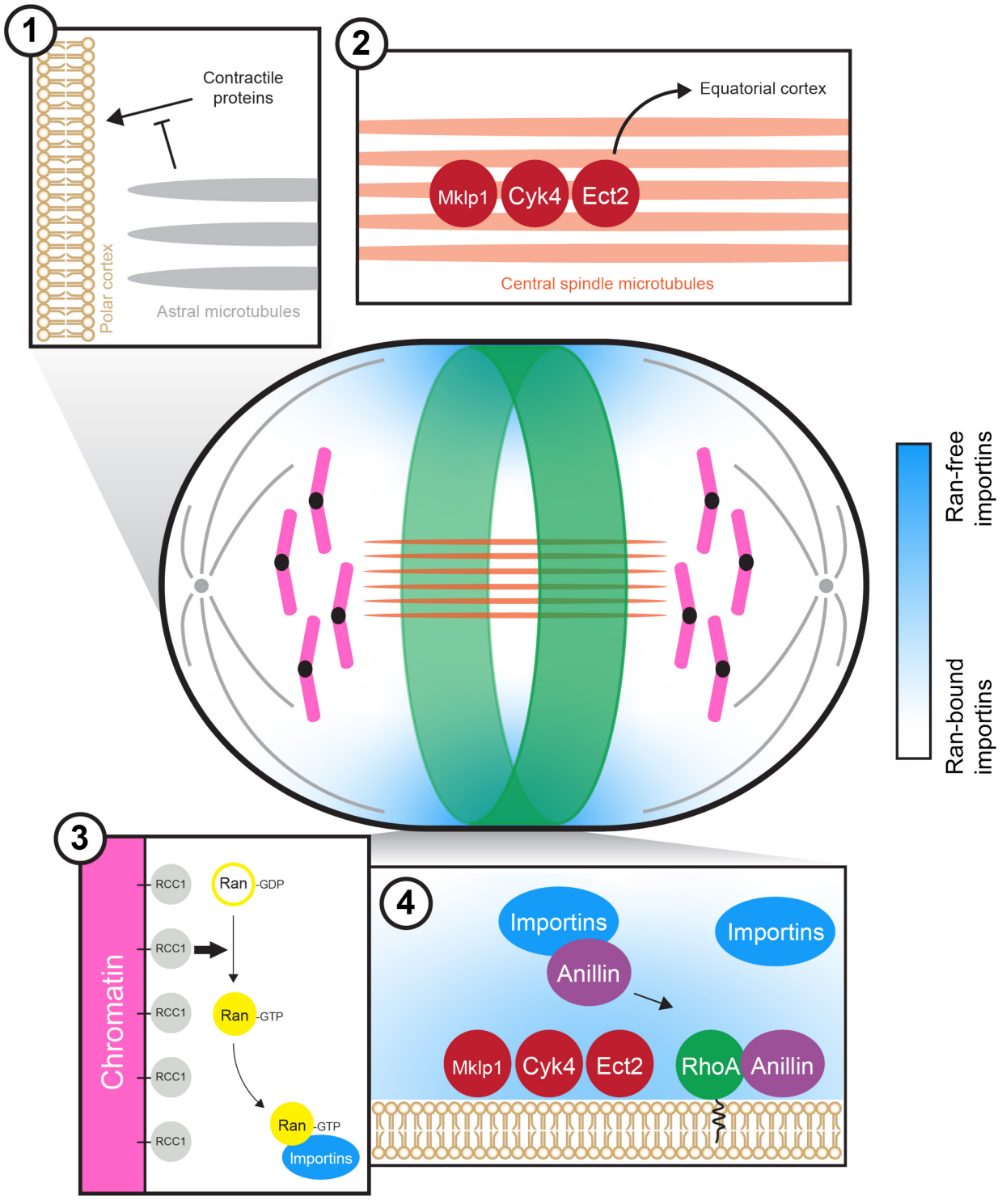
1
Contractile proteins
Polar cortex
Astral microtubules
2
Equatorial cortex
Mklp1
Cyk4
Ect2
Central spindle microtubules
Ran-free importins
Ran-bound importins
3
Chromatin
RCC1
Ran -GDP
RCC1
RCC1
Ran -GTP
RCC1
Ran -GTP
Importins
RCC1
4
Importins
Anillin
Importins
Mklp1
Cyk4
Ect2
RhoA
Anillin

Figure 3. Multiple pathways regulate cytokinesis.

Cartoon schematic of a dividing cell, with boxed inset showing the contributions of dominant pathways in cytokinesis. In (1), astral microtubules emanating from the poles (gray) inhibit the localization of cortical proteins at the poles, restricting their localization to the equatorial cortex. In (2), the central spindle (orange) recruits centralspindlin (Cyk4/Mklp1) and Ect2, and this interaction is required for Ect2 localization at the cortex, although the mechanism for this is not well understood. (3) The Ran-gradient (white to blue) regulates the binding of importins (blue) to partners in proximity to chromatin. Binding to Ran-GTP precludes importins from binding to partners. Because RCC1, the activator of Ran, is tethered to chromatin, Ran-GTP exists as a gradient in mitotic cells. Active Ran is in high concentration near chromatin, and low at the cortex. Conversely, more importins are 'free' to bind to partners near the cortex, where Ran-GTP concentration is low, and fewer importins can bind to partners near chromatin, where Ran-GTP concentration is high. (4) Our lab found that importins regulate cytokinesis through the cytokinesis regulator anillin.

asters narrows the breadth of RhoA, myosin and anillin (Murthy and Wadsworth, 2008; Zanin et al., 2013; van Oostende Triplet et al., 2014). How astral microtubules clear contractile proteins from the cortex is not well understood, but may differ depending on the protein. For instance, anillin binds to the tip of astral microtubules, which seems to restrict its localization to the cleavage furrow (van Oostende Triplet et al., 2014). Because anillin is a myosin crosslinker, this also restricts myosin at the equator. Similarly, asters clear the formin Diaph1/mDia1 from the polar cortex by delivering CLIP170, which displaces its activator IQGAP1 (Chen et al., 2021). These findings indicate that astral microtubules act directly on contractile proteins, or through intermediaries.

1.3.2.2 Spindle-independent pathways

Additional pathways also regulate the core RhoA module – either via feedback within the module, or by other GEFs and GAPs. For example, positive feedback within the Ect2-Cyk4 complex stimulates GEF activity, which was recently proposed to occur in part through the binding of active RhoA to a domain in Ect2 that releases it from autoinhibition (Zhang and Glotzer, 2015; Chen et al., 2020). Another major regulator of feedback is anillin, a highly conserved scaffold protein which stabilizes active RhoA for downstream signalling (Figure 2-4). Anillin has binding domains for actin, myosin, RhoA, septins and lipids and is required for ring positioning in many metazoan cell types (Budnar et al., 2019; Field and Alberts, 1995; Piekny and Maddox, 2010; Piekny and Glotzer, 2008). Anillin binds cooperatively to RhoA and phospholipids, and requires active RhoA for its cortical recruitment (Sun et al., 2015). Recent studies showed that anillin organizes lipid nanodomains and increase the membrane retention of active RhoA to facilitate its

interaction with effectors such as Rho kinase that control actomyosin assembly (Sun et al., 2015; Budnar et al., 2019).

Cues from cortically localized proteins and DNA also play a role in cytokinesis. In fact, furrowing can occur in the absence of microtubules. For instance, contractility and even furrowing can still be observed in cells treated with microtubule poisons (Canman et al., 2000; Cabernard et al., 2010). In Drosophila neuroblasts, the cortical Pins complex regulates myosin localization to generate basal contractility in the absence of a central spindle (Cabernard et al., 2010). Signals from DNA can also polarize the cortex. For example, the PP1-Sds22 phosphatase complex on kinetochores can clear cortical actin by dephosphorylating the actin crosslinker moesin when kinetochores come in close proximity with the cortex (Rodrigues et al., 2015). Proximity to DNA has also shown to regulate the cortical localization of myosin and anillin (Kotadia et al., 2012; Kiyomitsu and Cheeseman, 2013). The mechanism for this response was identified to be the Ran-GTP and importin pathway, and is described in the next section.

1.3.2.3 Ran pathway and importins

The GTPase Ran is best known as a regulator of nucleocytoplasmic transport in interphase cells (reviewed in Clarke and Zhang, 2008), but it also moonlights as a master regulator of the mitotic spindle during mitosis (Prosser and Pelletier, 2017). Ran regulates these processes through importins and exportins, although only importins have been implicated in mitosis. For transport, importins recognize a nuclear localization signal (NLS) on partner proteins, then translocate into the nucleus as a complex (discussed in the next section). There, the active GTP-bound Ran binds to importins, releasing the NLS-containing protein. This regulation is

inverted for exportins, which bind to nuclear export signals (NES). Because the RanGEF RCC1 is tethered to chromatin, the concentration of Ran-GTP is high in the nucleus and low in the cytosol where RanGAPs promote GTP-hydrolysis. This allows importins to bind to partner proteins in the cytosol, and release them in the nucleus upon binding to Ran-GTP. In mitosis, the nuclear envelope is broken down, and active Ran exists as a gradient (Kalab et al., 2002; Kaláb et al., 2006). This gradient was demonstrated using FRET probes in sea urchin embryos and mammalian cells, which showed that Ran-GTP is enriched near chromatin and steeply decreases towards the cortex. Because spindle assembly factors (SAFs) are inhibited by importin-binding to their NLS, this local enrichment of active Ran promotes the assembly of the mitotic spindle near chromatin (Schatz et al., 2003; Tsai et al., 2003; Ems-McClung et al., 2004; Blower et al., 2005; Albee et al., 2006; Tsai et al., 2006; Walczak and Heald, 2008; Weaver et al., 2015). For cytokinesis, this gradient may act as a mechanism to position contractile proteins at the cortex in relation to DNA. A study in mammalian cells showed that cells can elongate to correct for spindle mispositioning, which would otherwise lead to asymmetric cell division (Kiyomitsu and Cheeseman, 2013). This elongation appeared to respond to nearby chromatin and led to the clearing of anillin. When RCC1 is impaired using a temperature-sensitive allele, elongation and clearing of anillin at the membrane does not occur (Kiyomitsu and Cheeseman, 2013). This identified Ran-GTP as the mechanism by which chromatin polarizes the cortex. Consistent with this finding, our lab showed that expressing a constitutively active Ran (Q69L) tagged with a membrane-binding domain disrupted anillin localization and caused ring oscillations (Beaudet et al., 2017).

Our lab expanded this work. We hypothesize that the chromatin pathway is a global mechanism for regulating the function of contractile ring proteins for ring assembly and abscission during cytokinesis. We found that Ran regulates anillin recruitment to the equatorial cortex

through importins (Beaudet et al., 2017, 2020). Anillin has a cryptic NLS in its C-terminal which is not used for nuclear localization. Instead, we found that importin-β1 binds to this NLS, and that this binding facilitates the recruitment of anillin at the cortex. Mutating the C-terminal NLS decreases the breadth of anillin at the cell equator and causes cytokinesis failure. In anillin-depleted cells, expression of NLS mutant anillin failed to rescue cytokinesis in a third of cells, and increased binucleated cells by nearly 50% in an asynchronous population (Beaudet et al., 2020). We also found that the Rho-binding domain (RBD) of anillin inhibits the C-terminal NLS in its C2 domain. Our findings support a model where RhoA binds anillin, which increases accessibility of the NLS to importins. Binding of importin to anillin could then stabilize a conformation that increases accessibility of anillin for lipids, RhoA and other partners during cytokinesis. Taken together, we propose that a gradient of 'free' importins regulates contractile proteins at the cortex, where the concentration of Ran-GTP is lowest. This model provides a mechanistic explanation for how Ran-GTP clears cortical proteins like myosin and anillin when chromatin comes in proximity with the cortex (Kotadia et al., 2012; Kiyomitsu and Cheeseman, 2013; Beaudet et al., 2017, 2020). Given that other cytokinesis regulators also have NLS's, we propose that some of these proteins could also be regulated by importins for their function in cytokinesis.

1.3.2.4 Importins in nucleocytoplasmic transport

The importin family of proteins is composed of several importin-α and importin-β proteins. Importins recognize nuclear localization signals (NLSs) on cargo proteins to transport them into the nucleus. Classical NLSs are made up of basic residues (lysines and arginines), and are categorized as "monopartite", or "bipartite" when two basic clusters are divided by a spacer of 9-12 residues (Lu et al., 2021). These classical NLSs are recognized by an importin-α/β1

heterodimer, where an importin-α acts as an adaptor linking the NLS to importin-β1, which interacts with the nuclear pore complex for entry into the nucleus. In the heterodimer, binding of importin-β1 to the importin-β binding (IBB) domain of importin-α is proposed to relieve auto-inhibition on importin-α, allowing it to bind to an NLS. However, importin-αs and importin-β1 can bind to classical NLSs as monomers, suggesting that whether a cargo is imported by a monomer (α or β1) or the heterodimer (α/β1) is NLS-specific (Köhler et al., 1999; Forwood et al., 2001; Miyamoto et al., 2002; Kotera et al., 2005; Mehmood et al., 2011; Yamada et al., 2024). Non-classical NLSs are NLSs that are not enriched in basic residues (Süel et al., 2008; Lu et al., 2021). For example, the PY-NLS is composed of a long sequence containing either hydrophobic or basic residues and ending in PY, and is recognized by importin-β2. In the nucleus, binding to Ran-GTP leads to the dissociation of the cargo protein.

1.3.2.5 Ect2 and its regulation in cytokinesis

As described above, Ect2 is the key activator of RhoA for ring assembly in cytokinesis. Thus, tight spatiotemporal regulation of Ect2 is needed to ensure that contractility is restricted to the equatorial cortex. Ect2 is composed of N-terminal BRCT domains, a DH domain for GEF activity, a PH domain for lipid-binding, and a polybasic cluster region (PBC) at its C-terminal end. The N-terminal BRCT regions inhibit the DH domain, required for GEF activity (Saito et al., 2004; Kim et al., 2005; Frenette et al., 2012; Figure 2). In interphase cells, Ect2 is localized in the nucleus through importins interacting with its central NLS in the S-loop region (Tatsumoto et al., 1999; Chalamalasetty et al., 2006; Suzuki et al., 2015). During mitosis, phosphorylation of the S-loop region by Cdk1 is proposed to cause the BRCTs to fold and inhibit the DH. This auto-inhibition is relieved as Cdk1 activity decreases for anaphase. As described previously, Ect2 must

interact with Cyk4 to activate RhoA at the equatorial cortex (Yüce et al., 2005; Kamijo et al., 2006). Plk1 promotes this interaction by phosphorylating Cyk4, which binds Ect2 at its BRCTs (Wolfe et al., 2009; Zou et al., 2014). How Ect2 is recruited to the membrane is not well understood, but its lipid-binding PH domain is required for membrane localization and function (Su et al., 2011; Frenette et al., 2012). A single point mutation in the PH domain disrupts Ect2's membrane localization and causes cytokinesis failure due to decreased RhoA activation (Frenette et al., 2012). A later study showed that a small region of the PH domain may also inhibit the DH domain based on an X-ray crystal structure of Ect2 (Chen et al., 2020). In support of this, point mutations predicted to relieve this inhibition increased GEF activity and caused cell shape changes characteristic of overactive Ect2. Active RhoA was proposed to relieve this inhibition by binding to the PH domain, although this was not shown (Chen et al., 2020). The C-terminal PBC region may also play a role in mediating Ect2's membrane localization for cytokinesis and has a Cdk1 phosphorylation site that could impact this binding (Su et al., 2011). This region is predicted to be disordered, and was not captured via crystallization for the X-ray structure. Interestingly, this region harbors a predicted NLS (Liot et al., 2011). This NLS is unable to support nuclear localization in the full-length protein, which suggests that it is auto-inhibited. This indicates that the PBC may participate in Ect2 folding, beyond its role in membrane association. Further investigating the role of the PBC and this C-terminal NLS is the focus of Chapter 2.

1.3.2.6 The intercellular bridge, midbody and abscission

After ring ingression, the nascent daughter cells remain connected by an intercellular bridge for several hours into G_1 until they are separated during abscission (Figure 4). The contractile ring matures into a structure termed the midbody, and becomes the anchor for the

recruitment of the abscission machinery (Echard, 2008). The intercellular bridge undergoes multiple structural changes between ring ingression and abscission. Reducing active RhoA may be critical to keep F-actin nucleators from accumulating at the intercellular bridge, as excess F-actin appears to delay or block abscission (Dambournet et al., 2011). Several mechanisms remodel the bridge to reduce contractility. First, the GTPase Rab11 and its effector Fip3 deliver p50rhoGAP-containing vesicles to the bridge, inactivating RhoA and narrowing the bridge (Schiel et al., 2012). Then, Rab35 acts on OCRL to reduce PIP_2 at the bridge, a lipid important for contractility (Dambournet et al., 2011). RhoA is also deactivated by the kinase PKCε, but the mechanism is unclear (Saurin et al., 2008). The clearing of the RhoA activator Ect2 also occurs following ingression, and this is further discussed in Chapter 3. The stabilization of the intercellular bridge allows for the recruitment of the ESCRT-III complex for abscission.

Other contractile ring proteins play important roles in abscission. The centralspindlin complex, anillin and septins anchor the midbody ring to the membrane. Centralspindlin recruits CEP55 via binding to MKLP1, which in turn recruits targeting factors for ESCRT-III to sites flanking the midbody (Morita et al., 2007; Carlton et al., 2008). In addition, the ATPase spastin is recruited to sever central spindle microtubules (Connell et al., 2009). At these secondary ingression sites, the ESCRT-III complex forms large filaments into a spiral that constricts the membrane (Guizetti et al., 2011; Elia et al., 2012). The expansion of this spiral appears to be blocked by branched F-actin away from the midbody (Advedissian et al., 2024). These pools of F-actin are proposed to act as a ‘plug’ to prevent the ESCRT-III filaments from over-elongating towards the daughter cells. Scission of the bridge physically separates the daughter cells into two. Interestingly, scission can occur on either side of the midbody, and additional studies demonstrated that these midbody remnants can be engulfed and function as signaling factors (Peterman et al., 2019).

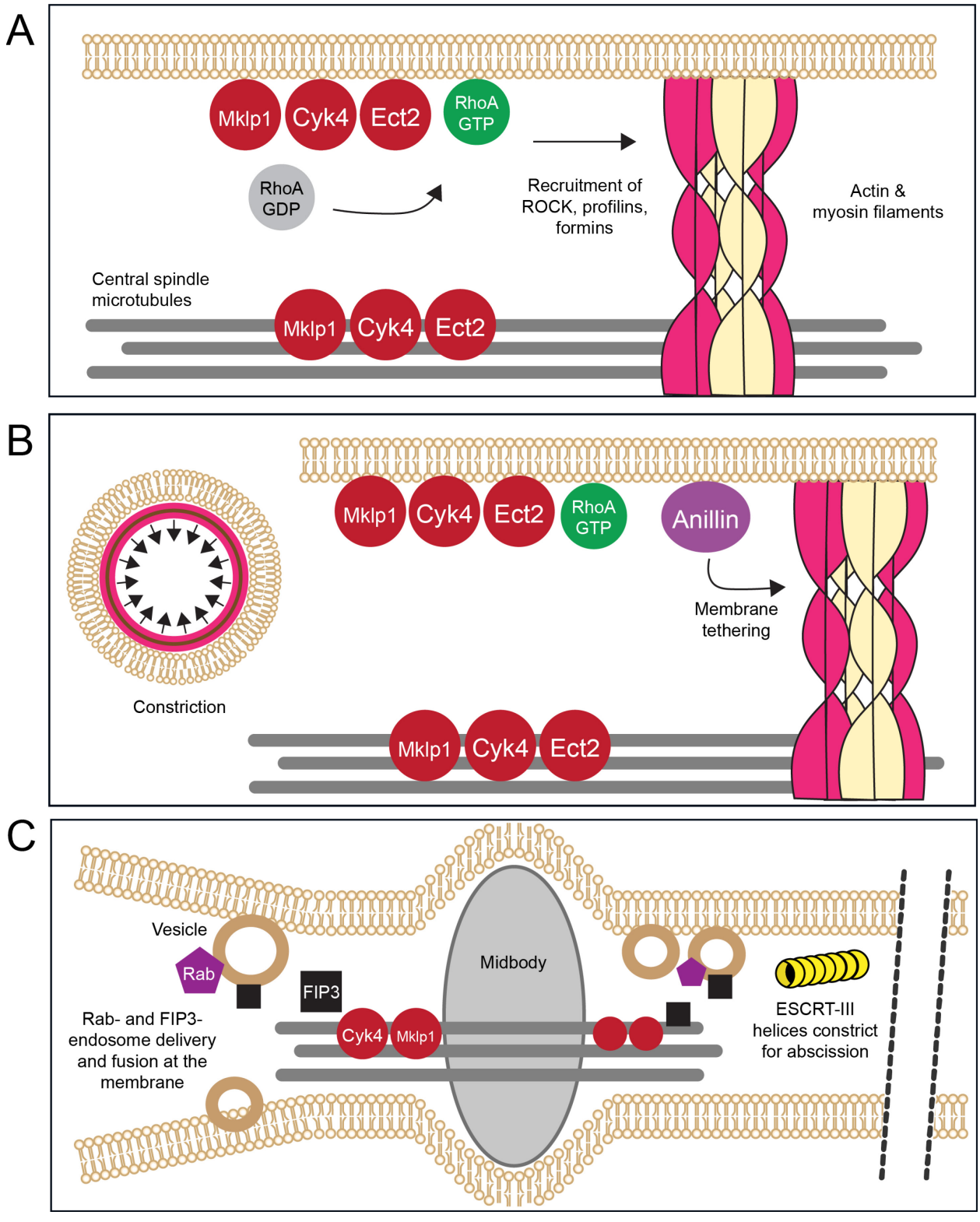
A
Mklp1
Cyk4
Ect2
RhoA GTP
RhoA GDP
Recruitment of ROCK, profilins, formins
Actin & myosin filaments
Central spindle microtubules
Mklp1
Cyk4
Ect2
B
Mklp1
Cyk4
Ect2
RhoA GTP
Anillin
Membrane tethering
Constriction
Mklp1
Cyk4
Ect2
C
Vesicle
Rab
FIP3
Midbody
Rab- and FIP3-endosome delivery and fusion at the membrane
Cyk4
Mklp1
ESCRT-III helices constrict for abscission

Figure 4. Cartoon images show a dividing cell from anaphase to abscission, zoomed-in on the equatorial region and the midbody

The ring is assembled by the central spindle pathway and is tethered to the membrane by anillin. After ring constriction, a midbody forms and controls abscission. Rab- and FIP3- endosomes are recruited by centralspindlin and localize to the midbody after Ect2 leaves and accumulates in the newly formed daughter cell nuclei (Simon et al., 2008; Green et al., 2012; Frémont and Echard, 2018). It is not clear if Ect2's nuclear localization is required for the transition to these other complexes, or to decrease in active RhoA. (A) Centralspindlin (Cyk4/Mklp1; red) activates and recruits Ect2 (red) to the equatorial cortex, and Ect2 activates RhoA (green) to recruit downstream effectors to the contractile ring. (B) RhoA recruits the scaffold protein anillin (purple) to tether the contractile ring to the overlying cortex for ring constriction. Anillin also stabilizes RhoA. (C) The contractile ring matures into the midbody. Ect2 presumably leaves the midbody, although the mechanism for this is not known, and it is unclear if RhoA activity must decrease for abscission. The recruitment of Rab11-Fip3 (black and purple) vesicles is required to stabilize and narrow the intercellular bridge. This is mediated through the interaction of Fip3 and Cyk4. During abscission, centralspindlin and anillin continue to maintain the cleavage furrow, tethering the midbody ring to the cortex (Mierzwa and Gerlich, 2014). The recruitment of ESCRT-III targeting factors recruits the complex to the intercellular bridge. ESCRT-III (yellow) form large helical filaments, which bind and twist the membrane, eventually causing scission of the bridge.

1.4 Cytokinesis defects, chromosomal instability and cancer

Aberrant cell division can contribute to chromosomal instability, a hallmark of many cancers (Hanahan and Weinberg, 2011). Cells with unstable genomes display an increased rate of mutations and chromosomal rearrangements; this heterogeneity can drive tumorigenesis by conferring fitness benefits like increased proliferation and cell-death avoidance, characteristic of cancers. Defects in chromosome segregation can result in cells with altered ploidy. Aneuploid cells have altered gene expression and proteomes, which can lead to further increasing instability and is strongly associated with tumorigenesis (Nicholson and Cimini, 2013). In support of this, cells with trisomies divide with segregation defects that correlate with the number of genes gained (Hintzen et al., 2022). Such defects can be caused by improper attachments of kinetochores, where chromosomes lag and form DNA bridges at the division plane. These lagging chromosomes have been shown to delay nuclear envelope reformation, with potentially deleterious effects on nuclear function of the daughter cells (Karg et al., 2015; Rodriguez-Muñoz et al., 2022). In addition to aneuploidy, lagging chromosomes that fail to be incorporated into the primary nuclei can form their own nuclear envelope, becoming micronuclei, and cause segregation errors in subsequent divisions (He et al., 2019). These micronuclei have fragile nuclear envelopes and can undergo chromothripsis: a catastrophic shattering of the chromosome, followed by re-arrangement and ligation (Crasta et al., 2012). These rearranged chromosomes can potentially become reincorporated into the primary nuclei in subsequent cell divisions and generate further chromosomal instability, in a feed-forward loop (Soto et al., 2018).

Cytokinesis failure has been proposed to drive chromosomal instability through the generation of aneuploid cells from the division of tetraploid cells (Lens and Medema, 2019). Cells that fail cytokinesis become binucleated, and this can occur either due to absent or incomplete

ingression, or failure to cut the intercellular bridge during abscission. The latter can lead to cells staying connected at their intercellular bridge, or regression of the bridge and multinucleation (Liu and Erikson, 2007). Cell division in multinucleated cells is error-prone, with an abnormal number of centrosomes and lagging chromosomes (Ganem et al., 2009; Kuznetsova et al., 2015). Although centrosome clustering at the poles typically result in the formation of bipolar spindles, rare tripolar divisions can be observed, but the resulting daughter cells are not viable (Ganem et al., 2009). This is unsurprising, as large-scale changes to the genome are unlikely to provide cells with fitness advantages characteristic of cancer cells. Instead, incremental changes may provide more fitness over time, suggesting an optimal level of chromosomal instability for tumorigenesis (Lens and Medema, 2019). Experiments in mice have demonstrated that tetraploidization due to cytokinesis failure can lead to aneuploidy and tumorigenesis (Fujiwara et al., 2005; Lv et al., 2012). Whether the same can occur in human cells remains to be determined.

1.5 Ect2 as a proto-oncogene

Ect2 was first discovered as a proto-oncogene with the ability to transform mouse fibroblast cells *in vitro* (Miki et al., 1993). Ect2-mediated transformation depended on truncation of the N-terminus and removal of the central nuclear localization signal (NLS), which directs Ect2 to the nucleus (Saito et al., 2004). Ect2 is gene amplified, overexpressed in various cancers (reviewed in Fields and Justilien, 2010), and is associated with poor prognosis in patients with NSCLC, esophageal squamous cell carcinoma, and colorectal cancer (Sano et al., 2006; Salhia et al., 2008; Hirata et al., 2009; Luo et al., 2015). However, because the Ect2 that is overexpressed in human cancers is full-length, the N-terminal truncation that displayed transforming ability in mice cells is not believed to be involved in tumorigenesis. The subcellular

localization of Ect2 appears to be significant for cancer progression, as mislocalization of Ect2 in the cytoplasm has been associated with poor prognosis in patients with breast cancer, colorectal cancer and lung adenocarcinoma (Kosibaty et al., 2019; Cook et al., 2021; Yi et al., 2022).

How Ect2 could drive tumorigenesis is unclear. In lung adenocarcinoma, Ect2 has been proposed to promote cancer progression by increasing focal adhesions through the kinase FAK (Kosibaty et al., 2021). Other studies demonstrated that Ect2 may be sequestered in the cytoplasm by the kinase PKCι in lung cancers, where it activates Rac1 to increase cell proliferation through ERK/MAPK signaling (Justilien and Fields, 2009; Fields and Justilien, 2010). On the other hand, nuclear Ect2 appears to activate ribosomal RNA genes, also through Rac1 activation (Justilien et al., 2019). Whether Ect2 can promote tumorigenesis in other cancer types through Rac1 is an important question.

1.6 Thesis overview

Cytokinesis is a dramatic event coordinated by multiple pathways. Seminal work in the past three decades has expanded our knowledge on how the division plane is defined and how the final cut is made. At the heart of this process are the GTPase RhoA and the RhoGEF Ect2, conserved throughout metazoans. As the activator of RhoA, Ect2 has become the focus of many studies in cell and cancer biology. Its importance in cytokinesis is well-established, yet important questions remain. Of its domains, the PBC region is the least studied and its role in cytokinesis is unclear. Importantly for us, an unmapped NLS is located in the PBC. Similarly, the central NLS is known to cause cytokinesis phenotypes when mutated, but the reason for this has not been determined. These make Ect2 a potential candidate for regulation by the Ran-importin pathway.

In Chapter 2, we investigated the role of importins in controlling the function of Ect2 via its C-terminal NLS. For the first time, we identified the residues that form this NLS. We found that the NLS spans residues from 800-818, and mutations that target at least two clusters of residues can abrogate its ability to bind to importins. Clusters of mutations within this NLS widen or abolish Ect2 at the equatorial membrane, which is also regulated by Cdk1 phosphorylation. We also determined that the N-terminal BRCT domains auto-inhibit the NLS, which would likely be relieved by Cyk4-binding. Thus, we have uncovered additional modes of spatiotemporal regulation for Ect2 by importins at the equatorial membrane where it controls RhoA activation for ring assembly.

In Chapter 3, we investigated the role of importins in controlling the nuclear transport and removal of Ect2 via the central, S-loop NLS for cytokinesis. Using time-lapse fluorescence microscopy, we showed that abolishing nuclear localization maintains Ect2 at the midbody for a long time after ingression has completed, and a significant proportion of cells fail cytokinesis. In cells expressing mutant Ect2, active RhoA persists at the intercellular bridge and we observed bridge instability. We propose that abscission fails in these cells due to persistent ring components and contractility at the bridge. Our results support the notion that RhoA activity must decrease to form a stable midbody for abscission.

In Chapter 4, we identified novel proteins that could be regulated by the Ran-importin pathway during mitotic exit. Using a proteomics approach, we performed a TurboID proximity-biotinylation assay to identify the interactome of importin-β1 during mitotic exit. Our assay yielded 24 high-confidence interactors, with 13 common to previously published interactions. Of the 11 novel interactors, we confirmed binding for the proteins abi-2, dyskerin and Dock7. Preliminary results using shRNA-knockdown suggests that annexin A1 may be weakly required for cytokinesis. We also found that the C-terminus of Dock7 localizes to the midbody, which suggests

a potential role in the later stages of cytokinesis. Whether these proteins have functions in cytokinesis and if they are regulated by importins will be interesting questions to explore.

These studies generate new knowledge on how cytokinesis occurs in human cells. Expanding on previous work, our findings provide mechanistic insight into Ect2-RhoA regulation. As a protein overexpressed in many cancers, new knowledge of Ect2 function may help us better understand cancer progression. Our work opens new avenues of research to study the scope of the Ran-importin pathway in cytokinesis.

Chapter 2

The PBC of Ect2 controls membrane localization

2.1 Preamble

In cytokinesis, the contractile ring is formed upon activation of the GTPase RhoA by the RhoGEF Ect2. Studies on Ect2 regulation have focused on its N-terminal region, the BRCT domains, and little is known about the polybasic cluster region (PBC) at its C-terminus. In addition, this region is predicted to hold a cryptic C-terminal NLS, similar to anillin, which suggests the PBC could be regulated by importins. In this chapter, we identify the residues critical to this NLS and show that it is required for Ect2 function in cytokinesis.

2.2 Abstract

Cytokinesis, the final step of mitosis, describes the physical separation of a dividing cell into two daughters. Multiple pathways couple the segregation of chromosomes in anaphase to the formation and constriction of the contractile ring, which pinches to divide the cell. In anaphase, the centralspindlin complex recruits Ect2 to the central spindle and overlying cortex, where it activates RhoA to assemble the contractile ring. The membrane association of Ect2 by its PH domain is required for its activity, but how this is regulated is not well understood. Adjacent to the PH is a polybasic cluster (region) which is also required for cytokinesis and membrane association, but its role in cytokinesis is unclear. We found that mutating the PBC in a region predicted to be a nuclear localization signal (NLS) impairs Ect2 recruitment at the equatorial cortex. We show that this NLS is required for cytokinesis, and that a phosphorylation site within this NLS controls the timing of Ect2 recruitment at the cortex during metaphase. We propose that

importin-binding to this NLS contributes to Ect2 localization at the membrane by promoting a conformation that has higher affinity for lipids. These findings show that the PBC region regulates Ect2 function and localization in cytokinesis.

2.3 Introduction

Cytokinesis occurs at the end of mitosis due to the assembly and constriction of a contractile ring, which divides the cell into two daughters. Failure to complete cytokinesis can result in the misallocation of cell fate determinants and chromosomes, which can cause developmental diseases. The ring assembles between the segregating chromosomes and is spatiotemporally coupled to DNA position through multiple mechanisms. Assembly of the contractile ring depends on the activation of the GTPase RhoA by the guanine nucleotide exchange factor (GEF) Ect2 at the equatorial cortex. In anaphase, an array of antiparallel microtubules forms between the segregating sister chromatids. The centralspindlin complex comprised of Kif23/MKLP1 and RacGAP/Cyk4 is required for central spindle assembly and also recruits Ect2 (Kamijo et al., 2006). The interaction between Ect2-Cyk4 is essential for RhoA activation, which subsequently activates formins and Rho kinase for actin polymerization and myosin activation, respectively (Green et al., 2012). At the poles, astral microtubules negatively regulate the contractile machinery, ensuring their narrow enrichment at the equatorial plane to form the ring (van Oostende Triplet et al., 2014). After ingression, the ring matures into the midbody at the centre of an intercellular bridge connecting the two daughter cells. The cutting of this bridge is mediated by the ESCRT-III complexes during abscission, which result in physical separation of the two daughter cells.

Ect2 activates RhoA at the equatorial cortex, but the mechanism controlling Ect2's membrane localization is not clear. Ect2 consists of N-terminal BRCT domains, an S-loop hinge region, a catalytic DH domain that activates RhoA, and pleckstrin homology (PH) and polybasic (PBC) regions that bind to phospholipids. In mitosis, Ect2 is phosphorylated by Cdk1, which keeps it from being active until mitotic exit, when dephosphorylation permits Ect2 to form a complex with Cyk4 (Yüce et al., 2005). Ect2 has several Cdk1 phosphorylation sites, and presumably one/more of these could cause autoinhibition via interactions between the BRCT domains and other regions of Ect2 to prevent accessibility of the DH domain for RhoA. Cyk4 also requires phosphorylation by Plk1 for Ect2-binding, which occurs via the BRCT domains (Clifford et al., 2008). While these interactions control Ect2-Cyk4 binding, they do not explain how Ect2 is recruited to the membrane. The PH and PBC domains have each been shown to be required for Ect2's membrane localization (Frenette et al., 2012; Su et al., 2011). RhoA was also proposed to promote Ect2's membrane association by binding to the PH domain in a positive-feedback loop, which is likely distinct vs. regions of the PH domain that are required for lipid-binding (Chen et al., 2020).

Compared to the rest of its structure, the polybasic cluster (PBC) of Ect2 is poorly studied. Previous work showed that the PBC is required for membrane association, but how this region is regulated is not well understood (Su et al., 2011). There is a Cdk1 site in the PBC, and a phosphodeficient mutation in a C-terminal fragment of Ect2 was shown to facilitate the fragment's localization at the cortex, supporting that phosphorylation prevents Ect2 from associating with the membrane (Su et al., 2011).

In addition, the PBC has a predicted cryptic NLS that has not been characterized (Liot et al., 2011). Our lab previously found that anillin also has a cryptic C-terminal NLS that has a role in cytokinesis rather than nuclear localization (Beaudet et al., 2017, 2020). Our model is that importins facilitate the recruitment of anillin at the cortex by binding to this C-terminal NLS,

enhancing anillin's affinity for lipids. It is possible that the C-terminal NLS of Ect2 is similarly regulated by importins. Deletion of the PBC has been shown to impair Ect2's ability to rescue cytokinesis in Ect2-depleted cells, leading to multinucleation (Su et al., 2011). Although the PBC is required for Ect2 function, specific lipid-binding residues have not been identified. The location of the predicted NLS has not been confirmed, and whether it plays a role in cytokinesis is unknown. Like anillin's C-terminal NLS, which we showed is inhibited by anillin's Rho-binding domain, the Ect2 C-terminal NLS appears to be auto-inhibited, but the domains which inhibit this region have also not been determined. NLSs are positively-charged residues and bind to importins through electrostatic interactions (Lu et al., 2021). Within this predicted NLS region is a phosphorylation site; this modification could interfere with binding to lipids directly or impact importin-binding (Su et al., 2011).

In this work, we have identified critical residues for Ect2's C-terminal NLS. This NLS is required for cytokinesis and unable to rescue Ect2 depletion. We also show that the accessibility of this NLS may be inhibited by both Cdk1 phosphorylation and by the BRCT regions through intramolecular folding. Our results show that, depending on the residues, mutating this C-terminal NLS can widen or abolish the localization of Ect2 at the cleavage furrow, showing that the PBC region regulates Ect2 localization.

2.4 Materials & Methods

2.4.1 Cell Culture and Transfection

HeLa cells were plated and grown in DMEM (Wisent), supplemented with 10% cosmic calf serum (Thermo Scientific) and were maintained at 37°C with 5% CO2. For transfection, cells were plated in DMEM media, and transfected using Lipofectamine 3000 according to the manufacturer's protocol (Invitrogen). Briefly, 2.5-5.0 of Lipofectamine was used per 2 ml of media with 2.5 µg DNA, 2.5-5.0 µL of P3000 and re-suspended in Opti-MEM (Gibco). Cells were imaged 24 h after transfection for localization experiments in interphase cells, and 48 h after transfection for rescue experiments where Ect2 was depleted with shRNA.

2.4.2 Constructs / Plasmids

All plasmids were maintained and cloned in *Escherichia coli* DH5α unless specified otherwise. Primers used for cloning and mutagenesis are listed in Table 1 and 2, and shRNA sequence is listed in Table 3. mNeonGreen was obtained from Allele Biotech, and 3xmNeonGreen was cloned by amplifying mNeonGreen and cloning three fragments in-frame into the pYTK001 backbone (Addgene #65108; Lee et al., 2015) using a Golden Gate cloning protocol (Engler et al., 2008). Scarlet-I-Ect2 was generated by first cloning mScarlet-I, amplified from mScarlet-I-mTurquoise2 (Addgene #98839; Mastop et al., 2017), and Ect2, amplified from myc:Ect2 (Yüce et al., 2005) into the pYTK001 backbone (Addgene #65108; Lee et al., 2015) by Golden Gate, then assembled into a modified pX459V2.0-HypaCas9 vector (Addgene #108294; Kato-Inui et al. 2018) for mammalian expression. A shRNA sequence targeting endogenous Ect2, designed after the siRNA described in Yüce et al., 2005, was cloned into the modified pX459V2.0-

HypaCas9 vector beforehand. Restriction enzymes used for Golden Gate assembly were BbsI, BsmBI-v2 and BsaI-hfv2 (New England Biolabs). Substitutions (Ect2 804AAVTA808, 814ATPAA818, 804AAVTAAFSFSATPAA818, 800AA801, 348AAA350, 565AAAA568 + P570S, W307A + P703D, T815A, T815D) and truncations (Ect2 774-883, Ect2 ΔBRCT0/1-137, Ect2 ΔBRCT1/138-236, Ect2 ΔBRCT2/237-326, Ect2 ΔBRCT0-1/1-236, Ect2 ΔBRCT0-1-2/1-326) were generated using a one-step PCR protocol using partially overlapping primers (Liu and Naismith, 2008). GST:importin-β was previously generated (Beaudet et al., 2020). All constructs were verified by sequencing (Genome Quebec, Plasmidsaurus, and FlowGenomics).

Table 1. List of cloning primers

Primers used to clone 3xmNG (repeats are labeled in parentheses), mScarlet-I and Ect2 into the pYTK001 backbone. Primers are labeled as forward (fwd) or reverse (rev). Sequences are listed in the 5'-3' orientation.

Cloning Primer	Sequence
3xmNG (1) - fwd	GCATCGTCTCATCGGTCTCACCATGGTGAGCAAGGGC
3xmNG (1) - rev	ATGCCGTCTCAGGACCCTCCTGAACCCCCCTTGTACAGCTCGTCCATG
3xmNG (2) - fwd	GCATCGTCTCAGTCCATGGTGAGCAAGGGC
3xmNG (2) - rev	ATGCCGTCTCACGACCCTCCTGAACCCCCCTTGTACAGCTCGTCCATG
3xmNG (3) - fwd	GCATCGTCTCAGTCGATGGTGAGCAAGGGC
3xmNG (3) - rev	ATGCCGTCTCAGGTCTCAAGACCCTCCTGAACCCCCCTTGTACAGCTCGTCCATG
mScarlet-I N-terminus - fwd	GCATCGTCTCATCGGTCTCACCATGGTGAGCAAGGGCGAG
mScarlet-I N-terminus - rev	GGCATGGACGAGCTGTACAAGGGGGGTTCAGGAGGGTCTTGAGACCTGAGACGGCAT
Ect2 - fwd	GCATCGTCTCATCGGTCTCAGTCTATGGCTGAAAATAGTGTATTAACATCCACTAC
Ect2 - rev	GTCATACGTTAAGTAGATCTACAACTCATTTGATATGAGTGAGACCTGAGACGGCAT

Table 2. List of primers for substitution mutations and truncations

Primers used for substitution mutations and truncations. Primers are labeled as forward (fwd) or reverse (rev). Sequences are listed in the 5'-3' orientation.

Ect2 mutation and truncation	Sequence
328-388 - fwd	GCATCGTCTCATCGGTCTCAGTCTACTCCTGAGCTCAAGAAATCAGTG
328-388 - rev	ATGCCGTCTCAGGTCTCACTCAGATATCTAGGAGTGACCCTATGGAAAG
348AAA350 - fwd	AATAGAGCAGCAGCTAGATTAAAAGAAACACTTGCTCAGCTTTCAAGAGAG
348AAA350 - rev	TTTTAATCTAGCTGCTGCTCTATTGCTGTTAGGGGTATTTAGAGAAAGCATTGAC
565AAAA568 - fwd	GAGCAGCAGCAGCATTACCCAGTGTTGCATTACTTTTAAATGATCTTAAGAAGCATAC
565AAAA568 - rev	TAATGCTGCTGCTGCTCGGATAAGAAGTTCAACAAGGCTCTGCC
565AAAA568 + P570S - fwd	GCATTATCCAGTGTTGCATTACTTTTAAATGATCTTAAGAAGCATACAGCTG
565AAAA568 + P570S - rev	CAACACTGGATAATGCTGCTGCTGCTCG
774-883 - fwd	GTCTCAGTCTTATACTGCTGATCCAGAATCCTTTGAAGTAAATACAAAAGATATGGA
774-883 - rev	AGCAGTATAAGACTGAGACCGACTACGGTTATCCACAGAATCA
800AA801 - fwd	AATAGCAGCGACTTCAAAAAAGGTTACAAGAGCA
800AA801 - rev	AGTCGCTGCTATTGCTCTTGATGCTCTACTC
804AAVTA808 - fwd	CAATAAAAAAGACTTCAGCTGCAGTTACAGCAGCATTCTCTTTCTC
804AAVTA808 - rev	CTCTTTCTCTTACGACGACATTGACGTCGACTTCAGAAAAAATAAC
814ATPAA818 - fwd	CCAGCAGCTGCTCTTGCAGCGGCTCTTATGACATC
814ATPAA818 - rev	GAGCAGCTGCTGGAGTTGCGGAGAAAGAGAATGCTC
814ATPAA818 + 804AAVTA808 fwd	TCTTGCAGCGGCTCTTATGACATCCCACGGCTCAG
814ATPAA818 + 804AAVTA808 rev	AGCCGCTGCAAGAGCAGCTGCTGGAGTTGC
P703D - fwd	CCTAATGGATCTTTCTCAGATTAAGAAGGTATTGGACATAAGAGAGACA
P703D - rev	TGAGAAAGATCCATTAGGTGAATATGCTTAAGAGAAGCTGGG
T815A - fwd	CCAAAGCTCCAAAAAGAGCTCTTCGAAGGGC
T815A - rev	CTTTTTGGAGCTTTGGAGAAAGAGAATGCTCTTGTAACC
T815D - fwd	CTCCAAAGATCCAAAAAGAGCTCTTCGAAGGG
T815D - rev	TTTTGGATCTTTGGAGAAAGAGAATGCTCTTGTAACCTT
W307A - fwd	GGTTCGCGGGAAGCATTCAAATGGATGCCC
W307A - rev	CCCGCGAACCACTCTTGCTTGACAACATAAAGTTTCTTTG
ΔBRCT/1-137 - fwd	AGTCTCGCCCGTTGTATTGTACAAGTATGATGAATCTAGTACTATGCTTTACTG
ΔBRCT/1-137 - rev	CGGGCGAGACTGAGACCGACTACGGTTATCCA
ΔBRCT0-1/1-236 - fwd	TCAGTCTGTTCCTCCATTTCAAGATTGTATTTTAAGTTTCCTGGGATTTTCAGA
ΔBRCT0-1/1-236 - rev	GGAGGAACAGACTGAGACCGACTACGGTTATCCACA
ΔBRCT0-1-2/1-326 - fwd	GTCTCAGTCTAATACTCCTGAGCTCAAGAAATCAGTGTCAATGC
ΔBRCT0-1-2/1-326 - rev	AGGAGTATTAGACTGAGACCGACTACGGTTATCCACAGAATCA
ΔBRCT1/138-236 - fwd	TTTTCATGTGTTCCTCCATTTCAAGATTGTATTTTAAGTTTCCTGGGATTTTCAGA
ΔBRCT1/138-236 - rev	GGAGGAACACATGAAAATGGCAAAGGCTCTCCTTTTTG
ΔBRCT2/237-326 - fwd	AGAAATGAATTTAAAAATACTCCTGAGCTCAAGAAATCAGTGTCAATGCT
ΔBRCT2/237-326 - rev	CAGGAGTATTTTTAAATTCATTTCTAAAGTCATCAACTGCTGCATAGAAATCC

Table 3. List of shRNA sequence

Primers used to clone shRNA sequence into expression vectors. Primers are labeled as forward (fwd) or reverse (rev). Sequences are listed in the 5'-3' orientation.

shRNA	Sequence
shECT2 - fwd	CACCGAAGGCGGAATGAACAGGATTTATCAAGAGAAAATCCTGTTCATTCCGCCTT
shECT2 - rev	GAAGGCGGAATGAACAGGATTTATCAAGAGAAAATCCTGTTCATTCCGCCTTTTTT

2.4.3 Microscopy

To image cells, they were plated and transfected on 25-mm round coverslips (no. 1.5) or 22x22-mm square coverslips (no 1.5) and incubated with Hoechst 34580 (Invitrogen) at 1.3 μM or SYTO Deep Red (Invitrogen) at 50 nM for 30 min and placed in a Chamlide magnetic chamber (Quorum). Cells were kept at 37°C with 5% CO_2. Live imaging of timelapse rescue experiments was performed on an inverted Nikon Eclipse Ti microscope with a Livescan Swept Field confocal unit (Nikon), using the 100×/1.45 CFI PLAN APO VC oil immersion objective (Nikon; pixel size 0.0625 μm), a piezo Z stage (MadCity Labs), and with the Evolve EMCCD camera (Photometrics). Timelapse images were acquired with 500 ms exposures using the 488-nm and 561-nm lasers (100 mW; Agilent) set at 40% and 20%, respectively, and with 100 ms exposure using the 640-nm laser set at 17% power, and multiple Z-stacks of 1.0 μm were taken every 120 s per cell using NIS-Elements acquisition software (Nikon). For localization experiments, images were acquired with 200 ms exposures using 405-nm and 488-nm at 10% power, and multiple Z-stacks of 0.5 μm with the quad filter. For localization experiments, cells were imaged using the Nikon-TIE inverted epifluorescence microscope with the Lambda XL LED light source, using the 60x/1.4 PLAN APO λ oil objective (Nikon; pixel size 0.26 μm), a Piezo Z stage (ASI), and with the Photometrics Evolve 512 EMCCD camera. Images were acquired with 60 ms exposures using the 405-nm and 488-nm LEDs set at 5% and 20% power, respectively, and multiple Z-stacks of 2.0 μm were taken using NIS-Elements (Nikon). For rescue experiments and localization experiments, cells were imaged on an inverted Nikon Eclipse Ti2 microscope with a CSU-X1 spinning disk (Yokogawa), using the 60×/1.4 CFI PLAN APO VC oil immersion objective (Nikon) or a 20×/0.75 CFI PLAN APO air objective (Nikon) with a piezo Z stage (MadCityLabs), and with the Zyla camera (Andor). Images for timelapse experiments were acquired with 200 ms exposures using the 405-nm and 561-nm lasers (OMICs) set at 10% and 15% power, and multiple Z-stacks of 1.0 μm were taken

using μManager (NIH) every 120 s. For localization experiments and population rescue experiments, images were acquired with 300 ms using 488-nm and 638-nm at 100% and 10% power, or 405-nm and 561-nm lasers. Binning was set at 1x1 for localization experiments, 2x2 for timelapse rescue experiments, and 3x3 for population rescue experiments. Image files were exported as TIFFs, which were opened with Fiji (NIH) and converted into maximum intensity Z-stack projections. Projections and merged color images were then converted into 8-bit images and imported into Illustrator (Adobe) to make figures.

2.4.4 Pull-down assays

Recombinant proteins GST and GST: importin-β were made from *Escherichia coli* BL21 cells. Bacteria were resuspended in lysis buffer (2.5 mM $MgCl_2$, 50 mM Tris, 150 mM NaCl, pH 7.5, 0.5% Triton X-100, 1 mM dithiothreitol [DTT], 1 mM phenylmethanesulfonyl fluoride [PMSF], and 1× protease inhibitors [Roche]), incubated with 1 mg/mL lysozyme on ice for 30 min, then sonicated three times. Extracts were incubated with pre-equilibrated glutathione sepharose 4B (GE Lifesciences) overnight at 4°C with rotation. After washing, beads were stored as a 50% slurry at 4°C. Protein concentration was determined by running samples by SDS–PAGE and measuring the density of bands in comparison to known concentrations of bovine serum albumin. To test for binding, proteins were pulled down from cell lysates after transfection. Transfected HeLa cells were lysed in 50 mM Tris, pH 7.6, 150 mM NaCl, 5 mM $MgCl_2$, 0.5% Triton X-100, 1 mM DTT, 1 mM PMSF with 1× protease inhibitors (Roche), and incubated with 5–10 μg of purified GST-tagged importin-β protein on beads at 4°C overnight. After binding, beads were washed three to four times with 50 mM Tris, pH 7.6, 150 mM NaCl, 5 mM $MgCl_2$ before adding SDS sample buffer to denature the proteins for SDS PAGE. All samples were run by SDS–PAGE and

wet-transferred to nitrocellulose membrane for Western blotting. All blots were reversibly stained with Ponceau S to show total protein. The blots were blocked with 5% milk for 20 min, then incubated with 1:10,000 mouse anti-mNeonGreen antibodies (ChromoTek) in 1× TBS-T (0.150 M NaCl, 0.1 M Tris pH 7.4, 0.5% Triton X-100) for 1–2 h at room temperature. After washing the membrane three to four times with 1× TBS-T, secondary antibodies (anti-rabbit HRP [horseradish peroxidase]; New England Biolabs) were added as per manufacturer's instructions in 1× TBS-T for 2 h. The blots were developed using enhanced chemiluminescence (ECL) Western blotting detection reagents (Cytiva) and visualized on a GE Amersham Imager 600 or ChemiDoc XRS+ (Bio-Rad). All results from each pull-down assay were replicated in at least three distinct experiments to ensure reproducibility. Band intensity was quantified using ImageJ, then imported into Excel (Microsoft) for formatting. Data were then imported to Prism (Version 10.20, Graphpad). Images were converted to 8 bit by Fiji, and made into figures using Illustrator (Adobe).

2.4.5 Analysis

All images acquired using NIS Elements (Nikon) were opened in Fiji (Version 2.3, NIH) or Cellprofiler (Broad Institute) for analysis. Linescans were performed and measured using a macro in Fiji modified from Ozugergin et al., 2022. The macro was designed to isolate the desired channel from the image file, subtract background signal, and perform a bleach correction. The desired timepoint and three central Z slices were selected manually, and the macro generated a Z- stack sum-slice projection. A five-pixel-wide line was then traced along the cortex of the cell, from one pole to the other, along with a straight one- pixel- wide line to define the midplane. The macro then measured the fluorescence intensity of each pixel along the length of the linescan and positioned the pixels in relation to the midplane. For breadth measurements, the number of

pixels above 50% of the normalized peak intensities were counted for each linescan and converted to microns. Pixels with intensities higher than the cutoff value outside of the peak region were excluded from these calculations. For analysis of the cortical enrichment, cell images were converted to a Z-stack maximum intensity projection of 3 slices. Four circular regions of interest on the cortex and in the cytosol were measured for mean gray value, and average values were calculated from the four measurements. The ratio of the average cortical signal was divided by the average cytosolic signal, and this analysis was repeated for each timepoint analyzed, from 4 min before anaphase onset to 2 min after anaphase onset. All data were imported into Excel (Microsoft) for formatting, then to Prism (Version 9.3, GraphPad) for further analysis. All images and graphs were transferred to Illustrator (Adobe) to make figures.

For analysis of mononucleate and multinucleate cells in rescue experiments, counting was performed manually on FIJI using the CellCounter plugin. For Figure S2, a custom pipeline in CellProfiler v4.2.8 was developed. First, cells were segmented using DIC images with Cellpose-SAM to produce labeled matrices as input segmentation masks in CellProfiler. The pipeline segmented nuclei using the nuclei model of Cellpose2 (RunCellpose), then shrunk them to a single point to avoid misattribution of nuclei to adjacent cells (ExpandOrShrinkObjects). The fluorescence intensity of mScarlet-I was measured for each object (MeasureObjectIntensity), allowing each segmented cell to be filtered based on integrated intensity (FilterObjects) based on controls. Finally, segmented and shrunk nuclei were related to segmented cells within the set intensity thresholds (RelateObjects), and classified as mononucleate or multinucleate (ClassifyObjects). Data were imported into Excel (Microsoft) for formatting. An average of the percent of multinucleated cells of each field of view was calculated, and images where no cells were segmented were excluded. Data were then imported to Prism (Version 9.3, GraphPad) for

further analysis. All of the images and graphs were transferred to Illustrator (Adobe) to make figures.

2.4.6 Statistical analysis

Line graphs, bar graphs and box-and-whisker plots were generated using Prism (Version 9.3, GraphPad). Data were tested for normality, and statistical significance was tested using Student's t-test, a one-way ANOVA or Welch's ANOVA, followed by multiple comparisons using Tukey's post-hoc test if the data were normally distributed, or using a non-parametric test if the data were not normally distributed. Significance levels were defined as: $p > 0.05$ non-significant (ns); *$p \leq 0.05$; **$p \leq 0.01$.

2.5 Results

2.5.1 Mapping the C-terminal NLS of Ect2 (localization and pull-down)

Ect2 localizes to the nucleus in interphase cells via a previously identified NLS located in its S-loop region. However, Ect2 also has a cryptic, poorly-studied NLS in its polybasic cluster (PBC) region, located at its C-terminus, which appears to be inhibited in the full-length protein. This classical bipartite NLS is predicted to span residues 800 to 826 in isoform 2 (Figure 5A). To identify the residues that constitute this NLS, we mutated three clusters of basic residues (800-801; 804-808; 814-818) alone or in tandem in a PBC-containing fragment (774-883) by substituting the basic residues to Ala and assessing whether nuclear localization was impaired. In addition, since small proteins can passively diffuse through the nuclear pore complexes, we tagged the PBC with three tandem repeats of mNeonGreen to increase the size of the fusion protein (Timney et al., 2016; Winogradoff et al., 2022). While the 3xmNeonGreen-PBC localized to the nuclei in HeLa cells, mutations in two clusters of the NLS reduced nuclear localization, while it was abolished when two clusters were mutated ($PBC^{mut804-818}$; $PBC^{mut800-801/814-818}$) (Figure 5B and S1A). These experiments confirm that the C-terminal NLS is located between residues 800-818. For downstream experiments, we focused on $PBC^{mut804-818}$ as the NLS mutant, and $PBC^{mut800-801}$ as a partial mutant.

Since the PBC NLS had not been previously shown to bind to importins, we wanted to assess whether the NLS could bind to importin-β1, and how the mutations impacted this binding. We used purified recombinant GST:importin-β1 to pull-down mNeonGreen-PBC from HeLa cell

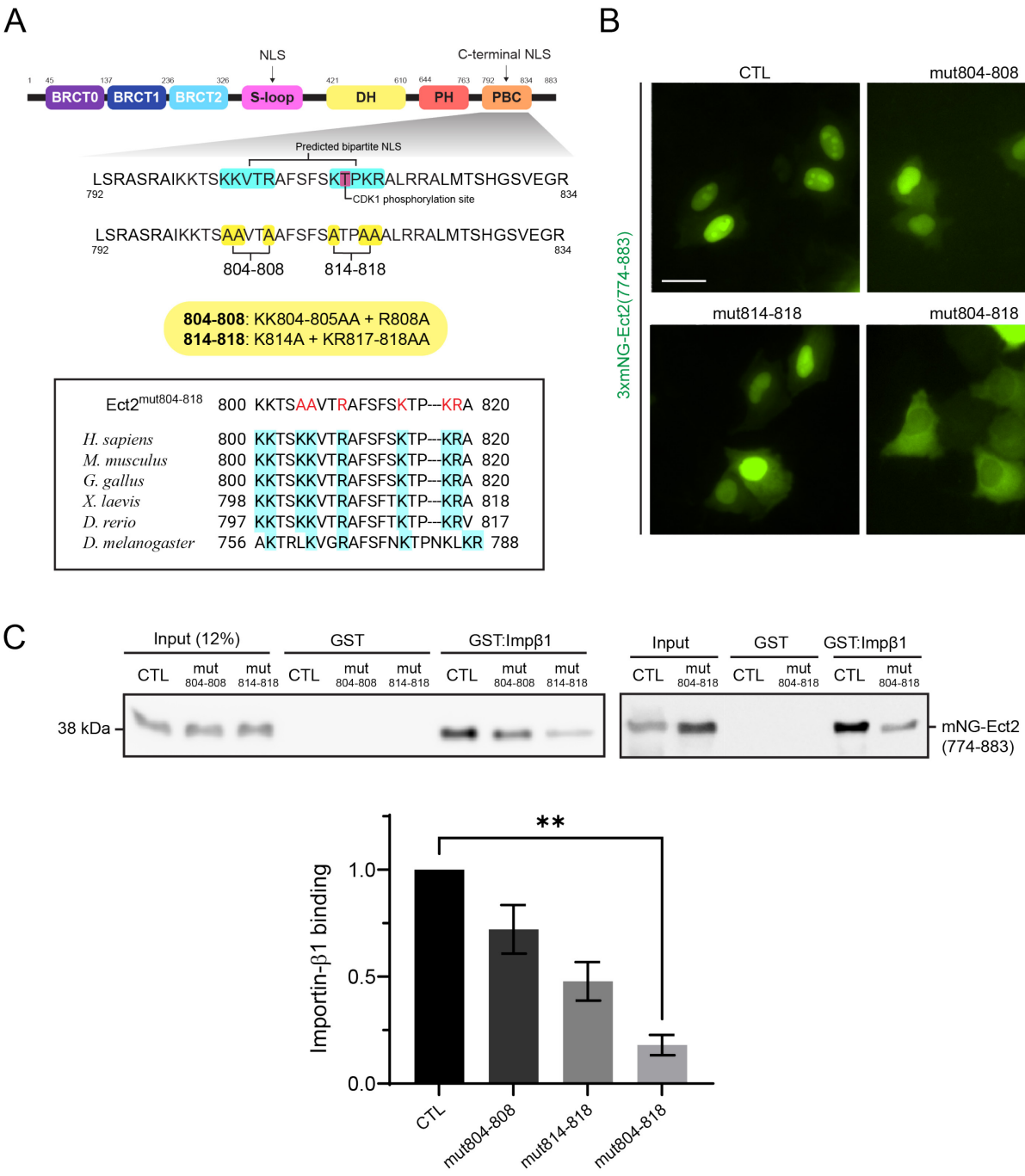
A
NLS
C-terminal NLS
1
45
137
236
326
421
610
644
763
792
834
883
BRCT0
BRCT1
BRCT2
S-loop
DH
PH
PBC
Predicted bipartite NLS
LSRASRAIKKTSKKVTRAFSFSKTPKRALRRALMTSHGSVEGR
792
834
CDK1 phosphorylation site
LSRASRAIKKTSAAVTAAFSFSATPAAALRRALMTSHGSVEGR
792
834
804-808
814-818
804-808: KK804-805AA + R808A
814-818: K814A + KR817-818AA
Ect2mut804-818 800 KKTSAAVTRAFSFSKTP---KRA 820
H. sapiens 800 KKTSKKVTRAFSFSKTP---KRA 820
M. musculus 800 KKTSKKVTRAFSFSKTP---KRA 820
G. gallus 800 KKTSKKVTRAFSFSKTP---KRA 820
X. laevis 798 KKTSKKVTRAFSFTKTP---KRA 818
D. rerio 797 KKTSKKVTRAFSFTKTP---KRV 817
D. melanogaster 756 AKTRLKVGRAFSFNKTPNKLKR 788
B
CTL
mut804-808
mut814-818
mut804-818
3xmNG-Ect2(774-883)
C
Input (12%)
GST
GST:Impβ1
CTL
mut 804-808
mut 814-818
38 kDa
mNG-Ect2 (774-883)
Importin-β1 binding
1.0
0.5
0.0
**
CTL
mut804-808
mut814-818
mut804-818

Figure 5. Mutating the C-terminal NLS of Ect2 impairs importin-binding.

(A) Cartoon diagram of the structures of Ect2. The predicted C-terminal NLS is labeled in cyan, with alanine substitutions in yellow (Liot et al., 2011). A putative Cdk1 phosphorylation site at Thr815 is highlighted in red (Su et al., 2011), Below, an alignment showing conservation of the PBC, with conserved basic residues highlighted in cyan. (B) Images show HeLa cells expressing 3xmNG:Ect2 (774-883) (green; control or mutants). Scale bar is 30 μm. Cartoon structure of 3xmNG-Ect2 (774-883) is shown above. (C) Immunoblots of pull-down assays of purified GST:importin-β1 with mNG:Ect2 (774-883) (control or NLS mutants) from HeLa cell lysates. Below, a bar graph of the means of densitometry measurements of immunoblots, normalized to input and to the control (n = 3). Error bars show standard deviation. Data were analyzed by ANOVA and are labeled for significance: ** for $p < 0.01$.

lysate. As expected, mNeonGreen-PBC bound to GST:importin-β1 and not to GST. Further, while binding to the upstream or downstream NLS mutants decreased compared to non-mutant PBC, it was strongly reduced with the double mutant PBC$^{mut804-818}$ (Figure 5C). Notably, binding to GST:importin-β1 was more strongly affected by the downstream vs. upstream NLS mutant, suggesting that the downstream residues may be more critical for importin-binding to the NLS than the upstream residues. However, this could be specific to importin-β1 vs. importin-α. Together, these results show that the PBC NLS residues can bind to importins, which can mediate the localization of the PBC to the nucleus.

2.5.2 The PBC NLS is required for Ect2 function in cytokinesis

A previous study showed that deletion of the PBC impaired the ability of Ect2 to rescue Ect2-depletion in HeLa cells, leading to multinucleation – a readout for cytokinesis failure – in approximately half of the cells (Su et al., 2011). To determine whether mutating the nuclear localization had similar effects, we performed cell population rescue experiments where we knocked down endogenous Ect2 in HeLa cells using shRNA and expressed RNAi-resistant mScarlet-I:Ect2 (control or mutant) and counted the number of mononucleate and multinucleate cells after 48h. For controls, we expressed Ect2 wild-type (Ect2^{WT}) and a loss-of-function mutant (Ect2^{LOF}; Su et al., 2011; Chen et al., 2020).

We found that expressing Ect2$^{mut804-818}$ led to 41.7% binucleate cells, compared to 9.1% with Ect2^{WT} and 62% with Ect2^{LOF} (Figure 6B.). Mutating the upstream cluster (Ect2$^{mut800-801}$) led

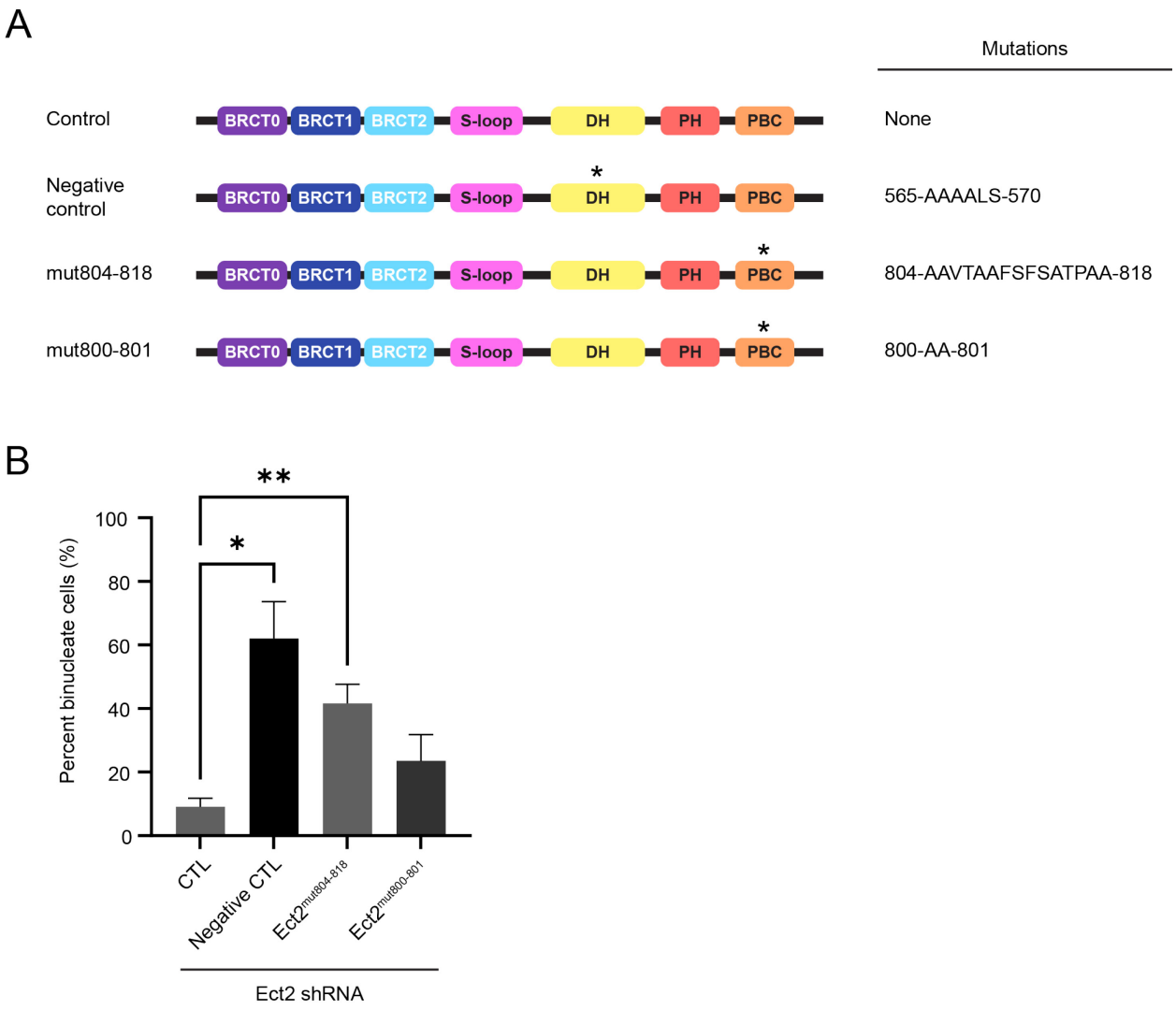

Figure 6. The C-terminal NLS of Ect2 is required for cytokinesis.

(A) Cartoon schematic of full-length Ect2 with control, negative control (loss-of-function) and C-terminal NLS mutations. Asterisk (*) denotes mutations, listed on the right. (B) Graph showing percentage of binucleate cells in rescue assays. HeLa cells were transfected with a plasmid encoding shRNA against endogenous Ect2 and expressing RNAi-resistant mScarlet-I:Ect2 (control or NLS mutants) as in (A). The means of each condition are as follows: control, 9.1%; negative control, 62.0%; $Ect2^{mut804-818}$, 43.7%; $Ect2^{mut800-801}$, 23.5%. Bars show standard deviation (N = 3, with n = 171-442 cells per replicate) and statistical analyses were done using ANOVA and Tukey post-hoc test (* for $p < 0.05$; ** for $p < 0.01$).

to a mild increase of binucleate cells (25.6%), but this was not significant. This indicates that the C-terminal NLS is required for cytokinesis.

Typically, the counting of monunucleate and multinucleate cells in these rescue experiments is performed manually. In an attempt to automate this process, we developed an image analysis pipeline on Cellprofiler (Figure S2). In our pipeline, cells and nuclei are segmented using the deep learning-based segmentation tool Cellpose-SAM and its pre-trained models (Pachitariu et al., 2025; pre-print). By quantifying the fluorescence intensity of mScarlet-I:Ect2, we were able to set thresholds of expression for rescue based on controls. Although promising, this pipeline was not able to resolve transfected binucleate cells as consistently as manual counting.

2.5.3 The PBC NLS controls the membrane localization of Ect2

Our lab previously found that mutating the C-terminal NLS of anillin reduces the breadth of anillin recruitment at the cleavage furrow (Beaudet et al., 2017). We wanted to determine whether mutating the C-terminal NLS of Ect2 similarly impaired Ect2 localization during cytokinesis. For this, we expressed mScarlet-I:Ect2 in HeLa cells and performed live-cell imaging (Figure 7A). We measured the fluorescence intensity of Ect2 (control or NLS mutant) along the cortex as cells were beginning to ingress. The breadth of Ect2 localization was measured as the number of the pixels > 50% of maximum fluorescence intensity, which was normalized by calculating the ratio vs. the length (the number of pixels; Figure 7B). We found that Ect2$^{mut804\text{-}818}$ localization at the cleavage furrow was lost, suggesting that mutating the C-terminal NLS prevents Ect2 from being recruited to the cleavage furrow in cytokinesis. A small visible foci near the furrow with Ect2$^{mut804\text{-}818}$ can be observed in some cells, which we believe to be a pool of Ect2$^{mut804\text{-}818}$ on

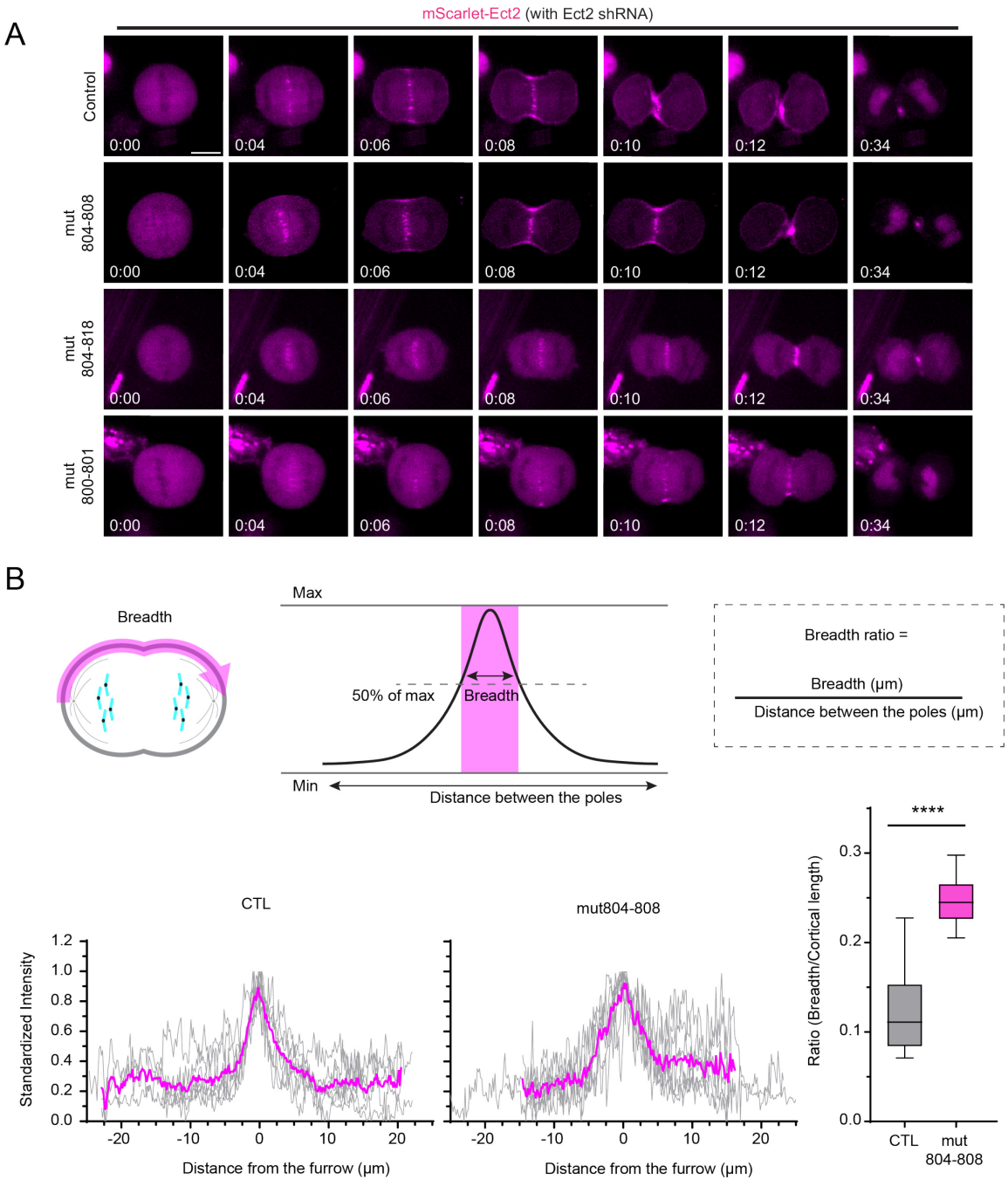
A
mScarlet-Ect2 (with Ect2 shRNA)
Control
mut 804-808
mut 804-818
mut 800-801
0:00
0:04
0:06
0:08
0:10
0:12
0:34
B
Breadth
Max
50% of max
Breadth
Min
Distance between the poles
Breadth ratio =
Breadth (μm)
Distance between the poles (μm)
CTL
mut804-808
Standardized Intensity
Distance from the furrow (μm)
Ratio (Breadth/Cortical length)
****
CTL
mut 804-808

Figure 7. Mutating the C-terminal NLS of Ect2 abolishes membrane recruitment.

(A) Timelapse images of HeLa cells expressing RNAi-resistant mScarlet-I:Ect2 (control or NLS mutants) and depleted of endogenous Ect2 using shRNA. Scale bar is 10 μm and time is in hours:minutes. (t = 0 is anaphase onset) (B) Cortical line scans of the wild-type Ect2 and $Ect2^{mut804\text{-}808}$ during membrane ingression. Breadth was calculated from the cortical linescans as depicted on the cartoon. On the right, box-and-whiskers plot of the breadth as a ratio of the cortical length (n = 6 cells for Ect2; n = 7 cells for $Ect2^{mut804\text{-}808}$). Statistical analysis was done using ANOVA (**** $p < 0.0001$).

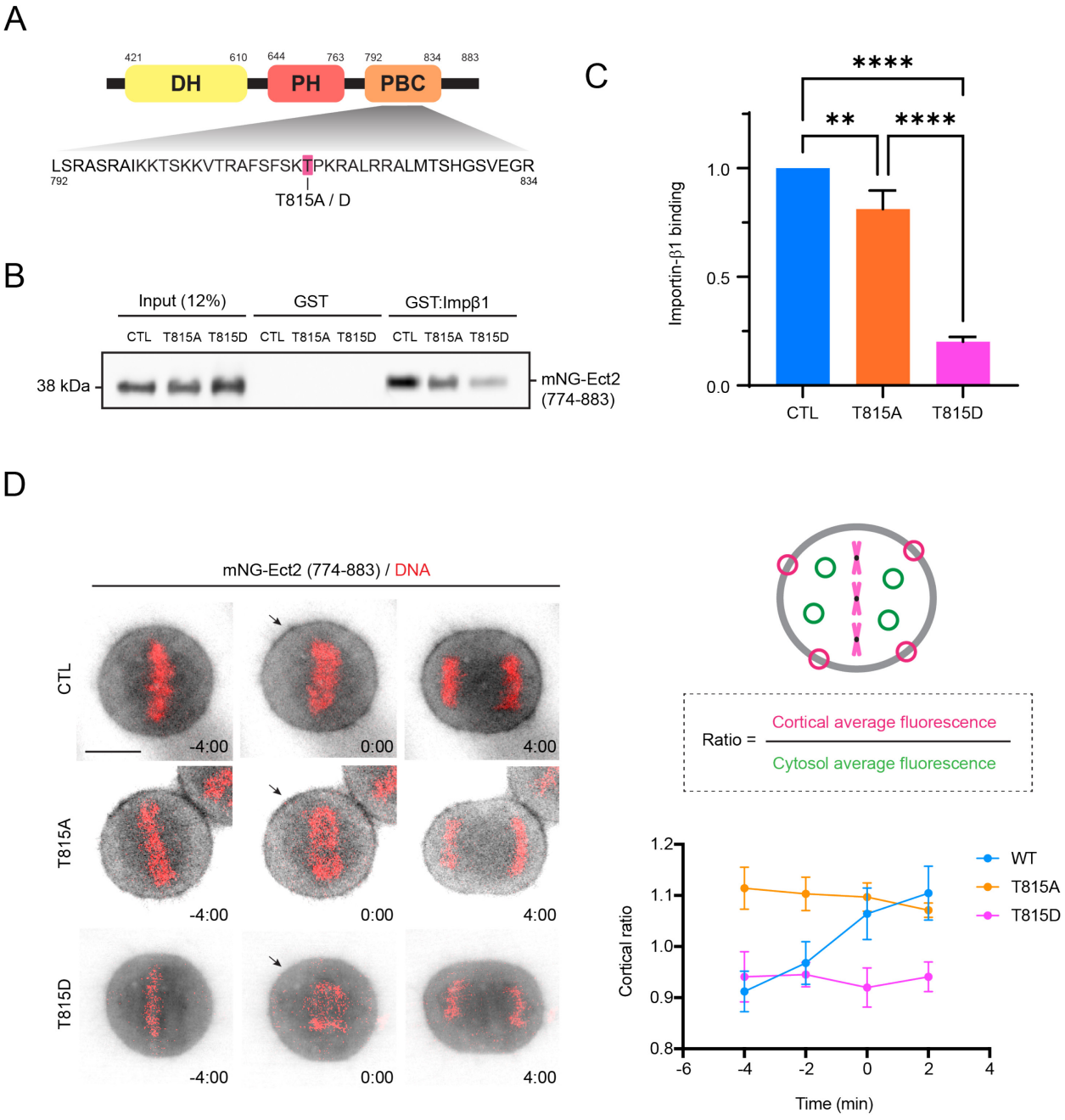
A
421
610
644
763
792
834
883
DH
PH
PBC
LSRASRAIKKTSKKVTRAFSFSKTPKRALRRALMTSHGSVEGR
792
834
T815A / D
B
Input (12%)
GST
GST:Impβ1
CTL T815A T815D CTL T815A T815D CTL T815A T815D
38 kDa
mNG-Ect2
(774-883)
C
****
**
****
Importin-β1 binding
1.0
0.5
0.0
CTL
T815A
T815D
D
mNG-Ect2 (774-883) / DNA
CTL
T815A
T815D
-4:00
0:00
4:00
Ratio =
Cortical average fluorescence
Cytosol average fluorescence
Cortical ratio
1.2
1.1
1.0
0.9
0.8
-6
-4
-2
0
2
4
Time (min)
WT
T815A
T815D

Figure 8. Thr815 controls the timing of membrane recruitment in the PBC.

(A) Cartoon shows the structure of the C-terminus of Ect2, highlighting the Thr815 phosphorylation residue in red. (B) Immunoblot of pull-down assay of mNG-Ect2 (774-883) non-mutant, with phosphodeficient (T815A) or phosphomimetic (T815D) mutations from HeLa cell lysates with GST-importin-β1 (n = 3). (C) A bar graph of the means of densitometry measurements, normalized to input and to the control. Statistical analysis was done using ANOVA: **p≤0.01; ****p≤0.0001. Error bars show standard deviation. (D) Timelapse images of HeLa cells overexpressing mNG-Ect2 (774-883) non-mutant (n = 7 cells) or with phosphodeficient (T815A; n = 6 cells) or phosphomimetic (T815D; n = 6 cells) mutations (grayscale) with DNA (red, Hoechst). Black arrows point to the membrane. Time is in minutes:seconds (t = 0:00 is anaphase onset). The scale bar is 10 μm. On the right, a cartoon shows how the ratio of the fluorescence intensity in regions of interest at the membrane vs. cytosol (cortical ratio) was calculated. On the bottom-right corner, a graph shows the cortical ratios during the metaphase-anaphase transition for cells shown in (D).

the central spindle near the membrane. Interestingly, Ect2$^{mut804-808}$ had a much larger breadth. These results suggest that mutating the C-terminal NLS of Ect2 severely impacts membrane recruitment of Ect2 during cytokinesis.

2.5.4 Binding of the PBC to importin-β1 is controlled by phosphorylation

There is a predicted Cdk1 phosphorylation site in the PBC that was previously shown to control membrane localization of this region. However, this effect could occur via affecting importin-binding, which could in turn affect the membrane recruitment of the PBC. In particular, the Thr residue (Thr815) in the NLS is in a consensus Cdk1 site. Thus, we predicted that mutating to a phosphomimetic residue (D) would keep the NLS acidic and block binding, while mutating to phosphodeficient (A) would permit binding. We generated the following mutants: Thr815 to Asp (T815D) or Ala (T815A), respectively, and performed pull-downs as described previously. Indeed, we observed a significant decrease in the binding of importin-β1 to the T815D mutant, supporting that phosphorylation of Thr815 could control importin-binding (Figure 8B-C).

We next wanted to assess whether nuclear localization was impacted by the phosphorylation state of the NLS. Since the phosphomimetic T815D mutation led to a significant decrease in importin-binding, it is possible that this mutation could disrupt nuclear localization. We expressed 3xmNG-PBC with the phosphomimetic mutation. Because impairing nuclear import required mutating two clusters of basic residues, we also combined the phosphomimetic mutation with mutations in residues 804-808. We found that the phosphomimetic localized to the nucleus (Figure S1B). When combined with mutations in residues 804-808, a weak cytosolic pool

can be observed. These results indicate that phosphorylation of Thr815 does not impact nuclear import via this NLS.

In parallel, we were interested in whether the T815D mutation could affect the timing of membrane recruitment during the metaphase-anaphase transition. We expressed mNeonGreen:PBC (control or mutant) in HeLa cells and measured the fluorescence intensity at the cortex vs. cytosol from 4 min before anaphase onset to 2 min after anaphase onset (Figure 8D). We found that the ratio of cortical:cytosol of PBC^{WT} increased over time, whereas it remained high with PBC^{T815A} and low with PBC^{T815D} with little change over time, indicating that phosphorylation of Th815 may act as a switch to control the timing of Ect2 recruitment at the cortex, at least for the PBC.

2.5.5 C-terminal NLS is auto-inhibited by the BRCT domains

In addition to phosphorylation, protein folding could also play a role in limiting access to this NLS. As mentioned previously, mutating the central NLS is sufficient to abolish nuclear localization, despite the presence of a functional C-terminal NLS. Ect2 has three BRCT regions (BRCT0, 1 and 2) that inhibit the DH domain in metaphase (Kim et al., 2005; Wolfe et al., 2009). We wanted to investigate whether these regions could also play a role in inhibiting the C-terminal NLS. We generated truncations of Ect2 where we deleted one, two or three of the BRCT regions and studied their localization in HeLa cells (Figure 9A). To study the function of the C-terminal NLS in isolation, we mutated the central NLS. In addition, because expressing a functional Ect2 without the regulatory BRCT domains causes ectopic RhoA activity and membrane ruffling, we generated loss-of-function mutations in the DH domain (Su et al. 2011; Chen et al. 2020). We

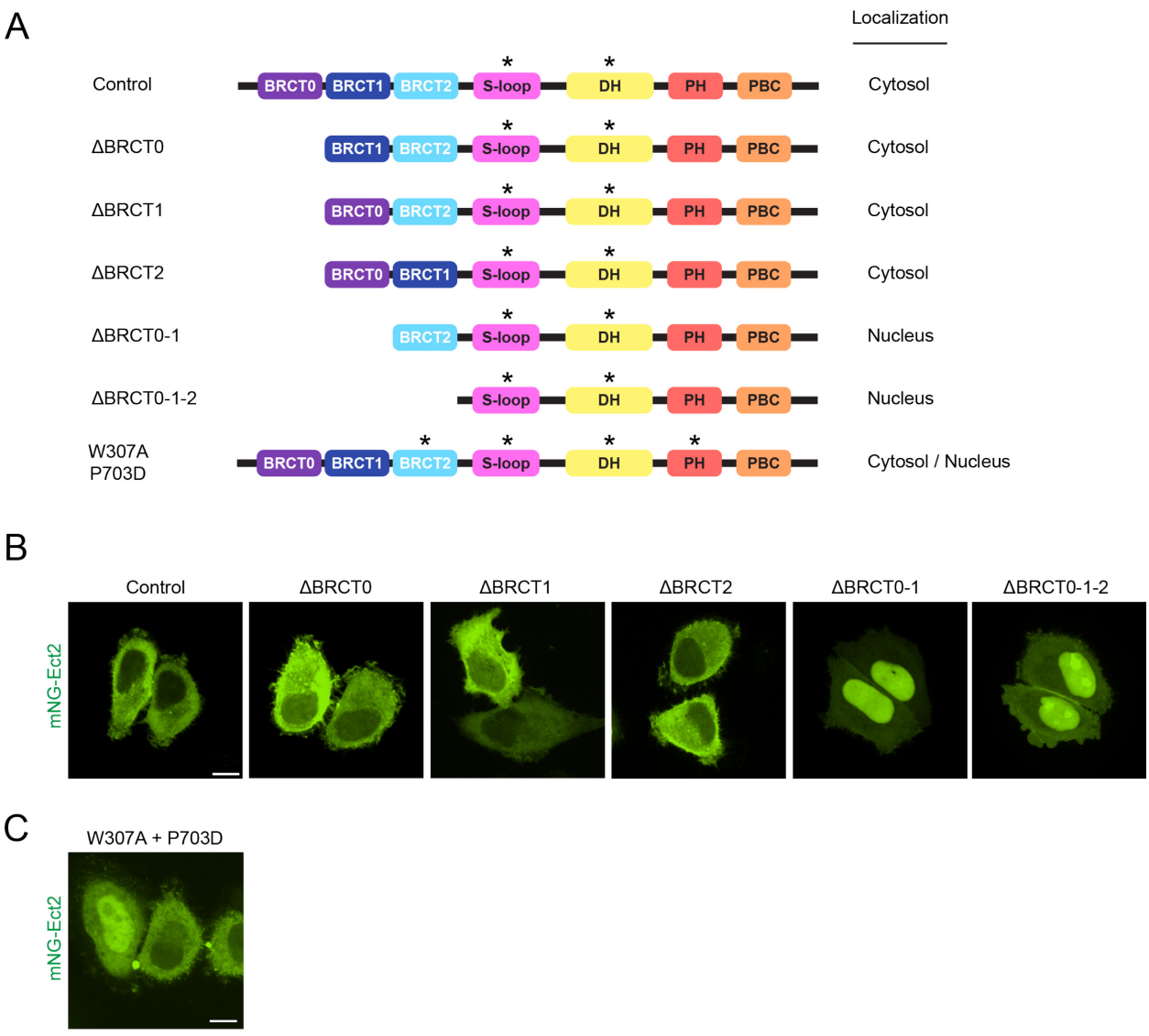

Figure 9. The BRCT domains inhibit the PBC.

(A) Cartoon schematic of Ect2 truncations and mutants, with summary of localization from (B-C) on the right. Asterisks (*) denote mutations. The central NLS and DH were mutated in all constructs. (B) Images show HeLa cells in interphase, expressing mNeonGreen:Ect2 (green) as depicted in (A). Scale bar is 10 μm. (C) HeLa cells expressing mNeonGreen:Ect2 in interphase with mutations from Chen et al. (2020). Scale bar is 10 μm.

observed that deletion of BRCT0 or BRCT1 showed cytosolic localization, but deletion of BRCT2 led to Ect2 being localized to both the nucleus and cytosol in a subset of cells (Figure 9B). Deletion of BRCT0 and BRCT1 or of all three BRCTs led to Ect2 being predominantly localized to the nucleus, although a cytosolic pool can still be observed. These results support that the BRCT regions inhibit the accessibility of the C-terminal NLS. despite the presence of a functional C-terminal NLS. Ect2 has three BRCT regions (BRCT0, 1 and 2) that inhibit the DH domain in metaphase (Kim et al., 2005; Wolfe et al., 2009). We wanted to investigate whether these regions could also play a role in inhibiting the C-terminal NLS. We generated truncations of Ect2 where we deleted one, two or three of the BRCT regions and studied their localization in HeLa cells (Figure 9A). To study the function of the C-terminal despite the presence of a functional C-terminal NLS. Ect2 has three BRCT regions (BRCT0, 1 and 2) that inhibit the DH domain in metaphase (Kim et al., 2005; Wolfe et al., 2009). We wanted to investigate whether these regions could also play a role in inhibiting the C-terminal NLS. We generated truncations of Ect2 where we deleted one, two or three of the BRCT regions and studied their localization in HeLa cells (Figure 9A). To study the function of the C-terminal NLS in isolation, we mutated the central NLS. In addition, because expressing a functional Ect2 without the regulatory BRCT domains causes ectopic RhoA activity and membrane ruffling, we generated loss-of-function mutations in the DH domain (Su et al. 2011; Chen et al. 2020). We observed that deletion of BRCT0 or BRCT1 showed cytosolic localization, but deletion of BRCT2 led to Ect2 being localized to both the nucleus and cytosol in a subset of cells (Figure 9B). Deletion of BRCT0 and BRCT1 or of all three BRCTs led to Ect2 being predominantly localized to the nucleus, although a cytosolic pool can still be observed. These results support that the BRCT regions inhibit the accessibility of the C-terminal NLS.

Previous work identified two residues which increase the catalytic activity of Ect2 for RhoA when they are mutated, and were proposed to relieve the auto-inhibition of adjacent domains on the DH (Chen et al., 2020). To test whether these mutations could relieve the C-terminal NLS from inhibition, we generated these mutations (W307A and P703D) in Ect2 where the central NLS and DH were mutated. This mutant localized to the cytosol or nucleus in cells, indicating that they can partially relieve the autoinhibition on the PBC (Figure 9C). This suggests that the PBC may be auto-inhibited by the same intramolecular folding that inhibits the DH.

2.6 Discussion

Our work uncovers the mechanism controlling Ect2's recruitment to the equatorial membrane during mitotic exit. We mapped the bipartite NLS to residues 804-818 in the PBC, and showed that this site is autoinhibited by the N-terminal BRCT domains. Our results support that the NLS in the PBC is required for Ect2 function during cytokinesis, likely by controlling its localization to the equatorial membrane. Importin-binding to the NLS is inhibited by mutations that mimic Cdk1 phosphorylation, while mutations that reduce importin-binding cause a reduction in the membrane-associated pool of Ect2, similar to a lipid-binding mutant. Thus, we propose a model (Figure 10) where in metaphase, Cdk1 phosphorylates Thr342 and Ser345 in the S-loop region leading the BRCTs to fold-over and inhibit the DH domain, and Thr815, which prevents membrane association and may weaken binding to importins. In anaphase, as Cdk1 activity decreases, Ect2 is de-phosphorylated, which relieves the BRCT-mediated inhibition of the DH domain and allows the PBC to interact with importins. The BRCTs then bind to phosphorylated Cyk4 for binding to centralspindlin. Binding to importins may maintain a conformation that facilitates Ect2's binding to phospholipids for RhoA activation. Future experiments will test

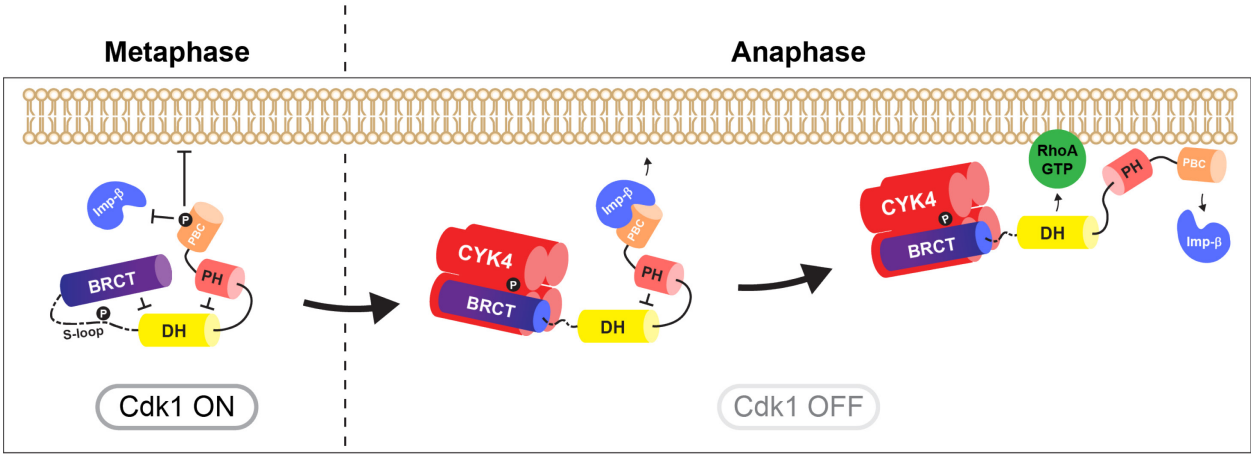

Figure 10. Model for importin-regulation of the PBC in cytokinesis.

During metaphase, Thr815 in the PBC domain is phosphorylated by Cdk1, preventing lipid-binding and importin-binding. In anaphase, Cdk1 levels decrease, and Ect2 is dephosphorylated. Importins are equatorially enriched where they bind to the importin-binding site in the PBC domain and facilitate Ect2's membrane recruitment. We speculate that importin-binding favors the hand-off of Ect2 to phospholipids, which have a higher affinity vs. importins.

whether lipid-binding is affected by the NLS mutations to determine if the observed phenotypes can be attributed partially to importins, or entirely to lipid-binding.

As with canoeing, the PBC appears to ‘steer’ from the back. We show that mutations in and around the NLS can significantly impact the membrane localization of Ect2 at the equatorial cortex. In this way, the PBC acts as a regulator of cortical recruitment to ‘fine-tune’ the localization of Ect2 during cytokinesis. However, the mechanism for this remains unclear. As described previously, we hypothesize that importin-binding induces a conformational change that alters the affinity of Ect2 for certain lipids. During cytokinesis, the cleavage furrow becomes enriched with $PI(4,5)P_2$ (Liu et al., 2012). Lipid overlay assays with purified Ect2 showed it can bind to $PI(4,5)P_2$ and $PI(3,4,5)P_3$, with no apparent preference (Su et al., 2011). Binding to importins could potentially alter Ect2’s affinity for $PI(4,5)P_2$ vs $PI(3,4,5)P_3$. When binding to importins is weakened, mutations in this region could shift affinity to other lipids or partners. For instance, the wider localization of $Ect2^{mut804\text{-}808}$ is reminiscent of the breadth of anillin or RhoA localization, and could potentially be due to a shift in affinity for RhoA or anillin when 804-808 are mutated. When binding to importins is more severely impaired as with $Ect2^{mut804\text{-}818}$, the narrower breadth could be caused by a loss in affinity for lipids, such that binding to partners would not be sufficient for cortical retention. On the other hand, since mutating residues 800-801 does not change nuclear localization on its own, the narrower breadth with $Ect2^{mut800\text{-}801}$ is likely driven by a loss of lipid-binding unrelated to importins.

While it was well-known that the BRCTs autoinhibit Ect2 function, the mechanism and extent of this inhibition was unclear. Here, we show that their inhibition likely extends to the PBC. The presence of the BRCTs could sterically hinder the PBC, or cause the positively-charged residues to be buried internally. The folding of the BRCTs and their distance to the PBC in the Ect2 structure is not experimentally known. Previously, a structure of Ect2 was resolved, but

lacked the BRCT0 and PBC regions (Chen et al., 2020). The intrinsically disordered nature of the PBC has so far precluded the resolution of a crystal structure of Ect2 that includes the PBC. Disordered regions can undergo folding transitions when bound to partners, and our pull-down experiments indicate that the PBC can be sufficiently ordered to bind to importins; alternatively, binding to importins may order the PBC. As with the S-loop, it is possible that phosphorylation of the PBC could play a role in regulating its folding, and thus mediate binding to partners like importins or lipids as mentioned previously.

Chapter 3

The nuclear localization of Ect2 is required for cytokinesis

3.1 Pre-amble

During mitosis, chromosomes are segregated to opposite poles and a contractile ring forms to divide the cell into two daughters. Cytokinesis, this physical separation, begins in anaphase when a contractile ring forms and pinches at the cell equator. After ingression, the daughter cells remain connected by an intercellular bridge for hours. At the same time, cells quickly re-form their nuclear envelope, kickstarting the nuclear import of proteins. The daughter cells become physically separated during abscission, when the intercellular bridge is cut. Here, we show that the nuclear sequestration of Ect2 after ingression is required for the stability of the intercellular bridge and abscission. We propose that this mechanism regulates other contractile proteins to promote abscission.

3.2 Abstract

Multiple pathways regulate cytokinesis, the physical separation of a cell into two daughters. The activation of RhoA by Ect2 is required, but it is unclear how RhoA activity is decreased after ingression for abscission. Here, we show that the nuclear re-sequestration of Ect2 is required for cytokinesis. A NLS mutant of Ect2 remains at the midbody and causes cytokinesis failure, and we show that this is due to increased RhoA activity in the intercellular bridge. We propose that this is due to increased F-actin, which destabilizes the bridge and inhibits abscission.

3.3 Introduction

During cytokinesis, an actomyosin ring pinches the membrane of a dividing cell, separating it into two daughters. Ring ingression is spatiotemporally coupled with chromosome segregation. This ensures that genetic material and cell fate determinants are equally allocated. However, aberrant cytokinesis can result in the uneven distribution of these factors, causing chromosomal instability and contributing to developmental diseases and cancer. Multiple pathways regulate the recruitment and localization of contractile ring proteins at the equatorial cortex during anaphase. Assembly of the contractile ring mainly depends on the small GTPase RhoA and its activation by the GEF Ect2. Ect2 activation is spatiotemporally coordinated by binding to RacGAP/Cyk4, part of the centralspindlin complex, during mitotic exit (Kamijo et al., 2006; Wolfe et al., 2009). Centralspindlin is also required for central spindle assembly, and this regulation of Ect2 by Cyk4-binding is proposed to ensure that Ect2 activates RhoA in the equatorial plane. Once active, RhoA binds to effectors for contractile ring assembly and positioning. After ingression, the ring transitions to a midbody ring, which surrounds the midbody at a bridge of microtubules that connects the two daughter cells. At this stage, contractile ring proteins are initially at the midbody, but are cleared by mechanisms that reduce F-actin and/or that shed RhoA-anillin-septin complexes (Echard, 2008). Ect2 is transiently localized to the midbody but then re-localizes to the reforming daughter nuclei, while RhoA is presumably inactivated, although the mechanisms for this are not well understood. The bridge is finally cut when the recruitment of the ESCRT-III machinery at the intercellular bridge triggers abscission, physically separating the two daughter cells. It is not clear what the cytokinesis machinery – such as RhoA and Ect2– can interfere with abscission complexes, and whether their removal is required for abscission.

Reducing active RhoA at the midbody may be critical to reduce contractile ring proteins for the later stages of cytokinesis. Excess RhoA could lead to the retention of regulators that polymerize F-actin, causing downstream effects that block abscission. A recent study showed that branched F-actin nucleated by Arp2/3 acts as a ‘plug’ to prevent the over-elongation of the ESCRT-III machinery in the intercellular bridge, which would prevent abscission by impairing the spastin-mediated severing of microtubules (Advedissian et al., 2024). The RhoA effector citron kinase also plays a role during the midbody ring transition by forming an inter-dependent complex with anillin (El Amine et al., 2013). However, as mentioned above, depending on the cell type, anillin may also be shed through its interaction with septins and RhoA (El Amine et al., 2013). Thus, anillin may be part of two independent complexes that are required for midbody maturation and shedding, through interactions with citron kinase or septins, respectively (Kechad et al., 2012; El Amine et al., 2013; Carim et al., 2020). However, the function of RhoA during late cytokinesis is not well-understood. Contractile proteins still play a role in secondary ingression, and mechanisms may be needed to ensure a careful balance of ring proteins for this event. A small pool of anillin may be required to anchor branched F-actin to the membrane at these secondary sites. RhoA may only be needed at this stage for anillin recruitment, and low levels of RhoA-mediated F-actin is possibly tolerated rather than required. Together, these findings suggest that a balance between contractile protein removal and retention at the midbody and/or bridge is essential for successful abscission. Depending on the cell type, one mechanism for inhibiting RhoA after ingression could be through the delivery of p190RhoGAP-containing vesicles to the intercellular bridge, while another non-mutually exclusive mechanism could be via the removal of Ect2.

Ect2 may also need to be removed from the midbody for the recruitment of proteins controlling midbody maturation and abscission. A previous study showed that as Ect2 leaves the

midbody, Cyk4 transitions to forming new complexes with Fip3, which could recruit recycling endosomes required for abscission (Simon et al., 2008). After ingression, the GTPase Rab11 and its effector Fip3 deliver vesicles to the intercellular bridge, and this is required to stabilize and narrow the intercellular bridge (Mierzwa and Gerlich, 2014). Ect2 may compete with Fip3 for Cyk4-binding, as overexpression of Ect2 N-term which binds to Cyk4 inhibits Fip3 recruitment to the midbody (Simon et al., 2008). However, the timing of Ect2's localization at the midbody is not clear as there have been no spatiotemporal studies with high resolution done in human cells to properly characterize endogenous Ect2 during the later stages of cytokinesis.

Whether Ect2 needs to be reduced at the midbody for a decrease in active RhoA or for new Cyk4-complexes, nuclear import could act as a removal mechanism. Nuclear import already plays a significant role in the spatiotemporal regulation of mitosis. Prior to mitosis, spindle assembly factors are localized in the nucleus, then released during prometaphase to form the mitotic spindle. In interphase, these factors are sequestered in the nucleus by importins, which bind to their nuclear localization signals (NLS). Since several essential cytokinesis regulators have NLSs and localize to the nucleus in interphase, nuclear sequestration is likely to play a regulatory role. Deletions that block the nuclear localization of Ect2 cause multinucleation, while the overexpression of a cytosolic N-terminal fragment causes a gain-of-function phenotype and induces malignant transformation in cultured cells (Tatsumoto et al., 1999; Saito et al., 2004; Chalamalasetty et al., 2006). However, these studies were either done before there were extensive tools available for live-cell imaging studies, and/or in the presence of endogenous Ect2, and it is not clear how mutating the NLS disrupts Ect2 function. Mislocalized Ect2 is also associated with poor prognosis in patients with colorectal or lung cancers, although the mechanism is unknown. Similarly, a NLS mutant of Mklp1/Kif23, which forms the centralspindlin complex with Cyk4, is unable to rescue the depletion of endogenous protein, leading to cell

multinucleation (Liu and Erikson, 2007). Although mutating the N-terminal NLS of anillin does not lead to cytokinesis failure in HeLa cells, cytosolic anillin causes abnormal cell shape changes (Chen et al., 2015). We hypothesize that the nuclear re-sequestration of contractile proteins after ring ingression may play a significant role in regulating the later stages of cytokinesis, as a mechanism to control midbody maturation and/or abscission.

Ect2 has a functional NLS that controls its nuclear import in interphase cells. Whether the pool of Ect2 in the newly formed daughter nuclei is the result of re-localized Ect2 from the midbody or from *de novo* translation is unknown. Ect2 has TEK and D-box domains that target the protein for degradation by the APC^{Cdh1} (Liot et al., 2011). Abolishing nuclear localization impairs Ect2 degradation, suggesting that Ect2 re-localizes from the midbody to the nucleus after ingression where it is targeted for degradation. Nuclear import could therefore act as a mechanism to remove Ect2 from the midbody and degrade it in the nucleus. Since there are no temporal studies of Ect2, it is not known how long Ect2 remains at the midbody for, and/or if any pools remain for the later stages of cytokinesis.

Here, we show that the removal of Ect2 from the midbody by nuclear import is required for cytokinesis. Mutating the NLS in the S-loop (domain between the N- and C-termini) causes Ect2 to remain at the midbody for much longer than wild-type Ect2 and leads to failed cytokinesis in Ect2-depleted cells. In these cells, the intercellular bridge is unstable and blebs, and ring closure is partially impaired as seen with endogenous anillin as a ring marker. Cytokinesis failure caused by the NLS mutant can be rescued by adding a SV40NLS sequence at the C-terminus. Overexpressing a mutant where both the NLS and the DH-domain (essential for RhoA activity) are mutated does not cause cytokinesis failure, suggesting that the phenotype is caused by excess RhoA activity. Using the active RhoA reporter 2xrGBD, we show that active RhoA persists for longer in cells expressing the Ect2 NLS mutant. Together, these results support a model where

nuclear import actively removes Ect2 after ingression to prevent excess RhoA activity and intercellular bridge instability.

3.4 Materials & Methods

3.4.1 Cell Culture and Transfection

HeLa cells were plated and grown in DMEM (Wisent), supplemented with 10% cosmic calf serum (Thermo Scientific) and were maintained at 37°C with 5% CO2. For transfection, cells were plated in DMEM media, and transfected using Lipofectamine 3000 according to the manufacturer's protocol (Invitrogen). Briefly, 2.5 of Lipofectamine was used per 2 ml of media with 2.5 µg DNA, 2.5 µL of P3000 and 2.5 nM siRNAs, as described previously (Yüce et al., 2005; Piekny and Glotzer, 2008), and re-suspended in Opti-MEM (Gibco). Cells transfected with plasmids encoding both fluorescent reporter and shRNA were imaged 24–48 h after transfection, whereas cells co-transfected with plasmid DNA and siRNAs were fixed 30 h after co-transfection of DNA and siRNAs. HeLa cells endogenously-tagged with mNeonGreen at the anillin, Ect2 or RhoA loci were previously generated (Husser et al., 2022).

3.4.2 Constructs / Plasmids

All plasmids were maintained and cloned in Escherichia coli DH5α unless specified otherwise. Primers used for cloning, mutagenesis, insertions and truncations are listed in Table 4 and 5, and siRNA and shRNA sequences are listed in Table 6. The myc:Ect2 constructs were previously generated (Yüce et al., 2005). mScarlet-I-Ect2 was generated by first cloning mScarlet-I, amplified from mScarlet-I-mTurquoise2 (Addgene #98839; Mastop et al., 2017), and Ect2,

amplified from myc:Ect2 (Yüce et al., 2005) into the pYTK001 backbone (Addgene #65108; Lee et al., 2015) by Golden Gate using a standard protocol, then assembled into a modified pX459V2.0-HypaCas9 vector (Addgene #108294; Kato-Inui et al., 2018) for mammalian expression. A shRNA sequence targeting endogenous Ect2, designed after the siRNA described in Yüce et al., 2005, was cloned into the modified pX459V2.0-HypaCas9 vector beforehand. mNG-2xrGBD was generated by amplifying 2xrGBD from dTomato-2xrGBD (Addgene #129625; Mahlandt et al., 2021) and mNeonGreen (Allele Biotech) by Golden Gate into pYTK001 then a modified pX459V2.0-HypaCas9 vector as previously described. Restriction enzymes for Golden Gate assembly were BbsI, BsmBI-v2 and BsaI-hfv2 (New England Biolabs). Substitutions (Ect2 347AAAAA351, Ect2 348AAA350, Ect2 565AAA568 + P570S), insertions (Ect2 348AAA350 + SV40NLS) and truncations (Ect2 328-388) were generated using a one-step PCR protocol using partially overlapping primers (Liu and Naismith, 2008). GST:importin-β was previously generated (Beaudet et al., 2020). All constructs were verified by sequencing (Genome Quebec, Plasmidsaurus, and FlowGenomics).

Table 4. List of cloning primers

Primers used to clone 2xrGBD, Ect2, mNeonGreen and mScarlet-I into the pYTK001 backbone. Primers are labeled as forward (fwd) or reverse (rev). Sequences are listed in the 5'-3' orientation.

Cloning Primer	Sequence
2xrGBD - fwd	GCATCGTCTCATCGGTCTCAGTCTATCCCCCTCGAGTCCATCC
2xrGBD - rev	ATGCCGTCTCAGGTCTCACTCATTATCTAGAGCCTGTCTTCTCCAGCA
Ect2 - fwd	GCATCGTCTCATCGGTCTCAGTCTATGGCTGAAAATAGTGTATTAACATCCACTAC
Ect2 - rev	GTCATACGTTAAGTAGATCTACAACTCATTTGATATGAGTGAGACCTGAGACGGCAT
mNeonGreen N-terminus - fwd	GCATCGTCTCATCGGTCTCACCATGGTGAGCAAGGGCGAG
mNeonGreen N-terminus - rev	GGCATGGACGAGCTGTACAAGGGGGGTTCAGGAGGGTCTTGAGACCTGAGACGGCAT
mScarlet-I N-terminus - fwd	GCATCGTCTCATCGGTCTCACCATGGTGAGCAAGGGCGAG
mScarlet-I N-terminus - rev	GGCATGGACGAGCTGTACAAGGGGGGTTCAGGAGGGTCTTGAGACCTGAGACGGCAT

Table 5. List of primers for substitutions, insertions and truncations
Primers used for substitution mutations, insertions and truncations. Primers are labeled as forward (fwd) or reverse (rev). Sequences are listed in the 5'-3' orientation.

Ect2 mutation, insertion and truncation	Sequence
328-388 - fwd	GCATCGTCTCATCGGTCTCAGTCTACTCCTGAGCTCAAGAAATCAGTG
328-388 - rev	ATGCCGTCTCAGGTCTCACTCAGATATCTAGGAGTGACCCTATGGAAAG
347AAAAA351 - fwd	ACCCCTAACAGCAATGCCGCTGCAGCTGCTTTAAAAGAAACACTTGC
347AAAAA351 - rev	GCAAGTGTTTCTTTTAAAGCAGCTGCAGCGGCATTGCTGTTAGGGGT
348AAA350 - fwd	AATAGAGCAGCAGCTAGATTAAAAGAAACACTTGCTCAGCTTTCAAGAGAG
348AAA350 - rev	TTTTAATCTAGCTGCTGCTCTATTGCTGTTAGGGGTATTTAGAGAAAGCATTGAC
348AAA350 + SV40NLS - fwd	GGATCTGGAGGATCTGGATGAGTGAGACCAGACCAATAAAAAACGC
348AAA350 + SV40NLS - rev	TCCAGATCCTCCAGATCCGACTTTTCGTTTCTTCTTTGGTATCAAATGAGTTGTAGATC
565AAAA568 - fwd	GAGCAGCAGCAGCATTACCCAGTGTTGCATTACTTTTAAATGATCTTAAGAAGCATAC
565AAAA568 - rev	TAATGCTGCTGCTGCTCGGATAAGAAGTTCAACAAGGCTCTGCC
565AAAA568 + P570S - fwd	GCATTATCCAGTGTTGCATTACTTTTAAATGATCTTAAGAAGCATACAGCTG
565AAAA568 + P570S - rev	CAACACTGGATAATGCTGCTGCTGCTCG

Table 6. List of siRNA and shRNA sequences
Sequence of siRNAs and of primers used to clone shRNA sequence into expression vectors. Primers are labeled as forward (fwd) or reverse (rev). Sequences are listed in the 5'-3' orientation.

siRNA	Sequence
siEct2	GGCGGAAUGAACAGGAUUU
shRNA	**Sequence**
shECT2 - fwd	CACCGAAGGCGGAATGAACAGGATTTATCAAGAGAAAATCCTGTTCATTCCGCCTT
shECT2 - rev	GAAGGCGGAATGAACAGGATTTATCAAGAGAAAATCCTGTTCATTCCGCCTTTTTT

3.4.3 Cell fixation and Immunostaining

For fixed-cell imaging, HeLa cells were seeded to 50% confluency on 22x22mm glass coverslips etched using 0.1 M HCl. 30 hours after co-transfection of DNA and siRNAs, the cells were fixed using fresh, ice-cold 10% w/v trichloroacetic acid for 14 minutes before being washed three times with PBST (1 X PBS with 0.5% Triton X-100) as previously described (Yüce et al., 2005). Cells transfected with Myc::Ect2 constructs were immunostained for Myc using primary anti-Myc monoclonal antibodies (1:250; DSHB) and anti-mouse Alexa-568 (Invitrogen; 1:500), anillin using primary anti-anillin rabbit polyclonal antibodies (1:250; Piekny and Glotzer, 2008) and secondary anti-rabbit Alexa-488 antibodies Invitrogen; 1:400), and DAPI for DNA visualization (1/1000 dilution from 1mg/mL stock; Sigma). Cells were blocked the following day with normal

donkey serum (NDS; 5% in PBST) for 20 minutes before being incubated with the primary and secondary antibodies for 2 hours each, washing with PBST between antibodies, and incubating with DAPI for 5 minutes. Coverslips were mounted onto glass slides with mounting media (4% n-propyl gallate in 50% glycerol diluted in 50 mM Tris pH 9 and water) and sealed with nail polish to prevent drying.

3.4.4 Microscopy

Fixed cells transfected with Myc::Ect2 and co-stained for anillin and DNA (DAPI) were imaged using a Leica DMI6000B wide-field microscope with the 63×/1.4 PL APO oil immersion objective (pixel size 0.102 μm), and Z-stacks of 0.3 μm were acquired with a Hamamatsu OrcaR2 camera and Volocity software (PerkinElmer) using a piezo Z stage (MadCityLabs). Image files were exported as TIFFs, which were opened with Fiji (National Institutes of Health; NIH) and converted into maximum intensity Z-stack projections. Projections and merged color images were then converted into 8-bit images and imported into Illustrator (Adobe) to make figures. To perform live imaging, cells were plated and transfected on 25-mm round coverslips (no. 1.5) or 22x22-mm square coverslips (no 1.5) and incubated with Hoechst 34580 (Invitrogen) at 1.3 μM or SYTO Deep Red (Invitrogen) at 50 nM for 30 min and placed in a Chamlide magnetic chamber (Quorum). Cells were kept at 37°C with 5% CO2. Live imaging was performed on an inverted Nikon Eclipse Ti microscope with a Livescan Swept Field confocal unit (Nikon), using the 100×/1.45 CFI PLAN APO VC oil immersion objective (Nikon), a piezo Z stage (MadCity Labs), and with the Evolve EMCCD camera (Photometrics). Images were acquired with 400 ms exposures using the 405-nm, 561-nm and 640-nm lasers (100 mW; Agilent) set between 3 and 15% power, depending on the intensity of fluorescent signals (settings were kept constant for related experiments), and

multiple Z-stacks of 1.0 µm were taken every 120 s per cell using NIS-Elements acquisition software (Nikon), and a quad filter (430-485 + 520-550 + 590-630 +680-740; Chroma) or far-red filter. Cells were also imaged on an inverted Zeiss Axio Observer with a Cicero spinning disk (CrestOptics), using a 63×/1.4 PLAN APO DIC M27 oil immersion objective (Zeiss; pixel size 0.26 µm), with a piezo Z stage (MadCityLabs), and with the Orca Flash4.0 LT camera (Hamamatsu). Images were acquired with X ms exposures using the 555-nm and 637-nm powered by a LDi-5 laser launch (89North) set between 15-20% power. Multiple Z-stacks of 1.0 µm were taken every 120 s per cell for 60 min then every 10 min per cell for 3 hours, using Volocity (Quorum). Cells were also imaged on an inverted Nikon Eclipse Ti2 microscope with a CSU-X1 spinning disk (Yokogawa), using the 60×/1.4 CFI PLAN APO VC oil immersion objective (Nikon), with a piezo Z stage (MadCityLabs), and with the Zyla camera (Andor). Images acquired with 300 ms exposures using the 561-nm and 638-nm lasers (OMICs) set at 3% power, and multiple Z-stacks of 1.0 µm were taken every 120 s per cell, or 120 s per cell for 60 min then every 10 min for 3 hours using µManager (NIH). Image files were exported as TIFFs, which were opened with Fiji (NIH) and converted into maximum intensity Z-stack projec tions. Projections and merged color images were then converted into 8-bit images and imported into Illustrator (Adobe) to make figures.

3.4.5 Pull-down assays

The purified proteins GST and GST:importin-β1 were made from Escherichia coli BL21 cells. Bacteria were resuspended in lysis buffer (2.5 mM MgCl2, 50 mM Tris, 150 mM NaCl, pH 7.5, 0.5% Triton X-100, 1 mM dithiothreitol [DTT], 1 mM phenylmethanesulfonyl fluoride [PMSF], and 1× protease inhibitors [Roche]), incubated with 1 mg/ml lysozyme on ice for 30 min, then

sonicated three times. Extracts were incubated with preequilibrated glutathione sepharose 4B (GE Lifesciences) overnight at 4°C with rotation. After washing, beads were stored as a 50% slurry at 4°C. Protein concentration was determined by running samples by SDS–PAGE and measuring the density of bands in comparison to known concentrations of bovine serum albumin. To test for binding, proteins were pulled down from cell lysates after transfection. Transfected HeLa cells were lysed in 50 mM Tris, pH 7.6, 150 mM NaCl, 5 mM MgCl2, 0.5% Triton X-100, 1 mM DTT, 1 mM PMSF with 1× protease inhibitors (Roche), and incubated with 5–10 µg of purified GST-tagged importin-β protein on beads at 4°C overnight. After binding, beads were washed three to four times with 50 mM Tris, pH 7.6, 150 mM NaCl, 5 mM MgCl2 before adding SDS sample buffer to denature the proteins for SDS PAGE. All samples were run by SDS–PAGE and wet-transferred to nitrocellulose membrane for Western blotting. All blots were reversibly stained with Ponceau S to show total protein. The blots were blocked with 5% milk for 20 min, then incubated with 1:10,000 mouse anti-mNeonGreen antibodies (ChromoTek) in 1× TBS-T (0.150 M NaCl, 0.1 M Tris pH 7.4, 0.5% Triton X-100) for 1–2 h at room temperature. After washing the membrane three to four times with 1× TBS-T, secondary antibodies (anti-rabbit HRP [horseradish peroxidase]; New England Biolabs) were added as per manufacturer's instructions in 1× TBS-T for 2 h. The blots were developed using enhanced chemiluminescence (ECL) Western blotting detection reagents (Cytiva) and visualized on a GE Amersham Imager 600 or ChemiDoc XRS+ (Bio-Rad). All results from each pull-down assay were replicated in at least three distinct experiments to ensure reproducibility. Images were converted to 8 bit by Fiji, and made into figures using Illustrator (Adobe).

3.4.6 Analysis

All images acquired using NIS Elements (Nikon) were opened in Fiji (Version 2.3, NIH) or IMARIS (Oxford Instruments) for analysis. Linescans were performed and measured using a macro in Fiji modified from Ozugergin et al., 2022. The macro was designed to isolate the desired channel from the image file, subtract background signal, and perform a bleach correction. The desired timepoint and three central Z slices were picked manually, and the macro generated a Z-stack sum-slice projection. A five-pixel-wide line was then traced along the cortex of the cell, from one pole to the other, along with a straight one- pixel- wide line to define the midplane. The macro then measured the fluorescence intensity of each pixel along the length of the linescan and positioned the pixels in relation to the midplane. For breadth measurements, the number of pixels above 50% of the normalized peak intensities were counted for each linescan and converted to microns. Pixels with intensities higher than the cutoff value outside of the peak region were excluded from these calculations. To measure the ratio of cortical accumulation versus pole, the area under the curve of the fluorescence intensity delineated by the breadth was divided by the area under the curve of the same for the average of the first and last 10% pixels of the linescan. Kymographs were performed and measured using a macro in Fiji. The macro was designed to isolate the desired channel, and a five-pixel-wide line was drawn manually over the furrow region at every timepoint until closure. Then, the distance between the two sides of the membrane was measured at each timepoint using the straight-line tool, and measurements were exported to Excel (Microsoft). The distance between the two sides at anaphase onset was set to a maximum value (100%) and used to normalize the distance throughout ingression. As the closure times were variable among cells, measurements were terminated when at least three cells had completed cytokinesis. For measurement of fluorescence intensity over time, images were analyzed using Imaris. The signal at the intercellular bridge or midbody was modeled as a spot

or surface and tracked over time and its sum of fluorescence intensity over time was determined. For the ratio of sum-intensity at closure and before closure, the sum intensity of fluorescence intensity at closure was divided by the same at the timepoint before closure. All data were imported into Excel (Microsoft) for formatting, then to Prism (Version 9.3, GraphPad) for further analysis. All of the images and graphs were transferred to Illustrator (Adobe) to make figures.

3.4.7 Statistical analysis

Line graphs, bar graphs and box-and-whisker plots were generated using Prism (Version 9.3, GraphPad). Data were tested for normality, and statistical significance was tested using Student's t-test or a one-way ANOVA followed by multiple comparisons using Tukey's post-hoc test if the data were normally distributed, or using a non-parametric test if the data were not normally distributed. Significance levels were defined as: $p>0.05$ non- significant (ns), $*p\leq0.05$; $**p\leq0.01$.

3.5 Results

3.5.1 Ect2 is sequestered to the daughter cell nuclei via transport from the midbody after ring ingression

Ect2 localization changes throughout the cell cycle. In interphase cells, Ect2 is in the nucleus, then becomes cytosolic after nuclear envelope breakdown. During mitotic exit, Ect2 is enriched at the central spindle and overlying equatorial cortex where it controls assembly of the contractile ring for cytokinesis, and subsequently Ect2 localizes to the midbody. Ect2 decreases at the midbody and re-appears in the daughter cell nuclei, but it is not clear if this change in Ect2 is required for the later stages of cytokinesis. Further, the timing of this change in Ect2 was not known as previous studies relied on antibodies in fixed cells, or using over-expression. We previously endogenously tagged Ect2 with mNeonGreen in HeLa cells (Husser et al., 2022). Using these cells, we imaged Ect2 with high spatiotemporal resolution throughout cytokinesis, including abscission (Figure 11B). We quantified the reduction in Ect2 at the midbody over time and saw a steady decrease in signal that was no longer visible by 100 minutes post-ingression, which corresponded with an increase in nuclear Ect2 (Figure 11C). This suggests that Ect2 is indeed re-sequestered in the nucleus. Future experiments can confirm this by using fluorescence recovery after photobleaching and comparing the nuclear signal increase over time in cells where the midbody pool was bleached vs. not bleached.

3.5.2 Ect2's nuclear localization is required for cytokinesis

Previous studies showed that the centrally-located NLS is required for nuclear localization and over-expression of the N-terminal half of Ect2 caused cytokinesis failure (Figure 12A, Chalamalasetty et al., 2006). However, it was not known if Ect2's nuclear localization is required

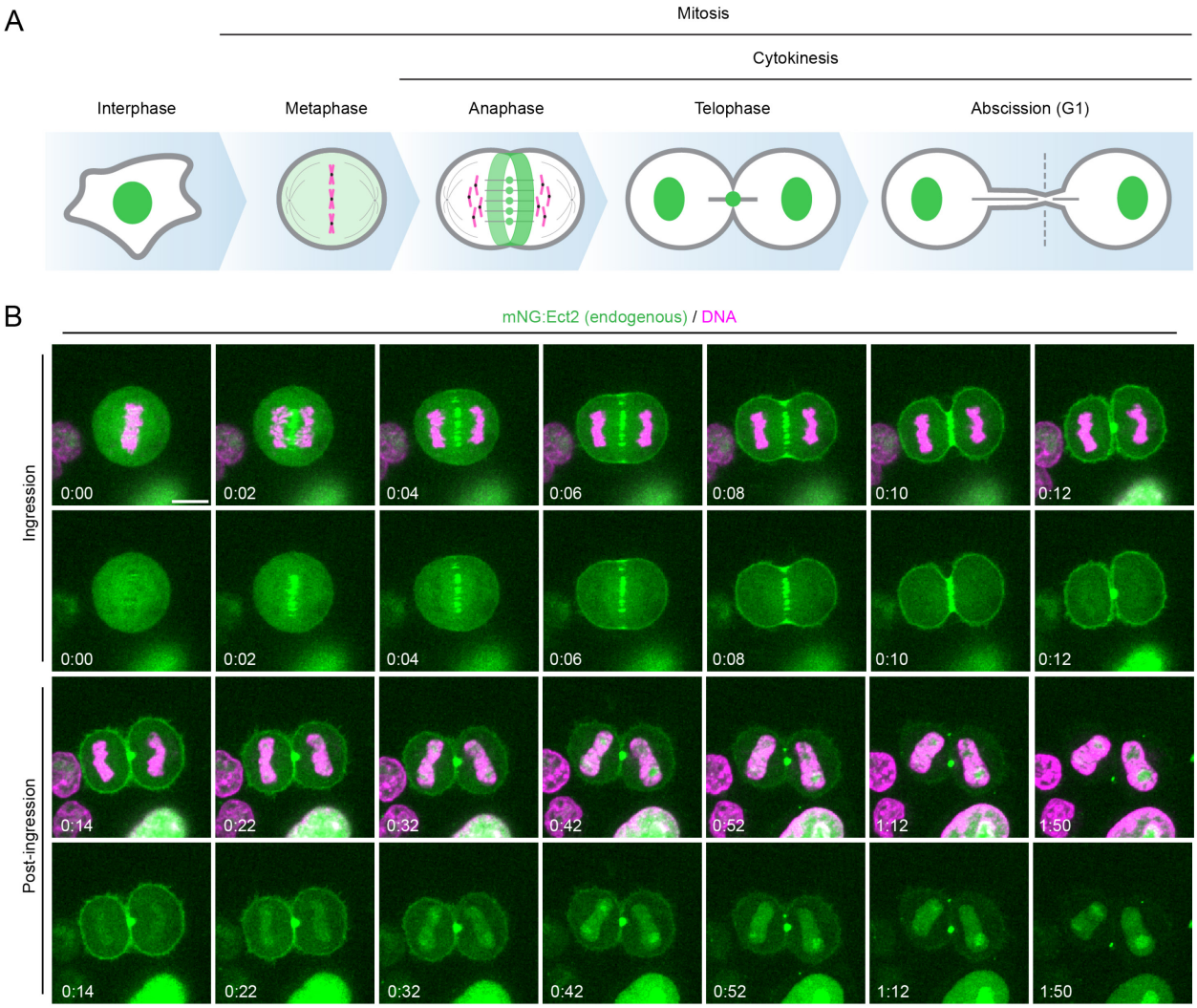
A
Mitosis
Cytokinesis
Interphase
Metaphase
Anaphase
Telophase
Abscission (G1)
B
mNG:Ect2 (endogenous) / DNA
Ingression
Post-ingression
0:00
0:02
0:04
0:06
0:08
0:10
0:12
0:14
0:22
0:32
0:42
0:52
1:12
1:50
C
Midbody signal
mNG:Ect2 (endogenous)
Ring closure (t = 0)
Nuclear signal
Midbody signal = sum intensity at midbody over time
Nuclear signal = averaged sum intensity of both nuclei over time
Midbody
Nuclei
Normalized intensity (%)
100
50
0
0
50
100
Time (min)

Figure 11. Ect2 decreases at the midbody with concomitant increase in the daughter cell nuclei.

(A) Cartoon cells show Ect2 localization (green; chromosomes are in pink) in the nucleus in interphase, and throughout mitosis where it transitions from being cytosolic, to the central spindle and ring, then to the midbody and nuclei of the daughter cells. (B) Timelapse images show a HeLa cell expressing endogenous mNeonGreen (mNG):Ect2 (green) co-stained for DNA (magenta, SYTO Deep Red). Images taken after ring closure are labeled as “post-ingression”. The scale bar is 10 μm. Time is in hours:minutes (t = 0 minutes refers to anaphase onset, and ring closure is at 12 minutes). (C) The schematic on the left shows how the midbody (green) and nuclear pools (magenta) of Ect2 were quantified by measuring the sum total fluorescence intensity over time after ring closure (note that the time t = 0 now refers to ring closure). On the right, a line graph shows a plot of the normalized fluorescence intensity (y-axis, %) of the midbody (green) and nuclear pool (magenta) over time (x-axis, minutes; n = 14 cells). The error bars show standard error of the mean (SEM).

for cytokinesis. To investigate the role of the NLS during cytokinesis, we mutated the NLS of Ect2 by substituting 348KRR350 to alanine residues (348KRR-AAA350; Ect2^{3A}; Figure 12A). HeLa cells rescued with RNAi-resistant Myc-tagged Ect2 or Ect2^{3A} and co-depleted for endogenous Ect2 via siRNAs revealed that mutating the NLS caused Ect2 to remain cytosolic in interphase cells (Figure 12B). To determine if the 3A mutant alters binding to importins, we performed a pull-down assay using recombinant Glutathione S-transferase (GST)-tagged importin-β1 (GST:importin-β1) and mNeonGreen:Ect2 (328-388) from HeLa cell lysates. Comparing the control to the 3A mutant revealed a decrease in binding (Figure 12C-D). This data shows that the 3A mutant sufficiently reduces nuclear localization and importin-binding. Next, we used this mutant to determine if the NLS is required for cytokinesis. To do this, we then performed rescue assays by expressing Myc-tagged RNAi-resistant Ect2 or Ect2^{3A} in cells co-depleted of endogenous Ect2 using siRNAs (Figure 12E). Since Ect2 depletion causes cells to fail during cytokinesis causing cells to become binucleate, we used the number of binucleate cells as an indicator of cytokinesis failure. While Ect2 RNAi caused 63.5% of binucleate cells, 17.7% of cells rescued with RNAi-resistant Ect2 were binucleate, and 49.2% of cells rescued with RNAi-resistant Ect2^{3A} were binucleate (Figure 12F). These findings support that a functional NLS is required for cytokinesis. Notably, we observed similar results when performing rescue assays with a mutant where residues 347RKRRR351 were substituted to alanine residues (Ect2^{5A}; Figure S3).

As previously reported, the over-expression of Ect2 can cause cytokinesis phenotypes. Indeed, over-expressing Ect2 caused 10.5% of cells to become binucleate (Figure 12F). Interestingly, over-expressing Ect2^{3A} caused a significant increase in the proportion of binucleate cells (37.1%) compared to Ect2, suggesting that the NLS mutant is dominant-negative. This data suggests that the levels of Ect2 in the cell are critical for its function in cytokinesis.

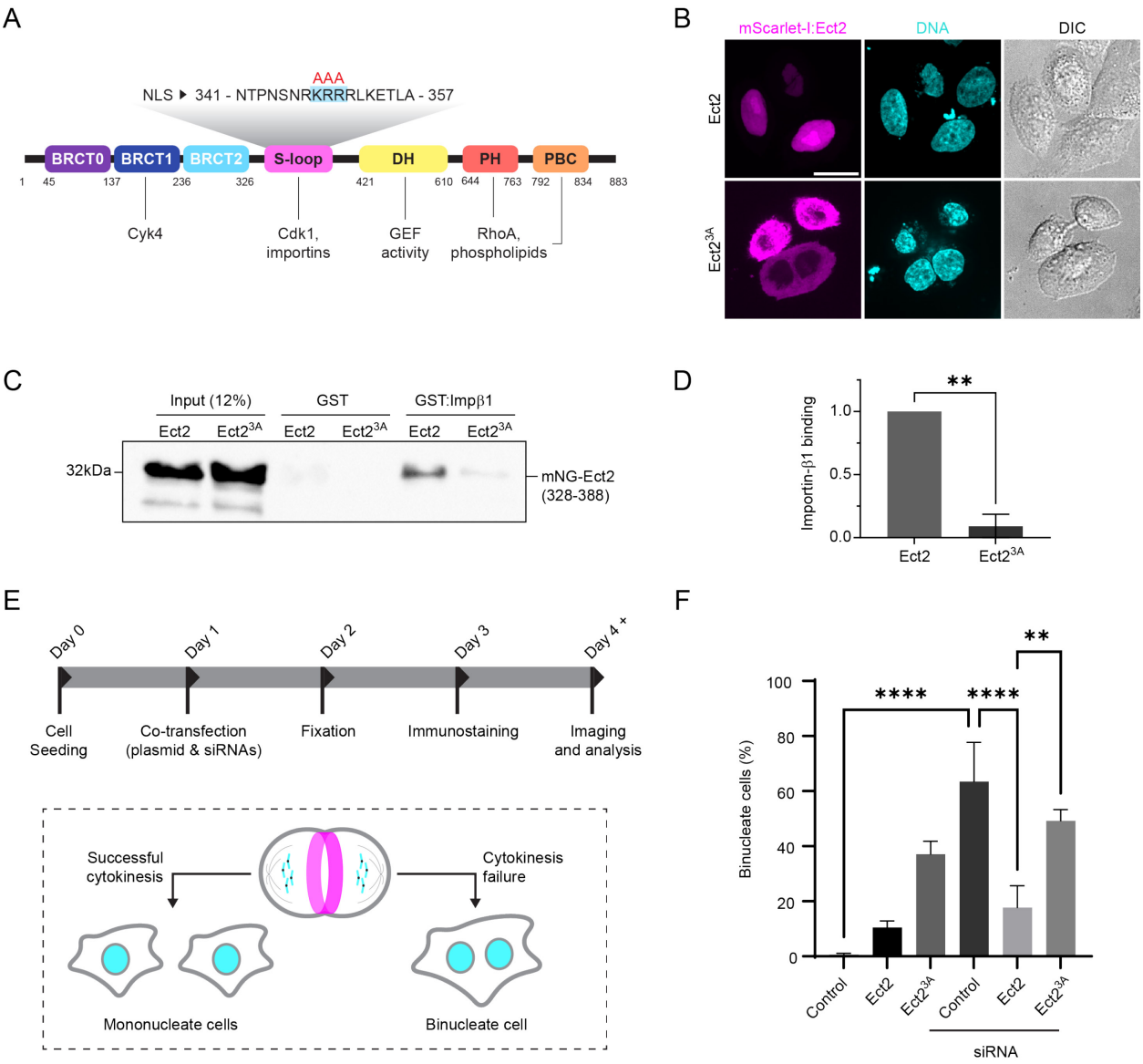

Figure 12. The NLS of Ect2 is required for cytokinesis.

(A) A cartoon structure of Ect2 is shown with binding domains as indicated. The BRCT domains bind to Cyk4/MgcRacGAP. The S-loop contains a Cdk1 phosphorylation site, and an NLS (sequence shown above with the mutations using in this study in red) that binds to importins and controls nuclear localization. The Dbl-Homology (DH) has GEF activity for RhoA, while the Pleckstrin Homology (PH) and PolyBasic Cluster (PBC) regions bind to phospholipids. (B) Images show HeLa cells expressing mScarlet-I:Ect2 (magenta; Ect2 or Ect2^{3A}), co-stained for DNA (cyan, Hoechst) and imaged with DIC (grayscale). The scale bar is 10 μm. (C) A western blot shows the binding of mNeonGreen (mNG)-tagged Ect2 (328-388; Ect2 or Ect2^{3A}) from HeLa cell lysates to purified recombinant GST:importin-β1 (GST:Impβ1). (D) A bar graph shows the mean densitometry measurements, normalized to input and to the control (Ect2, WT). Error bars show standard deviation (N = 3). Statistical analysis was done using Student's T-test (**, p<0.01). (E)

A timeline shows the experimental design for the rescue assay and a cartoon shows the consequences of successful cytokinesis or failure. (F) A bar graph shows the proportion of binucleate cells as a measure of failed cytokinesis (y-axis, %) in HeLa cells expressing RNAi-resistant myc:Ect2 (Ect2 or Ect2^{3A}) +/- Ect2 siRNA. Error bars show standard deviation (N = 3, with n = 26-249 cells per replicate). Statistical analyses were done using ANOVA and Tukey post-hoc test (ns, not significant; ***, $p<0.0002$; ****, $p<0.0001$).

3.5.3 The nuclear localization of Ect2 is required for cytokinesis post-ingression

To determine the cytokinesis phenotypes caused by the Ect2^{3A} mutant, we performed live-cell imaging. HeLa cells expressing RNAi-resistant mScarlet-I-tagged Ect2 co-depleted of endogenous Ect2 were imaged throughout cytokinesis (Figure 13A). During mitotic exit, Ect2 localized to the spindle midzone and equatorial cortex, then to the midbody and subsequently to the daughter nuclei after ingression as described previously (Figure 13A). Ect2^{3A} also localized to the spindle midzone and equatorial cortex, and subsequently to the midbody. However, the mutant remained at the midbody for much longer than control, and in a significant proportion of these cells, the ring/membrane regressed and became binucleate (Figure 13B). We quantified Ect2 at the midbody after ring ingression (Figure 13C). While Ect2^{WT} could not be detected 70 min after ring ingression, Ect2^{3A} could be detected for a longer period of time (Figure 13C). The proportion of cells that failed cytokinesis with Ect2^{3A} was similar to the population studies using fixed cells and myc-tagged Ect2^{3A} (Figures 12F and 13B). These results suggest that cytokinesis failure could arise because Ect2 remains at the midbody after ingression, rather than being sequestered to the daughter cell nuclei. To test this, we fused the SV40NLS to the C-terminus of Ect2^{3A} (Ect2$^{3A\text{-}SV40NLS}$) and expressed the mScarlet-tagged RNAi resistant mutant in cells co-depleted for endogenous Ect2. As shown in Figure 13A, adding the SV40NLS restored nuclear localization and Ect2$^{3A\text{-}SV40NLS}$ was reduced at the midbody compared to Ect2^{3A} and similar to Ect2 (Figure 13C). Interestingly, Ect2$^{3A\text{-}SV40NLS}$ can be observed at the daughter nuclei earlier than Ect2, indicating that the rate of nuclear import could vary with the NLS motif or their position in the protein. Notably, the proportion of Ect2$^{3A\text{-}SV40NLS}$ cells that failed cytokinesis was lower compared to Ect2^{3A} and similar to Ect2, showing that re-localizing Ect2^{3A} to the nuclei is sufficient to rescue cytokinesis failure (Figure 13B).

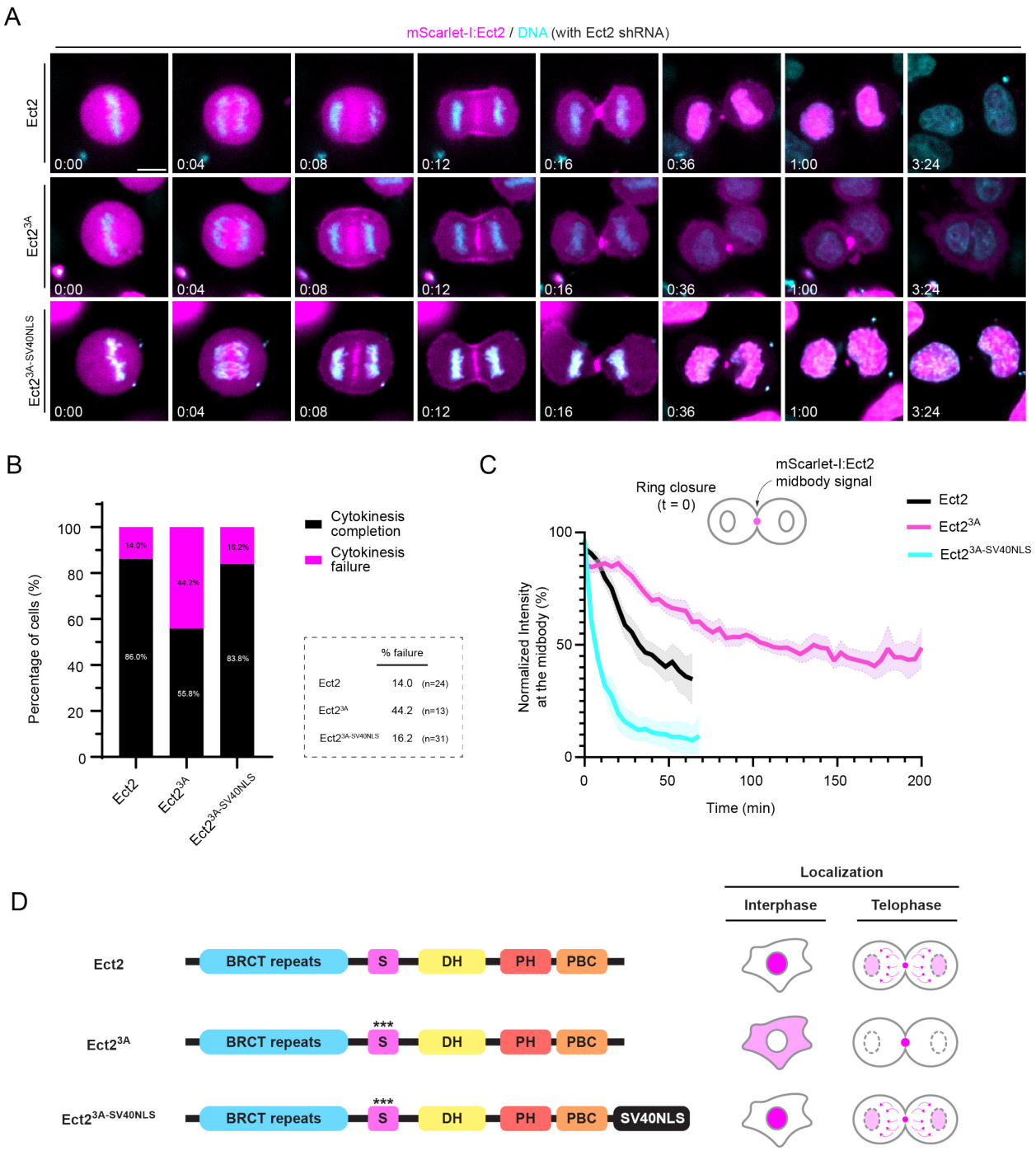

Figure 13. The nuclear localization of Ect2 is required to reduce its levels at the midbody.

(A) Timelapse images show HeLa cells expressing RNAi-resistant mScarlet-I-Ect2 (magenta; Ect2, Ect2^{3A}, Ect2$^{3A\text{-}SV40NLS}$) depleted of endogenous Ect2 using shRNA, co-stained for DNA (cyan, SYTO Deep Red). The scale bar is 10 μm. Time is in hours:minutes (t = 0 is anaphase

onset). (B) A bar graph indicates the proportion of cells that succeed (black) and fail (pink) cytokinesis for cells as shown in (A; Ect2 14% failure, n = 24; Ect2^{3A} 44.2% failure, n = 13; Ect2$^{3A\text{-}SV40NLS}$ 16.2% failure, n = 31). (C) A line graph shows the changes in normalized fluorescence intensity (y-axis, %) at the midbody over time (x-axis, minutes in cells as shown in A (Ect2, black, n = 10; Ect2^{3A}, pink, n = 15; Ect2$^{3A\text{-}SV40NLS}$, blue, n = 11). The cartoon above shows how the midbody intensity was quantified. The error bars indicate standard error of the mean (SEM). (D) Ect2 structures with the NLS mutations (***) and SV40NLS (black) in A-C are shown (left) along with their localization in cartoon cells in interphase and telophase (right).

To determine whether the nuclear localization of Ect2 is required in a non-cancer human cell type, we also analyzed phenotypes caused by the over-expression of Ect2 vs. Ect2^{3A} mutant in HEK293T cells (Figure 14A). We performed live-cell imaging of HEK293T cells expressing mScarlet-I:Ect2 or Ect2^{3A} throughout cytokinesis. As in HeLa cells, Ect2 localized to the central spindle and equatorial cortex, albeit with more variability, which could be due to over-expression. The localization of Ect2^{3A} at the midbody was retained in HEK293T cells, and there was a significant increase in the proportion of cells that failed cytokinesis (76.9% for Ect2^{3A} vs. none for Ect2; Figure 14B). These results show that the nuclear localization of Ect2 is required in other, non-cancer cell types.

3.5.4 The nuclear localization of Ect2 is required for midbody formation

Our data supports that preventing Ect2's nuclear localization after ingression causes cytokinesis failure. To determine how persistent Ect2^{3A} at the midbody causes cytokinesis failure, we characterized the different stages of cytokinesis compared to control cells. For example, earlier problems with ring assembly or ingression could impact midbody formation. We performed live-cell imaging of mScarlet-I-tagged RNAi-resistant Ect2 or Ect2^{3A} in HeLa cells where Ect2 was co-depleted and anillin was endogenously tagged with mNeonGreen to visualize the contractile ring (Figure S4). As shown in the images in Supplemental Figure S4, there was no obvious difference in the localization of anillin or Ect2^{3A} in the ring compared to control cells. We quantified this by measuring the breadth of anillin and Ect2 (control or 3A) as the cells begin to ingress. The fluorescence intensity was measured along the cortex, then the breadth was measured as the number of the pixels > 50% of maximum fluorescence intensity, which was normalized by calculating the ratio vs. the length (total number of pixels; Figure S5). There was no significant

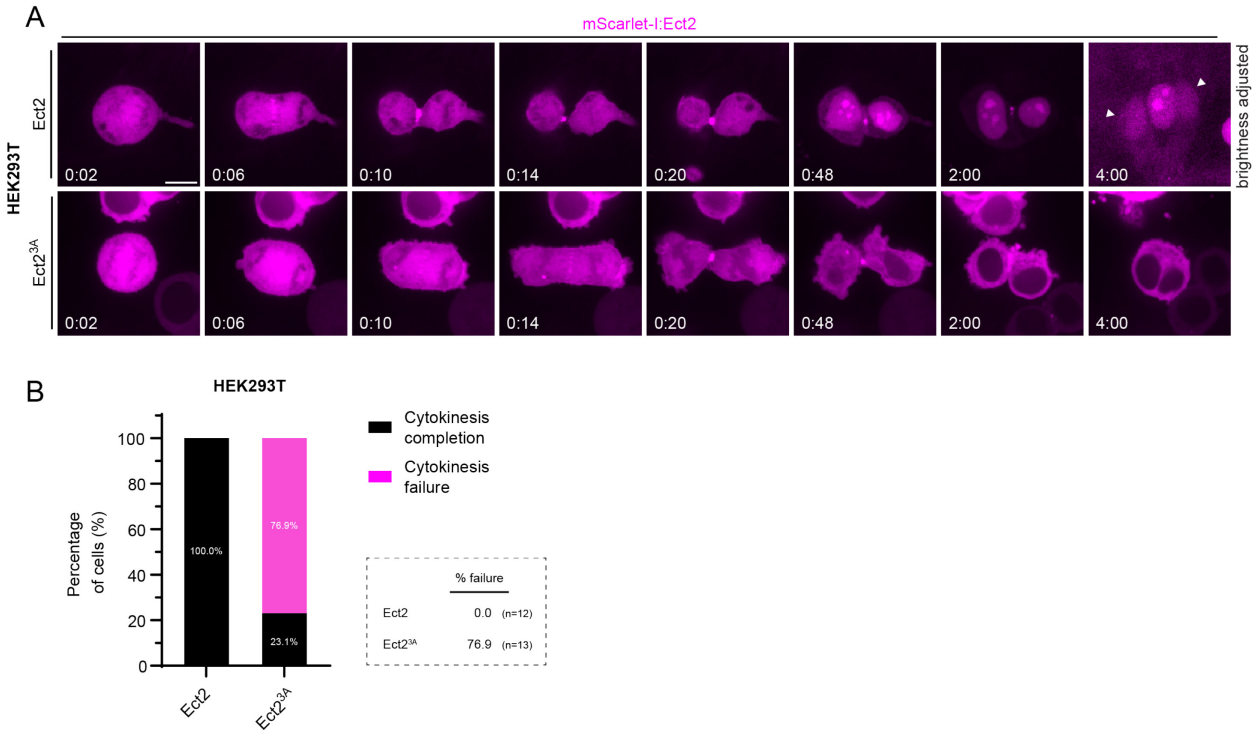

Figure 14. The NLS of Ect2 is required for cytokinesis in HEK293T cells.

(A) Timelapse images show HEK293T cells expressing mScarlet-I-Ect2 or Ect2^{3A} (magenta). The scale bar is 10 μm. Time is in hours:minutes (t = 0 is anaphase onset). The contrast was adjusted for the last panel (t = 4:00) of Ect2 due to low signal. White arrows point to the two nuclei of the original dividing cell. (B) A bar graph shows proportion of cells that succeed (black) or fail (pink) cytokinesis for cells treated as in A (Ect2 0% failure, n = 12; Ect2^{3A} 76.9% failure, n = 13).

difference for anillin or Ect2 in cells expressing control or the 3A mutant (Figure S5). This suggests that the NLS does not play a role in restricting the localization of Ect2 at the cleavage furrow. Then, to determine whether the duration of ingression was affected by the NLS mutation, we plotted kymographs of the division plane in cells expressing wild-type or mutant Ect2. We found that the duration of ingression in cells expressing Ect2^{3A} was slightly longer than control; the ring was almost entirely closed around 10-12 min after anaphase onset with control, whereas ring closure with Ect2^{3A} was closer to 14-16 min (Figure S6). Thus, there could be a minor delay in ring assembly or ingression. While anillin localization appeared similar to control cells during ring assembly and ingression, we observed a difference after ring closure during the ring-to-midbody transition (Figure S4). To quantify this, we measured changes in the ratio of anillin fluorescence intensity at closure (when a change in ring diameter cannot be detected) compared to the timepoint just before closure, which could indicate perturbations in the ring-to-midbody transition. Compared to control, cells expressing Ect2^{3A} show a greater range and variability in this ratio, suggesting that midbody formation is impaired in the mutant.

3.5.5 Nuclear Ect2 is required to decrease active RhoA for midbody formation

Our data supports that Ect2 nuclear localization is required to form a midbody after ring closure. To determine why persistent Ect2 could cause midbody phenotypes, we further characterized the intercellular bridge. We observed that the intercellular bridges of cells rescued with Ect2^{3A} appeared to be highly dynamic, with increased volume and blebbing compared to Ect2 (Figure S4). We hypothesized that persistent Ect2^{3A} at the midbody could sustain RhoA activity, leading to increased contractility, potentially making the intercellular bridge unstable. To investigate whether sustained RhoA activity causes cytokinesis failure when Ect2 remains at the midbody,

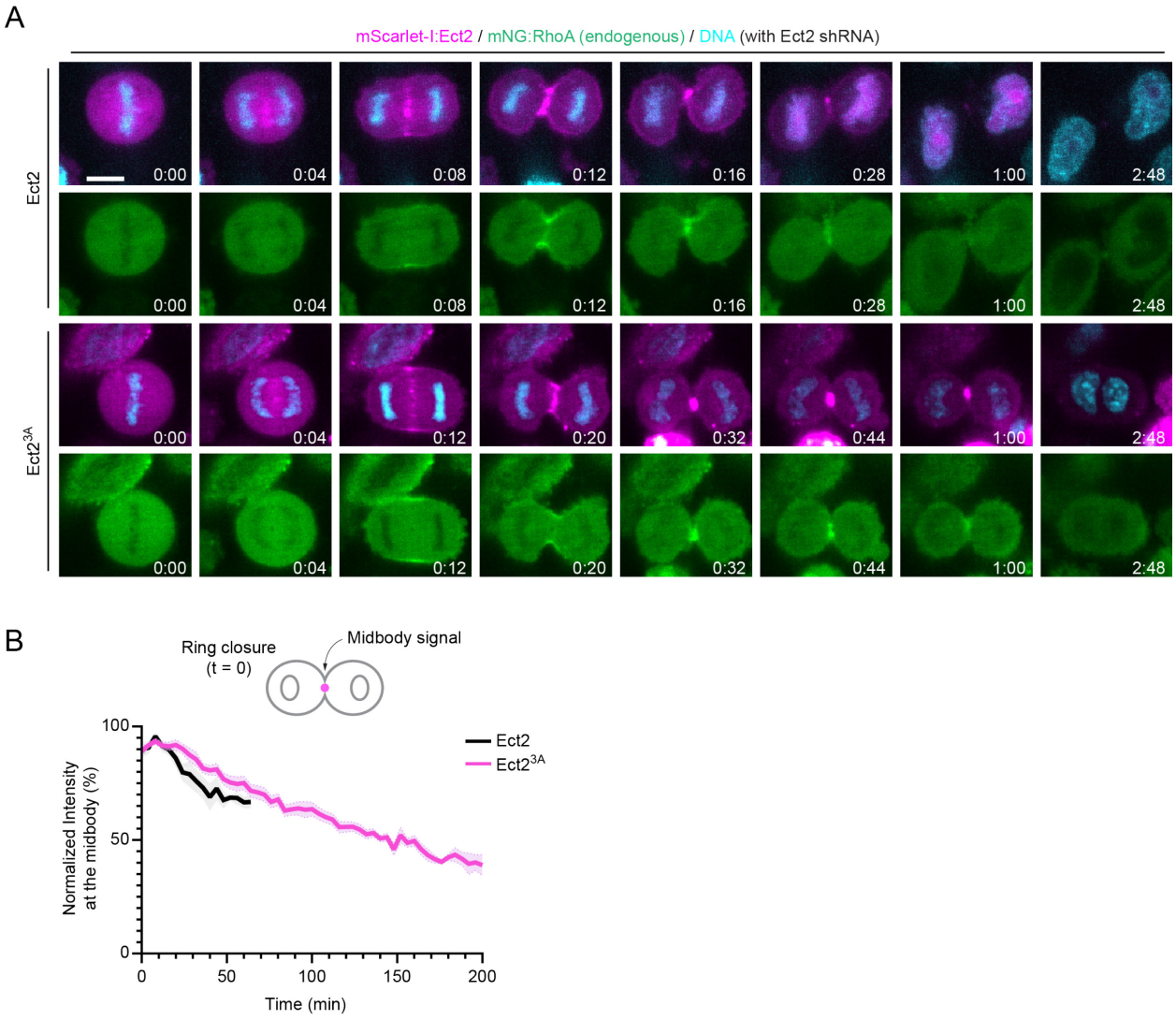

Figure 15. Total RhoA at the midbody decreases at a rate that is similar for Ect2 and NLS mutant Ect2.

(A) Timelapse images show HeLa cells with endogenous mNeonGreen:RhoA (green), co-expressing mScarlet-I:Ect2 or Ect2^{3A} (magenta), depleted for Ect2 with shRNA and co-stained for DNA (cyan, Hoechst). The scale bar is 10 μm. Time is in hours:minutes. (t = 0 is anaphase onset). (B) A line graph shows the normalized total fluorescence intensity (y-axis, %) of mNeonGreen:RhoA at the midbody in Ect2 (n = 10) or Ect2^{3A} cells (n = 15) over time (x-axis, minutes; ring closure t = 0). The error bars show standard error of the mean (SEM).

we imaged RhoA in HeLa cells where RhoA was endogenously tagged with mNeonGreen, rescued with RNAi-resistant mScarlet-I-Ect2 or Ect2^{3A} co-depleted for Ect2 (Figure 15A). We measured the changes in RhoA fluorescence at the midbody over time, using Ect2 as a marker. RhoA remained at the midbody with the Ect2^{3A} mutant, and over a longer time compared to Ect2 cells (Figure 15B). Since only a small pool of RhoA is active during cytokinesis, differences in active RhoA could be masked. To visualize active RhoA specifically, we co-expressed the RhoA biosensor (mNG-2 x RhoA-GTP binding domain from Rhotekin; rGBD) and measured changes in fluorescence at the midbody over time in cells rescued with mScarlet-I-tagged Ect2 or Ect2^{3A} mutant (Figure 16D, F). Indeed, active RhoA remained at the midbody for a longer period of time in Ect2^{3A}-expressing cells compared to control, indicating that Ect2^{3A} continues to activate RhoA at the intercellular bridge while it is retained at the midbody, causing cytokinesis failure and membrane regression. To test this, we mutated the DH domain, which is required to generate active RhoA, in Ect2^{3A} (Ect2$^{3A\text{-}DH}$; Figure 17A). We predicted that mutating the DH would prevent the dominant-negative effect caused by over-expression of the Ect2^{3A} mutant. Indeed, while the over-expression of Ect2^{3A} mutant causes 77.3% of cells to become binucleate, 16.7% of Ect2 and 8.3% of Ect2$^{3A\text{-}DH}$ cells became binucleate, respectively (Figure 17D). Taken together, these results show that Ect2^{3A} at the midbody causes cytokinesis failure through activating RhoA.

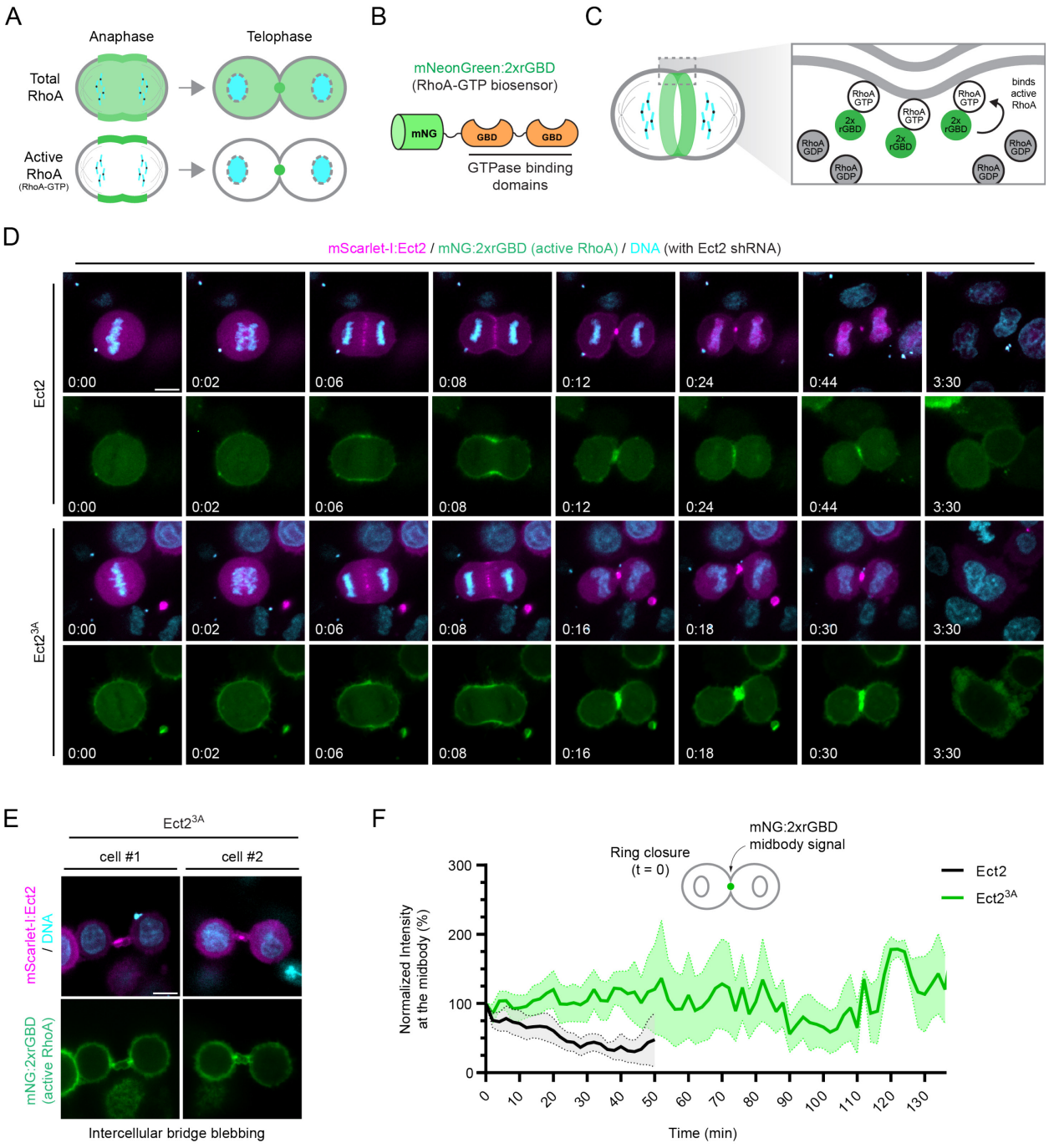

Figure 16. Ect2 nuclear localization is required to reduce active RhoA at the midbody and form a stable intercellular bridge.

(A) Cartoon pictures show the localization of total RhoA (light green) in cells compared to active RhoA (dark green). Chromosomes are in blue. (B) A schematic shows the structure of the RhoA-GTP biosensor with mNeonGreen (mNG, green) fused to two RhoA-GTP binding domains (GBD,

orange) from Rhotekin (Mahlandt et al., 2021). (C) A cartoon cell shows the localization of the biosensor (2xrGBD, green) for RhoA-GTP (white) at the equatorial cortex. RhoA-GDP is in grey. (D) Timelapse images show HeLa cells expressing RNAi-resistant mScarlet-I:Ect2 (magenta; Ect2 or Ect2^{3A}), depleted of endogenous Ect2 using shRNA, co-expressing mNG:2xrGBD (green), and co-stained for DNA (cyan, Hoechst). The scale bar is 10 μm. Times are indicated in hours:minutes (t = 0 anaphase onset). (E) Images show intercellular bridge blebbing two Ect2^{3A} cells from D. The scale bar is 10 μm. (F) A line graph shows the normalized fluorescence intensity of mNG:2xrGBD (y-axis, a.u.) starting after ring closure (t = 0) for cells imaged as shown in D rescued with Ect2 (black, n = 9) or Ect2^{3A} (green, n = 8). The filled-in region surrounding the solid lines indicate standard error of the mean (SEM).

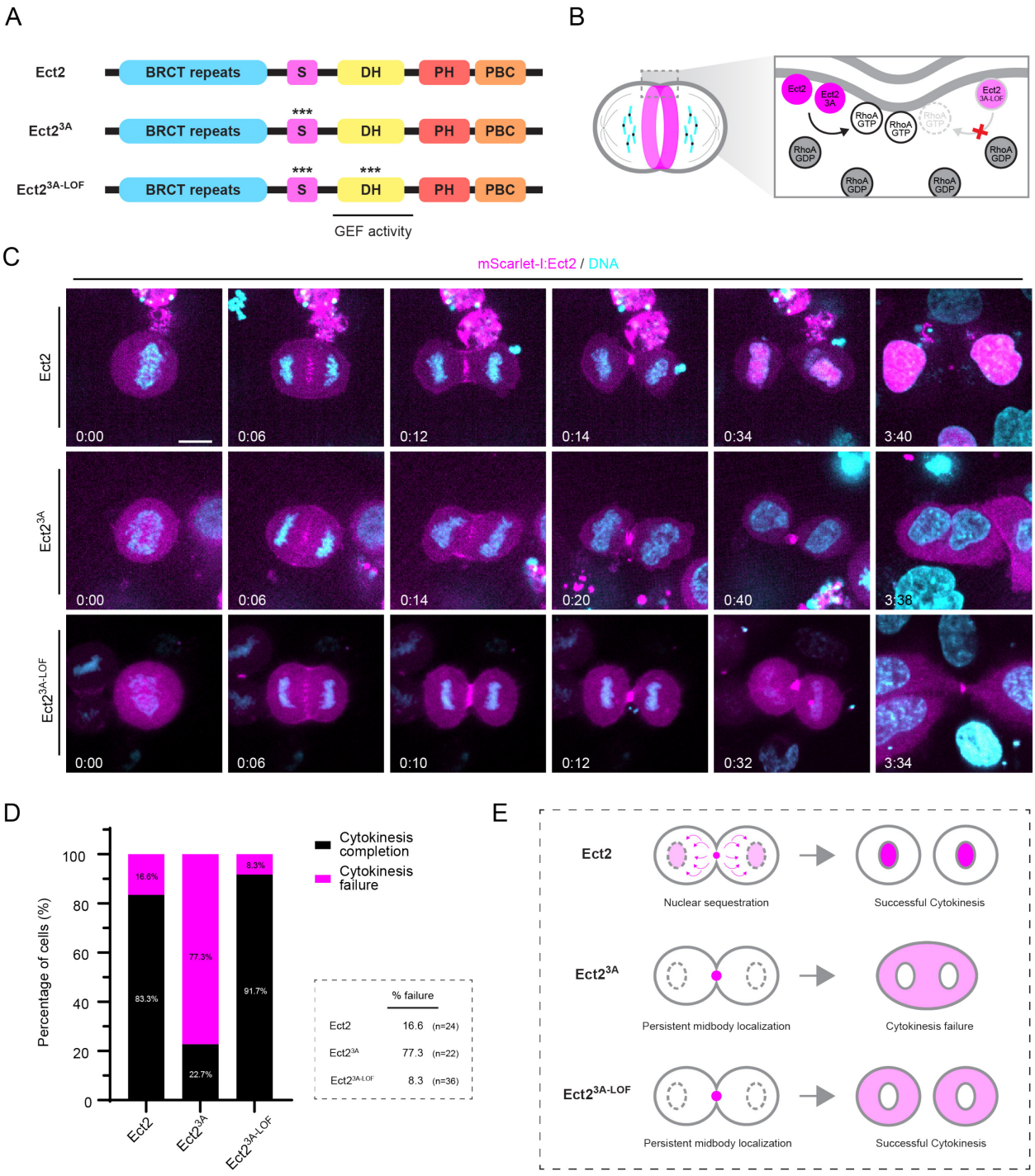
A
Ect2
BRCT repeats
S
DH
PH
PBC
Ect2^3A
***
Ect2^3A-LOF
GEF activity
B
Ect2
Ect2 3A
Ect2 3A-LOF
RhoA GTP
RhoA GDP
C
mScarlet-I:Ect2 / DNA
Ect2
Ect2^3A
Ect2^3A-LOF
0:00
0:06
0:12
0:14
0:34
3:40
0:20
0:40
3:38
0:10
0:32
3:34
D
Percentage of cells (%)
Cytokinesis completion
Cytokinesis failure
16.6%
83.3%
77.3%
22.7%
8.3%
91.7%
% failure
Ect2 16.6 (n=24)
Ect2^3A 77.3 (n=22)
Ect2^3A-LOF 8.3 (n=36)
E
Nuclear sequestration
Successful Cytokinesis
Persistent midbody localization
Cytokinesis failure
Persistent midbody localization
Successful Cytokinesis

Figure 17. A decrease in Ect2 activity is required to form a stable midbody.

(A) The structures of Ect2 with the location of the mutations (***) in the NLS and DH domain used in C-D are indicated for Ect2^{3A} and Ect2$^{3A\text{-}LOF}$. (B) A cartoon cell shows how Ect2 and Ect2^{3A} (dark pink) have functional DH domains and can activate RhoA (RhoA-GTP, white), whereas Ect2$^{3A\text{-}LOF}$ (light pink) cannot due to loss-of-function mutations in the DH domain. RhoA-GDP is shown in grey. (C) Timelapse images show HeLa cells expressing mScarlet-I:Ect2, Ect2^{3A} or Ect2$^{3A\text{-}LOF}$ (magenta), co-stained for DNA (cyan, SYTO Deep Red). The scale bar is 10 μm. Time is in hours:minutes. (t = 0 is anaphase onset). (D) A bar graph shows the proportion of cells that succeed (black) or fail (pink) cytokinesis for cells treated as shown in C (Ect2 16.6% failure, n = 24; Ect2^{3A} 77.3% failure, n = 22; and Ect2$^{3A\text{-}LOF}$ 8.3% failure, n = 36). (E) Cartoon cells show the changes in Ect2 localization (magenta) at the midbody and daughter cell nuclei when the NLS is mutated (Ect2^{3A}) and both the NLS and DH domains are mutated Ect2$^{3A\text{-}LOF}$.

3.6 Discussion

Our study showed the requirement of nuclear localization for Ect2 in cytokinesis. Using full-length Ect2, we showed here that mutating the NLS in the S-loop region causes cytokinesis failure in both HeLa and HEK293T cells. We found that cytokinesis can be restored by relocalizing the mutant to the nucleus, or by inactivation of the DH domain, which is required for nucleotide exchange to generate active RhoA. When the NLS is mutated, Ect2 remains at the midbody in cells, causing intercellular bridge instability and membrane regression. Using a RhoA biosensor, we showed that Ect2 continuously activates RhoA at the midbody and intercellular bridge, and we propose that this is the main cause of cytokinesis failure.

Previous work suggested that Ect2 delocalization from the midbody is important for abscission. Ect2 competes against Fip3, a protein required for abscission, for binding to Cyk4, potentially preventing Fip3 from localizing to the midbody for abscission (Wilson et al., 2005; Simon et al., 2008). Similarly, overexpression of the N-terminus of Ect2 (which binds to Cyk4) increases cell binucleation, potentially by inhibiting the Fip3-Cyk4 complex (Chalamalasetty et al., 2006). Our results are consistent with these reports, where persistence of Ect2 at the midbody leads to intercellular bridge instability and failed cytokinesis. In addition, overexpression of $Ect2^{3A-DH}$, which remains at the midbody but is unable to activate RhoA, causes a small percentage of cytokinesis failure, which is consistent with the proportion of cells that are binucleated when overexpressing the Ect2 N-terminus (Chalamalasetty et al., 2006). Thus, inhibition of the Fip3-Cyk4 complex may also contribute to cytokinesis failure with the NLS mutant.

We show here that nuclear localization removes Ect2 to reduce RhoA at the intercellular bridge (Figure 18). We hypothesize that nuclear re-sequestration acts as a transition mechanism between ingression and abscission, by removing ingression-promoting complexes for abscission

complexes to form and thus promote midbody maturation and abscission. This elegant mechanism could downregulate proteins as early as nuclear envelope reformation, which coincides with contractile ring closure. This regulation may be faster than targeting cytokinesis proteins for degradation or inhibition by post-translational modifications, which requires the synthesis and/or spatiotemporal control of specific enzymes. Since we showed that Ect^{3A} causes cytokinesis failure in both HeLa and HEK293T cells, this mechanism is potentially conserved.

Other cytokinesis proteins, such as anillin, Cyk4, Mklp1 and mDia2 have NLSs, and could be regulated in this manner. Interestingly, overexpression of an NLS mutant of Mklp1/Kif23 prevents abscission but does not cause cell binucleation; instead, the cells remain connected by an intercellular bridge (Liu and Erikson, 2007). How Mklp1 (or excess Mklp1) at the midbody could cause abscission failure is unclear. Unlike Ect2, Mklp1 remains at the midbody for a long time, and its re-sequestration has not yet been studied. Since phosphorylation of this NLS attenuates nuclear localization, it is possible that the NLS is phosphorylated throughout cytokinesis and subsequently dephosphorylated to re-sequester Mklp1 in the nucleus.

We also found a minor delay in the duration of ingression and impairment of ring closure when mutating the NLS of Ect2. Slower ingression kinetics could be due to the Ect2 mutant being less efficient at generating contractility through RhoA. It is possible that importin-binding to Ect2 at the cortex could play a minor role in regulating Ect2 function for ingression. Our lab previously found that mutating the C-terminal NLS of anillin increases the breadth of anillin enrichment at the cleavage furrow and decreases its stability at the cortex (Beaudet et al. 2017, and 2020). Our model is that importin-binding facilitates the recruitment of anillin at the cortex. Importins that can bind to anillin at the cortex could also bind to Ect2. Like anillin, importin-binding may facilitate Ect2 localization at the cleavage furrow to more effectively generate contractility. Alternatively, this delay could be explained by reduced lipid-binding. For instance, the positively charged residues

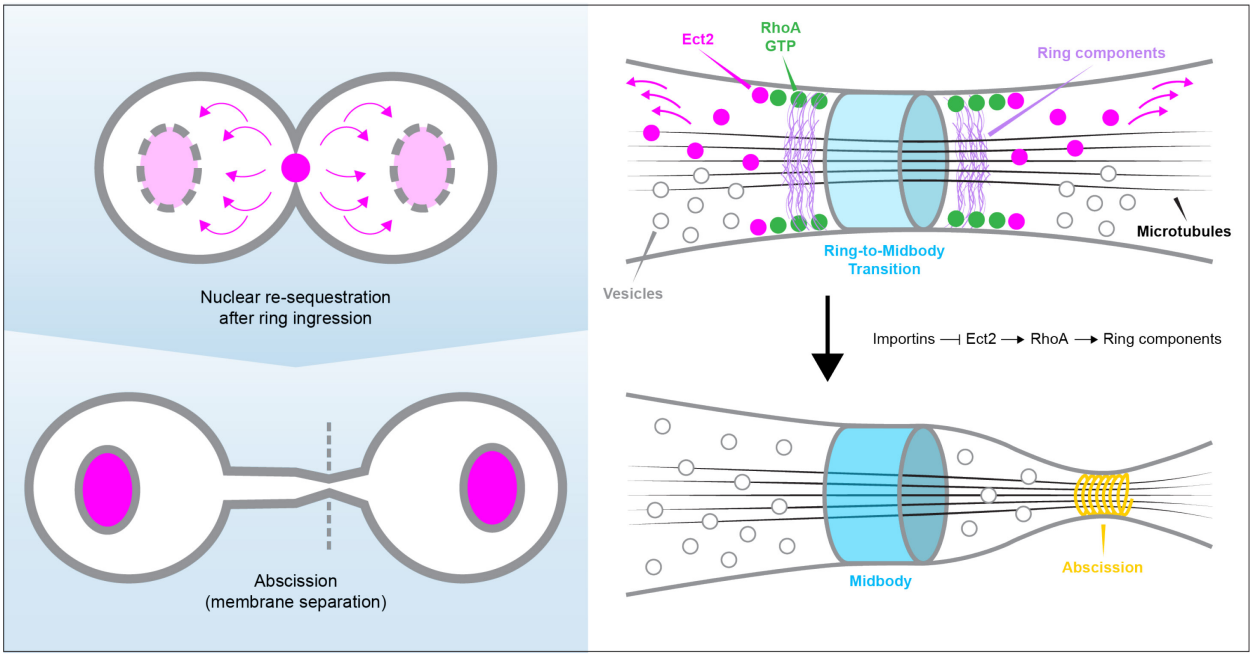

Figure 18. A model for nuclear sequestration as a regulatory mechanism for Ect2 function in cytokinesis.

After ring ingression and closure, Ect2 (pink) is removed from the midbody (blue) via nuclear transport by importins to reduce RhoA-GTP (green) at the intercellular bridge. A reduction in active RhoA is likely important to decrease ring components (purple) for intercellular bridge stability and midbody maturation for abscission (yellow). When the NLS of Ect2 is mutated it remains at the midbody and active RhoA persists causing intercellular bridge blebbing and cytokinesis failure, likely by sustaining ring components such as actin and myosin. This mechanism spatiotemporally couples ring closure with nuclear envelope reformation, and could regulate other contractile proteins.

of the NLS could contribute to lipid-binding for Ect2 cortical recruitment, although lipid-binding to the S-loop region has not been studied.

Although the midbody is an extremely dense structure, the removal of Ect2 occurs soon after ingression, likely before a stable midbody has fully formed. However, midbody assembly is not well-understood, and it is not clear when it becomes a more stable, dense structure. Presumably, Ect2 retains interactions with phospholipids in the overlying membrane, which could prevent Ect2 from being integrated into the denser regions of the midbody.

Ect2 has a cryptic C-terminal NLS that is not required for nuclear localization. This NLS has been understudied and could also act as a regulatory domain for importins, as described above. Interestingly, the C-terminal NLS appears to be auto-inhibited as only C-terminal fragments are nuclear (Liot et al., 2011). Other cytokinesis proteins, such as Mklp1 and anillin, have NLS's that are not primarily used for nuclear localization and are auto-inhibited. Clearly, NLSs are importin-binding regions that can be used either for nuclear localization or for modulating function. As described above, importin-binding to the NLS in anillin is spatiotemporally regulated and could facilitate recruitment to phospholipids in the equatorial membrane.

Ect2 is a proto-oncogene and is overexpressed in various cancers. The overexpression of a C-terminal fragment containing a mutant NLS confers transformation to HEK293 cells (Saito et al., 2004). Previous studies showed that mislocalization of Ect2 in the cytosol is associated with a poor prognosis in cancer patients with lung and colorectal cancers (Kosobaty et al., 2019; Cook et al., 2022; Yi et al., 2022). The mechanism for Ect2 in promoting tumorigenesis is believed to be through its function in activating both cytosolic and nuclear Rac1, resulting in an increase in ribosomal biogenesis and cell proliferation signaling pathways (Justilien and Fields, 2010). Ect2 may also regulate focal adhesions in cancer cells. In this work, our data suggest that mislocalized

Ect2 in cancer cells has the potential to cause cytokinesis failure, which can increase chromosomal instability, an important cancer hallmark. Whole genome-duplication by cytokinesis failure can contribute to aneuploidy, when binucleated cells avoid cell death and divide with lagging chromosomes, multiple poles or cleavage furrows (Lens and Medema, 2019). This work provides a new mechanism for how Ect2 could promote tumorigenesis.

Chapter 4

Identifying potential targets of the Ran-importin pathway In cytokinesis

4.1 Preamble

In mitosis, the nuclear envelope is defragmented, and the Ran-GTP and importin gradient regulates the assembly of the mitotic spindle. Work from our lab and other groups have shown that this pathway can also regulate the function of anillin, a core cytokinesis regulator. We propose that other contractile proteins are regulated by this pathway. We use a proteomics approach to determine the mitotic interactome of importin-β1 to identify potential targets of this pathway.

4.2 Abstract

During mitosis, multiple pathways regulate cytokinesis. Signals from the central spindle and astral microtubules promote and inhibit the localization of contractile proteins at the equator and at the poles, respectively. Chromatin-associated cues can also polarize the cortex through Ran and importins. We perform a proximity-biotinylation assay to determine the mitotic interactome of importin-β1. We found 24 high-confidence interactors, and validate interactions for the proteins abi-2, dyskerin, Dock7 and potentially annexin A1. Using a shRNA-mediated knockdown assay, we show that annexin A1 may be weakly required for cytokinesis. Localization experiments show that the C-terminus of Dock7 is localized to the midbody, suggesting a role for Dock7 in abscission. Our TurboID assay also identified a number of actin regulators. Further experiments can determine whether these proteins have roles in cytokinesis and whether they are regulated by the Ran-importin pathway.

4.3 Introduction

During mitosis, cells undergo extensive reorganization of the cytoskeleton. Once the nuclear envelope is disassembled, a host of spindle assembly factors are released from the nuclei and are activated to form the mitotic spindle near the chromosomes (Prosser and Pelletier, 2017). The anaphase spindle controls the segregation of chromosomes to the cell poles and is spatiotemporally coupled with cytokinesis, a process which describes the physical separation of the daughter cells. The central spindle recruits proteins to the equatorial cortex to regulate the assembly and ingression of a contractile ring, which physically pinches in the membrane to form two daughters. RhoA is the master regulator of ring kinetics and is activated at the equatorial cortex by the GEF Ect2 (Yüce et al., 2005; Green et al., 2012). Active RhoA recruits effector proteins to form actomyosin filaments. The scaffold protein anillin tethers the contractile ring to the overlying membrane and is also recruited by RhoA. After ingression, the contractile ring matures into the midbody at the center of an intercellular bridge, which controls abscission by the ESCRT-III complex (Mierzwa and Gerlich, 2014). Failure to segregate DNA or complete cytokinesis can result in cells with altered ploidy and chromosomal instability, a hallmark of cancer.

Multiple spindle-dependent and -independent pathways regulate cytokinesis. The central spindle recruits and activates the RhoA activator Ect2 through MgcRacGAP/Cyk4, and this interaction is necessary to activate Ect2 and ensures its distribution at the equatorial cortex. At the poles, astral microtubules negatively regulate the localization of contractile proteins (Lewellyn et al., 2010; Zanin et al., 2013; van Oostende Triplet et al., 2014; Mangal et al., 2018; Chen et al., 2021). In addition to microtubule-dependent mechanisms, cues from chromatin can regulate the positioning of contractile proteins at the cortex. The PP1-Sds22 phosphatase complex associated with kinetochores dephosphorylates the actin crosslinker moesin to cause the clearance of actin

when kinetochores come near the membrane (Rodrigues et al., 2015). Myosin and anillin also respond to chromatin via Ran GTPase and importins (Kotadia et al., 2012; Kiyomitsu et al., 2013; Beaudet et al., 2017). Ran in its active form is found near chromatin, where its activator RCC1 is tethered, and competes importins away from partner proteins. Thus, in dividing cells, active Ran exists as a gradient, high near chromatin and low near the cortex (Kaláb et al., 2006). In turn, importins free to bind partners also exist as a gradient, high near the cortex away from active Ran, and low near chromatin. This gradient controls spindle assembly factors, which are inhibited by binding to importins, and their subsequent release by active Ran near chromatin enables the assembly of the mitotic spindle. This same Ran-importin gradient also controls the cortex. Importin-binding to anillin facilitates its recruitment to the membrane to control ring positioning. Forcing constitutively active Ran to the equatorial cortex disrupts this importin-mediated regulation of anillin, leading to ruffling and cortical oscillations (Beaudet et al., 2017). In addition, an importin-binding mutant of anillin leads to cytokinesis failure in a third of anillin-depleted cells, indicating that importins regulate an important function of anillin (Beaudet et al., 2020). We propose that the Ran-importin gradient functions as a molecular ruler for the spatial recruitment of anillin to the cortex to ensure that the ring is positioned between the segregating chromosomes.

Importins are also known for their role in the nucleocytoplasmic import of proteins in interphase cells (Lu et al., 2021). Importins bind to positively-charged sequences called nuclear localization signals (NLS) in target proteins. Typically, importin-α forms a 1:1 complex with importin-β1, and importin-β1 binds to the target protein and relieves an auto-inhibitory importin-β1 binding (IBB) domain in importin-α for transport, whereas importin-β1 can bind to cargo and mediate transport on its own (Lu et al., 2021). We identified the NLS in anillin that binds directly to importin-β1, and that this binding is disrupted when the NLS is mutated. However, we did not study the role of importin-α, and we found that both importin-α and -β regulate ring kinetics in *C.*

elegans embryos (Ozugergin et al., 2022). Interestingly, this regulation occurs via ANI-1 (anillin homologue) in the somatic cell (AB) of the two-cell embryo, but not in the germline (P1), suggesting that the targets of the importin-pathway could be cell type-dependent.

Given that multiple cortical regulators contain NLS sequences, we predict that there could be more than one target of the Ran-importin pathway. To determine whether importins regulate other cytokinesis proteins, we performed a TurboID proximity-biotinylation assay using HEK293 cells synchronized for mitotic exit, with importin-β1 as the bait protein. We confirmed 13 previously published interactions and identified 11 potential novel interactors. Using pull-down assays, we confirmed binding of three of our potential novel interactors: abi-2, dyskerin and Dock7. To study whether these potential targets of the Ran-importin pathway are required for cytokinesis, we performed shRNA-knockdown assays and preliminary results suggest that annexin A1 may be weakly required for cytokinesis. We also characterized the subcellular localization of a subset of potential targets in interphase and during mitosis. We observed that dyskerin is nuclear in interphase, the C-terminus of Dock7 localizes to the midbody after ingression, septin 6 localizes to the equatorial cortex, and both septins 6 and 9 localize to the intercellular bridge. These results suggest that these potential targets may have roles in cytokinesis, which may be regulated by importins. Further studying this mechanism will reveal the scope of the Ran-importin pathway and provide a clearer picture of cytokinesis regulation.

4.4 Materials & Methods

4.4.1 Cell culture

HeLa and HEK293 cells were plated and grown in Dulbecco's Modified Eagle Medium (DMEM; Wisent), supplemented with 10% cosmic calf serum (CCS; Hyclone), and 2 mM L-glutamine (Wisent) and were maintained at 37°C with 5% CO_2. For immunofluorescence microscopy, cells were plated in DMEM media without antibiotics (Penillin/Streptomycin), and transfected the following day using Lipofectamine 3000 (Invitrogen) according to the manufacturer's protocol. For fluorescence and phase-contrast microscopy, cells were imaged 24 and 48 hours after DNA transfection, respectively. For *in situ* pull-down assays, cells were lysed 24 hours after DNA transfection. For proximity-based biotinylation, cells were seeded and transfected on the same day and lysates were collected 24-hours after DNA transfection.

4.4.2 Plasmids / Constructs

All plasmids were maintained and cloned in Escherichia coli DH5α unless specified otherwise. Primers used for cloning are listed in Table 7, and shRNA sequences are listed in Table 8. GST:Importin-β1 was made by cloning Importin-β1 cDNA from the pCMV6-Entry:Importin-β vector (Origene; #RC200659) into pGEX-4T using *NcoI* and *NotI* (New England Biolabs) as previously described (Beaudet et al., 2020). Mutant BirA* and Importin-β or mNeonGreen fusions were made by cloning Importin-β1 cDNA from the pCMV6-Entry:Importin-β vector (Origene; #RC200659) or mNeonGreen cDNA from the pNCS-mNeonGreen vector (Allele Biotech) into C1(1-29)-miniTurboID-V5_pCDNA3 (plasmid #107174) through HiFi assembly homologous recombination (New England Biolabs). miniTurboID (#107174) was a gift from Alice Ting; the C1(1-29) membrane targeting sites was removed from our fusions (Branon et al., 2018).

cDNA sequences for abi-2, annexin A1, Dock7 (C-terminus; 1506-2129) and dyskerin were amplified by PCR and ligated into expression vectors using golden gate cloning. Briefly, cDNA was cloned into an entry vector (pYTK001) using BsmbI and ligated with T7 ligase (New England Biolabs). Subsequently, cDNA was cloned into an expression vector (modified pX459V2.0 HypaCas9 vector; Addgene #108294) in-frame with mNeonGreen or mScarlet-I at the N-terminus (C2 of anillin, dyskerin) or at the C-terminus (abi-2, annexin A1, Dock7 C-terminus) using BsaI-HFV2 (New England Biolabs). Sequences for mDia2 and 14-3-3ε (YWHAE) were PCR-amplified from the ORFeome v7.1 into a pYTK001 vector using BsmBI-V2 restriction enzyme. Genes were cloned with mScarlet-I into a vector using BsaI-HFV2. GFP-SEPT6 and mCherry-SEPT9 were generously provided by Dr. Spiliotis (Drexel, PA, USA). Ect2 shRNA sequence was designed according to Yüce et al., 2005. All other shRNA sequences for were designed using the RNAi consortium shRNA library (Broad institute), and all shRNA sequences were cloned into vectors using BbsI (New England Biolabs). All constructs were verified by sequencing.

Table 7. List of cloning primers.

Primers used to clone Abi-2, Annexin A1, Dock7^{CT}, dyskerin, mDia2, mNeonGreen, mScarlet-I and 14-3-3ε into the pYTK001 backbone, and primers used to clone importin-β1 and mNeonGreen into the miniTurbo-encoding backbone. Primers are labeled as forward (fwd) or reverse (rev). Sequences are listed in the 5'-3' orientation.

Cloning Primer	Sequence
Abi-2 - fwd	GCATCGTCTCATCGGTCTCACCATGGCGGAGCTGCAGATG
Abi-2 - rev	ATGCCGTCTCAGGTCTCACCCCCTCAGAATAATGCATGATAGACTCAACG
Annexin A1 - fwd	GCATCGTCTCATCGGTCTCACCATGGCAATGGTATCAGAATTCCTCAAG
Annexin A1 - rev	ATGCCGTCTCAGGTCTCACCCCGTTTCCTCCACAAAGAGCCACC
Dock7 - fwd	GCATCGTCTCATCGGTCTCACCATGGCCTGTAACCAAAGTGCAG
Dock7 - rev	ATGCCGTCTCAGGTCTCACCCCGAGATCCATTTTGCGAAGGCTCA
Dyskerin - fwd	GCATCGTCTCATCGGTCTCAGTCTATGGCGGATGCGGAAGTAATTATT
Dyskerin - rev	ATGCCGTCTCAGGTCTCACTCACTCAGAAACCAATTCTACCTCTTTTGCT
mDia2 - fwd	GCATCGTCTCATCGGTCTCAGTCTATGAGTGAGGAGAGGAGCCTTTC
mDia2 - rev	ATGCCGTCTCAGGTCTCACTCATAAATACGGTTTATTACCATGGTTACAAACTTTCA
miniTurbo backbone - fwd	TAATACGACTCACTATAGGG
miniTurbo backbone - rev	CTGTCCCAGAATCTGTTTAGCGTTC
miniTurbo-importin-β1 - fwd	TACGACTCACTATAGGGAGACCCAGCCACCATGGCGATCGCCATGGAGCTG
miniTurbo-importin-β1 - rev	TCCGCTTCCTGATCCGCTTCCTGATCCGGCGCGCCTCTTCAGTTTCCTCAGTTCTTTTGTTGC
miniTurbo-mNeonGreen - fwd	GACTCACTATAGGGAGACCCAGCCACCATGGATGGTGAGCAAGGGCGAG
miniTurbo-mNeonGreen - rev	TCCGCTTCCTGATCCGCTTCCTGATCCGGCGCGCCTCTTCAGTTTCCTCAGTTCTTTTG
mNeonGreen C-terminus - fwd	GCATCGTCTCATCGGTCTCAGGGGGTTCAGGAGGGTCTATGGTGAGCAAGGGCGAG
mNeonGreen C-terminus - rev	GGCATGGACGAGCTGTACAAGTGAGTGAGACCTGAGACGGCAT
mNeonGreen N-terminus - fwd	GCATCGTCTCATCGGTCTCACCATGGTGAGCAAGGGCGAG
mNeonGreen N-terminus - rev	GGCATGGACGAGCTGTACAAGGGGGGTTCAGGAGGGTCTTGAGACCTGAGACGGCAT
mScarlet-I N-terminus - fwd	GCATCGTCTCATCGGTCTCACCATGGTGAGCAAGGGCGAG
mScarlet-I N-terminus - rev	GGCATGGACGAGCTGTACAAGGGGGGTTCAGGAGGGTCTTGAGACCTGAGACGGCAT
14-3-3ε - fwd	GCATCGTCTCATCGGTCTCAGTCTATGGATGATCGAGAGGATCTGGTG
14-3-3ε - rev	ATGCCGTCTCAGGTCTCACTCACTGATTTTCGTCTTCCACGTCCT

Table 8. List of shRNA sequences

Primers used to clone shRNA sequence into expression vectors. Primers are labeled as forward (fwd) or reverse (rev). Sequences are listed in the 5'-3' orientation.

shRNA	Sequence
shABI-2 (1) - fwd	CACCGACCTAGCCCAACCCGTAATATCTCGAGATATTACGGGTTGGGCTAGGT
shABI-2 (1) - rev	AAAAACCTAGCCCAACCCGTAATATCTCGAGATATTACGGGTTGGGCTAGGTC
shABI-2 (2) - fwd	CACCGGTCAGGTCTTCCCAGATTATCCTCGAGGATAATCTGGGAAGACCTGAC
shABI-2 (2) - rev	AAAAGTCAGGTCTTCCCAGATTATCCTCGAGGATAATCTGGGAAGACCTGACC
shANXA1 - fwd	CACCGCATAAGGCCATAATGGTTAAACTCGAGTTTAACCATTATGGCCTTATG
shANXA1 - rev	AAAACATAAGGCCATAATGGTTAAACTCGAGTTTAACCATTATGGCCTTATGC
shARP2 - fwd	CACCGTGCTGCTAGTCGTAGTCTTTACTCGAGTAAAGACTACGACTAGCAGCA
shARP2 - rev	AAAATGCTGCTAGTCGTAGTCTTTACTCGAGTAAAGACTACGACTAGCAGCAC
shARP3 (1) - fwd	CACCGCCCTTCCTGTATTGCTATTAACTCGAGTTAATAGCAATACAGGAAGGG
shARP3 (1) - rev	AAAACCCTTCCTGTATTGCTATTAACTCGAGTTAATAGCAATACAGGAAGGGC
shARP3 (2) - fwd	CACCGGTAACACCAAACATGATTATACTCGAGTATAATCATGTTTGGTGTTAC
shARP3 (2) - rev	AAAAGTAACACCAAACATGATTATACTCGAGTATAATCATGTTTGGTGTTACC
shDKC1 (1) - fwd	CACCGGCACCTACATTCGGACATTATCTCGAGATAATGTCCGAATGTAGGTGC
shDKC1 (1) - rev	AAAAGCACCTACATTCGGACATTATCTCGAGATAATGTCCGAATGTAGGTGCC
shDKC1 (2) - fwd	CACCGGGCACCTACATTCGGACATTACTCGAGTAATGTCCGAATGTAGGTGCC
shDKC1 (2) - rev	AAAAGGCACCTACATTCGGACATTACTCGAGTAATGTCCGAATGTAGGTGCCC
shDOCK7 - fwd	CACCGATGACTCAAAGGTACACTATACTCGAGTATAGTGTACCTTTGAGTCAT
shDOCK7 - rev	AAAAACGGGACGCTTACCAACTAAACTCGAGTTTAGTTGGTAAGCGTCCCGTC
shECT2 - fwd	CACCGAAGGCGGAATGAACAGGATTTATCAAGAGAAAATCCTGTTCATTCCGCCTT
shECT2 - rev	GAAGGCGGAATGAACAGGATTTATCAAGAGAAAATCCTGTTCATTCCGCCTTTTTT
shWASF2 (1) - fwd	CACCGAGGACGACTGGTCCGATTAACCTCGAGGTTAATCGGACCAGTCGTCCT
shWASF2 (1) - rev	AAAAAGGACGACTGGTCCGATTAACCTCGAGGTTAATCGGACCAGTCGTCCTC
shWASF2 (2) - fwd	CACCGTCCTCCAAGTCAACATGTATTCTCGAGAATACATGTTGACTTGGAGGA
shWASF2 (2) - rev	AAAATCCTCCAAGTCAACATGTATTCTCGAGAATACATGTTGACTTGGAGGAC
shYWHAE - fwd	CACCGCGACGAAATGGTGGAGTCAATCTCGAGATTGACTCCACCATTTCGTCG
shYWHAE - rev	AAAACGACGAAATGGTGGAGTCAATCTCGAGATTGACTCCACCATTTCGTCGC
shYWHAZ (1) - fwd	CACCGGCTGACAGTTGAAGAAAGAAACTCGAGTTTCTTTCTTCAACTGTCAGC
shYWHAZ (1) - rev	AAAAGCTGACAGTTGAAGAAAGAAACTCGAGTTTCTTTCTTCAACTGTCAGCC
shYWHAZ (2) - fwd	CACCGGCAATTACTGAGAGACAACTTCTCGAGAAGTTGTCTCTCAGTAATTGC
shYWHAZ (2) - rev	AAAAGCAATTACTGAGAGACAACTTCTCGAGAAGTTGTCTCTCAGTAATTGCC

4.4.3 Microscopy

To perform live imaging, cells were plated and transfected on 25-mm round coverslips (no. 1.5) and incubated with Hoechst 34580 (Invitrogen) at 1.3 μM for 30 min and placed in a Chamlide magnetic chamber (Quorum). Cells were kept at 37°C with 5% CO2. Live imaging of timelapse rescue experiments was performed on an inverted Nikon Eclipse Ti microscope with a Livescan Swept Field confocal unit (Nikon), using the 100×/1.45 CFI PLAN APO VC oil immersion objective (Nikon) for timelapse, or the 60×/1.40 CFI PLAN APO VC oil immersion objective (Nikon) for interphase localization, a piezo Z stage (MadCity Labs), and with the Andor IXON 897 EMCCD

camera. Timelapse Images were acquired using 400 ms exposures and using the 405 nm, 488 nm and 561 nm lasers (100 mW, Agilent) at 2-15% intensity depending on expression. Multiple Z-stacks of 1.0 µm were taken every 120 s per cell using NIS-Elements acquisition software (Nikon). Image files were exported as TIFFs, which were opened with Fiji (NIH) and converted into maximum intensity Z-stack projections. Projections and merged color images were then converted into 8-bit images and imported into Illustrator (Adobe) to make figures.

4.4.4 Pull-down assays

The following proteins were made from Escherichia coli BL21 cells: GST, GST:importin-β. Bacteria were resuspended in lysis buffer (2.5 mM MgCl2, 50 mM Tris, 150 mM NaCl, pH 7.5, 0.5% Triton X-100, 1 mM dithiothreitol [DTT], 1 mM phenylmethanesulfonyl fluoride [PMSF], and 1× protease inhibitors [Roche]), incubated with 1 mg/ml lysozyme on ice for 30 min, then sonicated three times. Extracts were incubated with preequilibrated glutathione sepharose 4B (GE Lifesciences) overnight at 4°C with rotation. After washing, beads were stored as a 50% slurry at 4°C. Protein concentration was determined by running samples by SDS–PAGE and measuring the density of bands in comparison to known concentrations of bovine serum albumin. To test for binding, proteins were pulled down from cell lysates after transfection. Transfected HeLa cells were lysed in 50 mM Tris, pH 7.6, 150 mM NaCl, 5 mM MgCl2, 0.5% Triton X-100, 1 mM DTT, 1 mM PMSF with 1× protease inhibitors (Roche), and incubated with 5–10 µg of purified GST-tagged importin-β protein on beads at 4°C overnight. After binding, beads were washed three to four times with 50 mM Tris, pH 7.6, 150 mM NaCl, 5 mM MgCl2 before adding SDS sample buffer to denature the proteins for SDS PAGE. All samples were run by SDS–PAGE and wet-transferred to nitrocellulose membrane for Western blotting. All blots were reversibly stained

with Ponceau S to show total protein. The blots were blocked with 5% milk for 20 min, then incubated with 1:10,000 mouse anti-mNeonGreen antibodies (ChromoTek) in 1× TBS-T (0.150 M NaCl, 0.1 M Tris pH 7.4, 0.5% Triton X-100) for 1–2 h at room temperature. After washing the membrane three to four times with 1× TBS-T, secondary antibodies (anti-rabbit HRP [horseradish peroxidase]; New England Biolabs) were added as per manufacturer's instructions in 1× TBS-T for 2 h. The blots were developed using enhanced chemiluminescence (ECL) Western blotting detection reagents (Cytiva) and visualized on a GE Amersham Imager 600 or ChemiDoc XRS+ (Bio-Rad). All results from each pull-down assay were replicated in at least three distinct experiments to ensure reproducibility. Band intensity was quantified using ImageJ, then imported into Excel (Microsoft) for formatting. Data was then imported to Prism (Version 10.20, Graphpad). Images were converted to 8 bit by Fiji, and made into figures using Illustrator (Adobe).

4.4.5 shRNA knockdown assay and analysis

For shRNA knockdown assays, cells were plated on 6-well dishes (Sarstedt) and transfected as described above. Cells were imaged by phase-contrast microscopy on a Nikon Eclipse TS100 microscope with a DS-Qi1Mc camera and using the 10×/0.25NA objective. Monunucleate and binucleate cells were counted in FIJI. Data was formatted in Excel, and statistical analysis was performed on Prism (Graphpad; v.10.20). Data were tested for normality, and statistical significance was tested a one-way ANOVA followed by multiple comparisons using Tukey's post-hoc test if the data were normally distributed, or using a non-parametric test if the data were not normally distributed. Significance levels were defined as: $p > 0.05$ non-significant (ns), *$p \leq 0.05$; ****$p \leq 0.0001$. Graphs were imported into Illustrator (Adobe) to make figures.

4.4.6 Proximity-based biotinylation and mass spectrometry analysis

HEK239 cells were seeded in 100 mm culture plates at 60-70% confluency and transfected with Importin-β:miniTurbo or mNeonGreen:miniTurbo (Branon et al. 2018). To synchronize cells in metaphase, cells were treated with S-trityl-L-cystein (STC) at 9 μM 8 hours-post transfection for 16 hours. Cells were released from STC and treated with RO-3306 (9 μM) and fed with biotin (100 μM; in DMEM) for 30 minutes, then lysed. Cell lysates were collected and clarified by centrifugation at 12,000 g for 3 minutes at 4°C. Protein concentrations of clarified lysates were quantified and equal amounts of total protein for control (transfected with mNeonGreen:miniTurbo) and experimental (transfected with Importin-β:miniTurbo) were incubated with pre-equilibrated streptavidin beads (Sigma-Aldrich) overnight at 4°C with shaking. After binding, beads were washed 3–4 X with 50 mM Tris pH 7.6, 150 mM NaCl, 5 mM $MgCl_2$ before adding SDS sample buffer and boiling to denature the proteins for SDS-PAGE. Samples were resolved by SDS-PAGE. For mass spectrometry analysis, polyacrylamide gels were stained with the mass spectrometry-safe stain Simply Blue (Invitrogen) for visualization of protein bands and amounts. Excised gel pieces were reduced with 50 mM NH_4HCO_3, 10 mM DTT for 30 minutes at room temperature, then alkylated with 50 mM NH_4HCO_3 and 50 mM iodoacetamide for 30 minutes at room temperature. Reduced and alkylated gel pieces were washed and dehydrated at room temperature with 50 mM NH_4HCO_3 for 15 minutes, with 25 mM NH_4HCO_3 containing 5% acetonitrile for 15 minutes, with 25 mM NH_4HCO_3 containing 50% acetonitrile for 30 minutes twice, and with 100% acetonitrile for 10 minutes. Dehydrated gel pieces were dried by SpeedVac (Savant) at 43°C and peptides were in-gel digested with proteomics-grade trypsin (Sigma-Aldrich) overnight at 30°C. Digested peptides were extracted from gel pieces and acidified with 60% acetonitrile containing 0.5% formic acid. Extracted peptides were evaporated to dryness by SpeedVac (Savant) at 43°C and stored at -20°C. Dried samples were resuspended and analyzed

using liquid chromatography-tandem MS at Concordia's Centre for Biological Applications of Mass Spectrometry (CBAMS). Liquid chromatography-tandem MS (LC-MS/MS) analyses were performed on a Thermo EASY nLC II LC system coupled to a Thermo LTQ Orbitrap Velos mass spectrometer equipped with a nanospray ion source at positive mode.

4.4.7 Analysis of mass spectrometry data

Mass spectrometry data was analyzed using the Trans-Proteomic Pipeline (Seattle Proteome Center). Tandem mass spectra were matched to peptide sequences using X!Tandem, and validation of matches was performed using PeptideProphet. Peptides were matched to proteins using ProteinProphet. Scoring of protein-protein interactions was performed using SAINT-Express (v3.6.1) (Teo et al., 2014). Mass spectrometry data from BirA*-tagged mNeonGreen was used as control. The experiment was performed in duplicate, and the control was performed once. The list of interactors was compared to published interactors of KPNB1 found on the curated database BIOGRID (v4.4.247). Functional annotation of the protein dataset was analyzed using DAVID v.2024q4 (LHRI) with a medium classification stringency and an EASE of 1.0, and with g:Profiler (https://biit.cs.ut.ee/gprofiler/gost). Volcano and box-and-whiskers plots were plotted on Prism (GraphPad; v10.20) and figures were prepared on Cytoscape and Illustrator (Adobe).

4.5 Results

4.5.1 TurboID identification of the mitotic KPNB1 interactome

To identify potential targets of the Ran-importin pathway in cytokinesis, we performed a proximity-based biotinylation assay (TurboID) using importin-β1 (KPNB1) as a bait protein in synchronized HEK293 cells. We arrested cells in prometaphase using S-trityl-L-cysteine (STC), which prevents cells from forming bipolar spindles by inhibiting the kinesin Eg5, then induced mitotic exit by inhibiting Cdk1 (Skoufias et al., 2006; Vassilev et al., 2006). During release, biotin was added to label proteins in the proximity of importin-β1 for 30 minutes (Figure 19A). To ensure biotinylation during this short-term treatment, we used miniTurbo, a highly-active mutant biotin ligase (BirA*; Branon et al., 2018). We also performed this experiment using a fusion of the fluorescent protein mNeonGreen and miniTurbo as a control to filter for background interactions in downstream analysis. We captured biotinylated proteins using streptavidin-conjugated beads and identified peptide species using LC-MS/MS and scored the interactions using SAINT Express, using data from mNeonGreen-TurboID as control. Our assay identified 24 high-confidence proximity interactors with Bayesian false discovery rates (BFDR) of 0.01 and lower (above 2.00 for log-transformed BFDR score; Figure 19B). We compared our dataset to a curated list of importin-β1 interactors obtained from the BioGRID repository (https://thebiogrid.org). We confirmed 13 interactions, common to both our dataset and BioGRID (Figure 19C). Unsurprisingly, these include various importin-α and nuclear pore complex proteins (Table 9). Our assay identified 11 potential novel interactions, which include various regulators of the cytoskeleton. Using the high-confidence interactors in Table 9, we performed an enrichment analysis using GO annotations and the Database for Annotation, Visualization and Integrated

A


Seeding, transfection
STC treatment
Release, RO-3306 and Biotin treatments
Lysate harvest
Time (hours)
0
6
22
22.5

B

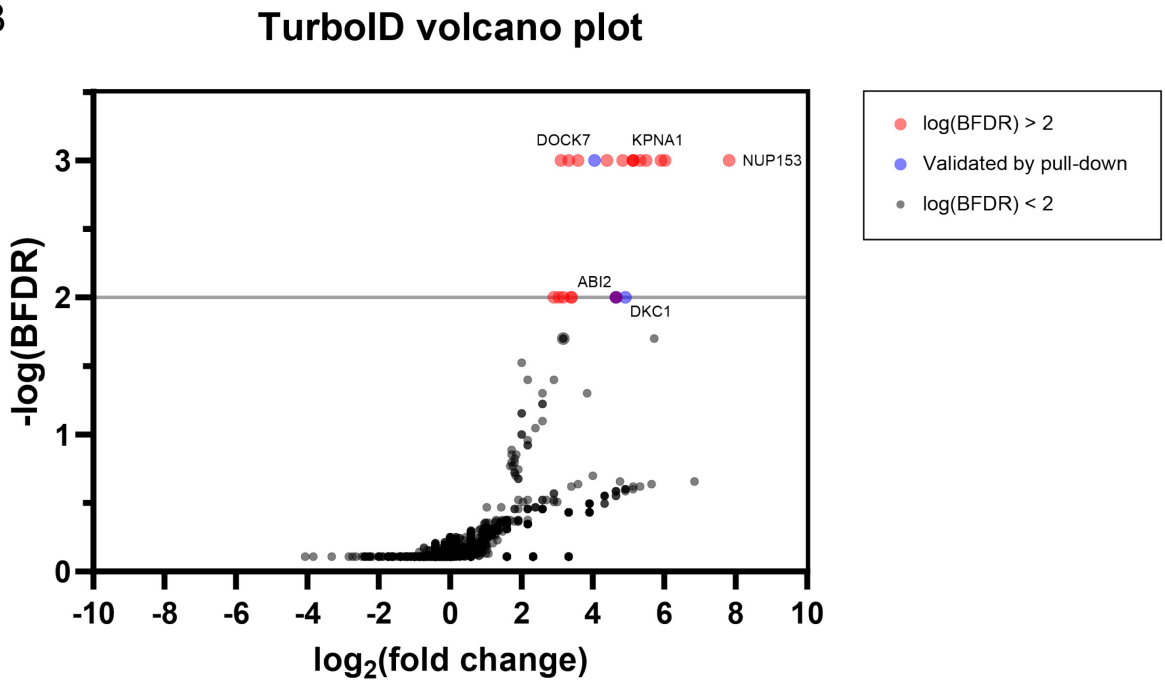
TurboID volcano plot
DOCK7
KPNA1
NUP153
ABI2
DKC1
log(BFDR) > 2
Validated by pull-down
log(BFDR) < 2
-log(BFDR)
log2(fold change)

C

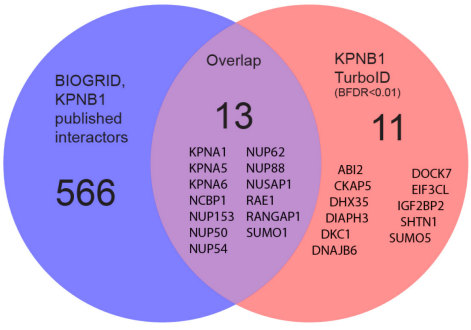
BIOGRID, KPNB1 published interactors
566
Overlap
13
KPNA1
KPNA5
KPNA6
NCBP1
NUP153
NUP50
NUP54
NUP62
NUP88
NUSAP1
RAE1
RANGAP1
SUMO1
KPNB1 TurboID (BFDR<0.01)
11
ABI2
CKAP5
DHX35
DIAPH3
DKC1
DNAJB6
DOCK7
EIF3CL
IGF2BP2
SHTN1
SUMO5

D

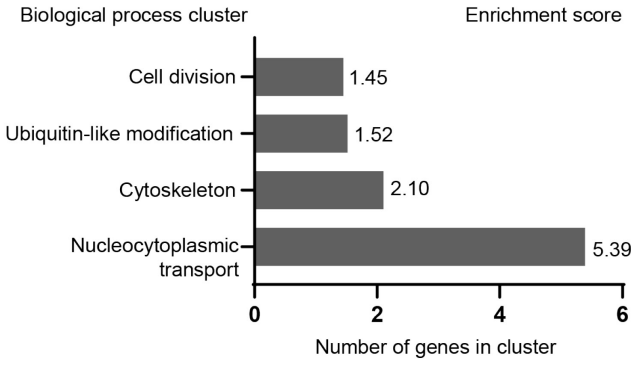
Biological process cluster
Enrichment score
Cell division
1.45
Ubiquitin-like modification
1.52
Cytoskeleton
2.10
Nucleocytoplasmic transport
5.39
Number of genes in cluster

Figure 19. A TurboID of importin-β1 identifies 11 potential novel interactors.

(A) Timeline of TurboID assay. HEK293 cells were seeded and transfected at t = 0. After 6 hours, cells were treated with STC for 16 hours, then released and treated with the Cdk1 inhibitor RO-3306 and fed with biotin for 30 minutes, then lysed. Biotinylated proteins were purified with streptavidin beads and analyzed by mass-spectrometry (n = 2). (B) Volcano plot of potential interactors obtained from SAINT-Express analysis, plotted with log-transformed Bayesian false discovery rate (BFDR) and fold change. Threshold for high-confidence interactors was set at BFDR = 0.01 and lower, and is at -log(BFDR) = 2 on the plot. Interactors with BFDR = 0 were treated as BFDR = 0.001 for graphing purposes. Interactors in red are above the threshold, and interactors in gray are below the threshold. Interactors in blue are above threshold, and validated in further experiments (Figure 20). (C) Comparison of high-confidence interactors (24) with interactors found by other groups in the BioGRID database. (D) Enrichment analysis of high-confidence interactors using DAVID showing four clusters of gene annotation for biological process, plotted by number of genes in the cluster and enrichment scores on the right.

Discovery (DAVID). These interactors formed four clusters: nucleocytoplasmic transport, cytoskeleton, ubiquitin-like modifications, and cell division (Figure 19D), confirming the robustness of mitotic enrichment. Using g:profiler (https://biit.cs.ut.ee/gprofiler/gost), we also generated an enrichment map of this list using GO annotations for biological processes (Figure S7). As expected, this list is enriched for functional annotations related to nucleocytoplasmic transport, cytoskeleton and microtubule organization during mitosis, with transport having the lowest adjusted p-value.

When comparing our dataset with BioGRID, we wanted to determine whether lower confidence interactors in our TurboID list overlaps with BioGRID. In addition to the 13 high-confidence interactors, 57 low-confidence potential interactors overlap with BioGRID. We plotted the interaction confidence scores of all 70 potential interactors and show that they span the entire range of SAINT-scores, and the lower two-thirds of BFDR scores (Figure S8). This is expected as proteomics methodologies differ in their ability to identify specific interactions (Lambert et al., 2015). This indicates that other low-confidence interactors in our list could be true interactors.

4.5.2 Validation of high-confidence potential interactors

Since BioID is a proximity-based approach, we wanted to validate a subset of interactions that are relevant for cytokinesis. From the list in Table 9, we selected several high-confidence potential interactors for further study, including several lower confidence potential interactors which have known or suspected roles in regulating the cytoskeleton (Table 10). We expressed mNeonGreen-tagged abi-2, annexin A1, dyskerin, and the C-terminus of Dock7 (Dock7^{CT}) in HeLa cells and used the cell lysate in pull-down assays with purified GST:importin-β1. As a positive control for binding, we used the C2 domain of anillin, which contains the NLS that binds to

Table 9. List of high-confidence interactors from TurboID of importin-β1.
List of 24 high-confidence interactors, by gene symbol, gene name and with interaction scores (SAINT), fold-change and Bayesian false discovery rate (BFDR). Notes describe known functions. Gene symbols marked with an asterisk (*) are common to BioGRID.

Gene Symbol	ENSEMBL ID	Gene name	Saint Score	FoldChange	BFDR	Notes
KPNA1*	ENSG00000114030	karyopherin subunit alpha 1	1.00	35	0	Nuclear transport
NUP88*	ENSG00000108559	nucleoporin 88	1.00	21	0	Nuclear transport
KPNA6*	ENSG00000025800	karyopherin subunit alpha 6	1.00	40	0	Nuclear transport
NUP153*	ENSG00000124789	nucleoporin 153	1.00	225	0	Nuclear transport
NCBP1*	ENSG00000136937	nuclear cap binding protein subunit 1	1.00	35	0	pre-RNA processing
EIF3CL	ENSG00000205609	eukaryotic translation initiation factor 3 subunit C-like	1.00	12	0	Translation initiation
NUSAP1*	ENSG00000137804	nucleolar and spindle associated protein 1	1.00	45	0	Microtubule-associated protein, spindle regulation
NUP50*	ENSG00000093000	nucleoporin 50	1.00	10	0	Nuclear transport
RAE1*	ENSG00000101146	ribonucleic acid export 1	1.00	28.5	0	mRNA export, spindle regulation
NUP54*	ENSG00000138750	nucleoporin 54	1.00	60	0	Nuclear transport
RANGAP1*	ENSG00000100401	Ran GTPase activating protein 1	1.00	8.59	0	Ran GAP
DOCK7	ENSG00000116641	dedicator of cytokinesis 7	1.00	16.5	0	Rho GEF
DKC1	ENSG00000130826	dyskerin pseudouridine synthase 1	0.98	30	0.01	rRNA processing
DNAJB6	ENSG00000105993	DnaJ heat shock protein family (Hsp40) member B6	0.98	35	0	Co-chaperone of HSP70
DIAPH3	ENSG00000139734	diaphanous related formin 3	0.98	65	0	Actin nucleation
KPNA5*	ENSG00000196911	karyopherin subunit alpha 5	0.97	25	0.01	Nuclear transport
NUP62*	ENSG00000213024	nucleoporin 62	0.97	10.5	0.01	Nuclear transport
SUMO5	ENSG00000241721	Small ubiquitin-related modifier 5	0.97	25	0.01	Sumoylation
DHX35	ENSG00000101452	DEAH-box helicase 35	0.97	25	0.01	RNA processing
ABI2	ENSG00000138443	abl interactor 2	0.97	25	0.01	Actin nucleation
IGF2BP2	ENSG00000073792	insulin like growth factor 2 mRNA binding protein 2	0.97	10.5	0.01	mRNA processing
SUMO1*	ENSG00000116030	small ubiquitin-like modifier 1	0.96	7.5	0.01	Sumoylation
SHTN1	ENSG00000187164	shootin 1	0.95	9	0.01	Actin regulation
CKAP5	ENSG00000175216	cytoskeleton associated protein 5	0.93	8.25	0.01	elongation, spindle

Table 10. List of interactors with suspected or known cytoskeleton regulation.
Interactors with suspected or known roles in regulating the cytoskeleton chosen for further study, sorted by gene symbol, gene name and with interaction scores (SAINT), fold-change and Bayesian false discovery rate (BFDR). Notes describe known functions. Gene symbols marked with an asterisk (*) are common to BioGRID.

Gene Symbol	ENSEMBL ID	Gene name	Saint Score	FoldChange	BFDR	Notes
DOCK7	ENSG00000116641	dedicator of cytokinesis 7	1.00	16.5	0	Rho GEF
DKC1	ENSG00000130826	dyskerin pseudouridine synthase 1	0.98	30	0.01	rRNA processing
DIAPH3	ENSG00000139734	diaphanous related formin 3	0.98	65	0	Actin nucleation
ABI2	ENSG00000138443	abl interactor 2	0.97	25	0.01	Actin nucleation
YWHAE*	ENSG00000108953	tyrosine 3-monooxygenase/tryptophan 5-monooxygenase activation protein epsilon	0.81	14.25	0.05	Adapter protein, cell signaling
YWHAZ	ENSG00000164924	tyrosine 3-monooxygenase/tryptophan 5-monooxygenase activation protein zeta	0.5	25	0.26	Adapter protein, cell signaling
WASF2	ENSG00000158195	WAS protein family member 2	0.35	3	0.45	Actin nucleation
ANXA1	ENSG00000135046	annexin A1	0.35	3	0.45	Calcium binding, phospholipase regulation
SEPT6	ENSG00000125354	septin 6	0.05	1.5	0.62	Cytoskeleton, cytokinesis
SEPT9	ENSG00000184640	septin 9	0.05	2	0.62	Cytoskeleton, cytokinesis
EZR	ENSG00000092820	ezrin	0.01	1.07	0.69	Cytoskeleton, macropinocytosis

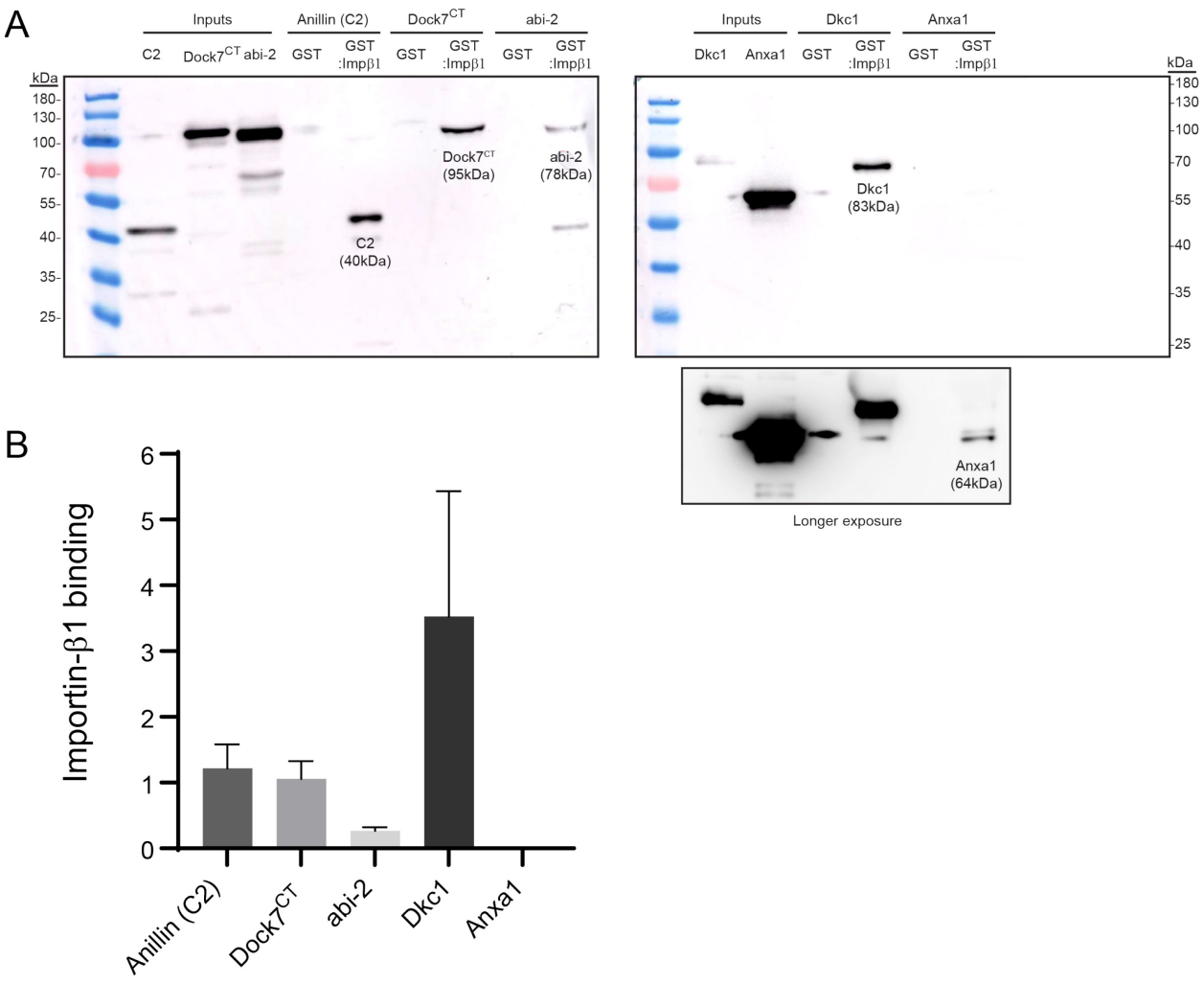

Figure 20. Dock7, abi-2 and dyskerin interact with importin-β1 in pull-down assays.

(A) Immunoblots of pull-down assays of mNeonGreen-tagged anillin (C2), Dock7^{CT}, abi-2, dyskerin (dkc1) and annexin A1 (Anxa1) from HeLa cell lysates with GST:importin (n = 3). Labels were shortened for clarity. Expected molecular size for each protein in fusion with mNeonGreen are labeled on each respective blots. The contrast of blot for dyskerin and annexin A1 was adjusted for visualization of the annexin A1 band (n = 1). (B) A bar graph of the means of densitometry measurements, normalized to input. Error bars show standard deviation.

importin-β1 (Beaudet et al., 2017, 2020). We confirm that abi-2, dyskerin and that Dock7^{CT} can bind to importin-β1, with dyskerin showing the strongest binding, followed by Dock7^{CT} and abi-2 (Figure 20). We could only detect faint binding with annexin A1 in one experiment, suggesting that this interaction is weak. These results are consistent with the BFDR values of these proteins in Tables 1 and 2, where the three proteins – abi-2, dyskerin and Dock7 – with BFDR with 0.01 or lower showed binding and where annexin A1, the lower confidence interactor, was the weakest. Together, these results confirm that abi-2, dyskerin and Dock7 interact directly or can form a complex with importin-β1.

4.5.3 Functional requirement of potential importin targets for cytokinesis

To determine whether the proteins identified in Table 10. are required for cytokinesis, we performed an shRNA-knockdown assay and counted the proportion of mononucleate and binucleate cells. Because the knockdown of a protein required for cytokinesis affects cells after chromosome segregation, binucleation is a common phenotype that indicates cytokinesis failure. We expanded our list to also test proteins which were not identified in our TurboID screen per se, but have functional relationships to those in our list. For example, since we identified regulators of branched actin nucleation – notably ABI2 and WASF2 – we included the known branched actin nucleators ARP2/3 in our assay. In the case of ANXA1, ARP2, DOCK7 and YWHAZ, only one shRNA sequence was cloned, whereas two shRNA sequences were cloned for ABI2, ARP2, DKC1, WASF2 and YWHAE. We performed phase-contrast microscopy and counted mononucleate and binucleate cells, and calculated a ratio of binucleate cells over total cells. As a negative control, we knocked down the essential cytokinesis regulator Ect2 (Yüce et al., 2005). Our results indicate that knockdown of annexin A1 (ANXA1) leads to a higher ratio of binucleate

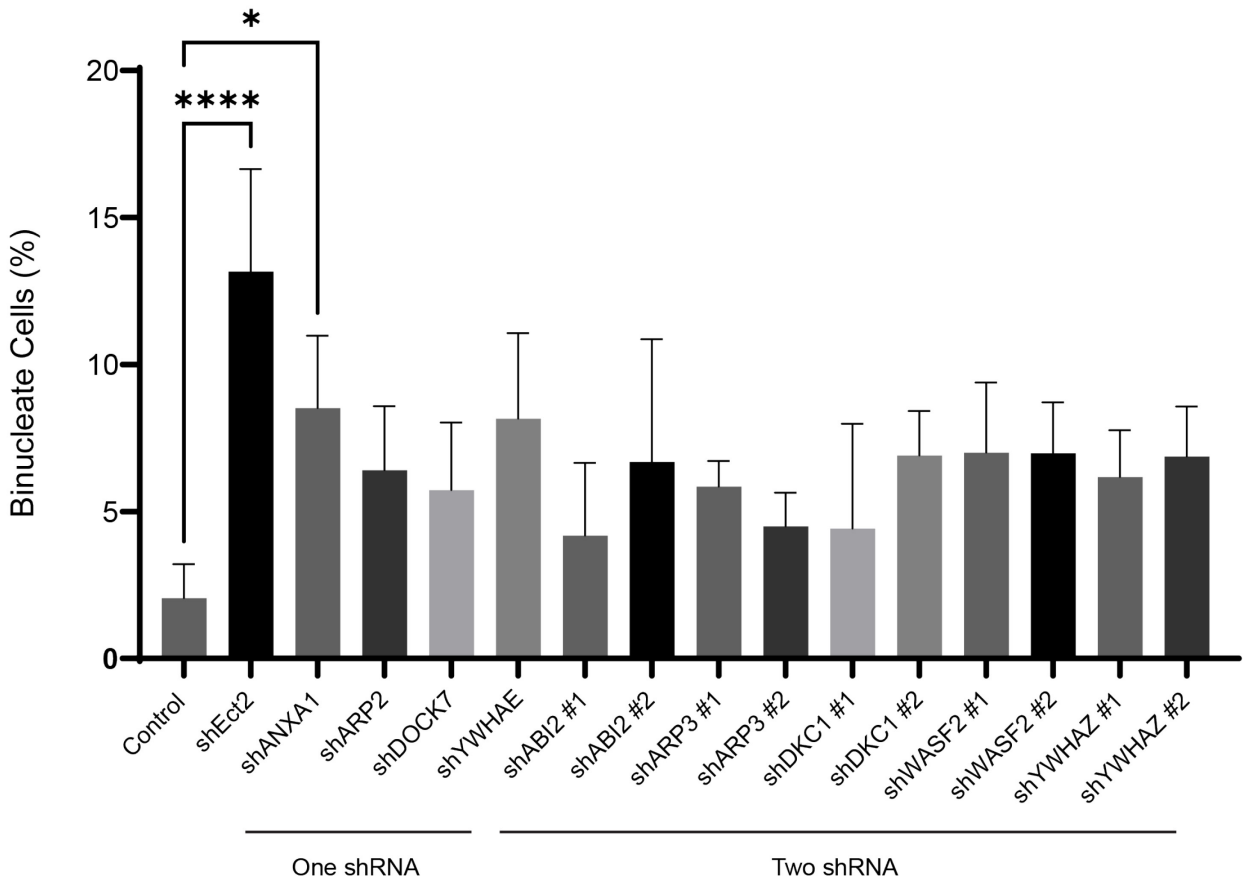

Figure 21. Annexin A1 may be weakly required for cytokinesis.

Bar graph of proportion of binucleate cells from shRNA-knockdown assays in HeLa cells (N=3 replicates; n = 69-361 cells per replicate). Statistical analyses were done using ANOVA and Tukey post-hoc test (*, $p<0.05$; ****, $p<0.0001$). Error bars show standard deviation.

cells (8.51%) compared to control (2.0%; Figure 21). These results suggest that annexin A1 may be required for cytokinesis and merits further exploration. However, the Ect2 control shRNA were weaker (13.2%) compared to siRNA (Yüce et al., 2005), and these findings need to be repeated using siRNAs, with alternate shRNA sequences or with a fluorescent reporter to identify transfected cells.

4.5.4 Characterization of subcellular localization of potential interactors

Because importins typically bind proteins for nuclear import, we wanted to determine whether these potential targets are localized to the nucleus. However, the NLS site in anillin that is required for cytokinesis is *not* used for nuclear import, and importin-binding may not always control nucleocytoplasmic transport. We expressed a subset of potential targets from our list in Table 10 as fusions with fluorophores and observed their localization in interphase cells. We also performed time-lapse fluorescence microscopy to study their localization throughout mitosis (Figure 22 and S10). Dyskerin and Sept9 localized to the nucleus, suggesting that importin-binding controls the nuclear import of these proteins. Interestingly, we found that Dock7^{CT} localizes to the midbody, suggesting that Dock7 may be involved in abscission and that the C-terminus may target the protein to the midbody. Consistent with previous work, we found that Sept6 and Sept9 both localize to the intercellular bridge flanking the midbody, and that Sept6 localizes to the equatorial cortex during ingression (Spiliotis et al., 2005; Estey et al., 2010). Interestingly, 14-3-3ε (YWHAE) was diffuse, but a punctate pattern was also observed at the midzone for one cell, suggesting that 14-3-3ε may localize dynamically to the central spindle (Figure S10). Abi-2 was diffuse and cytosolic during mitosis, but formed bright puncta immediately after ingression, as well as during interphase (Figure 22). Because the overexpression of mDia2

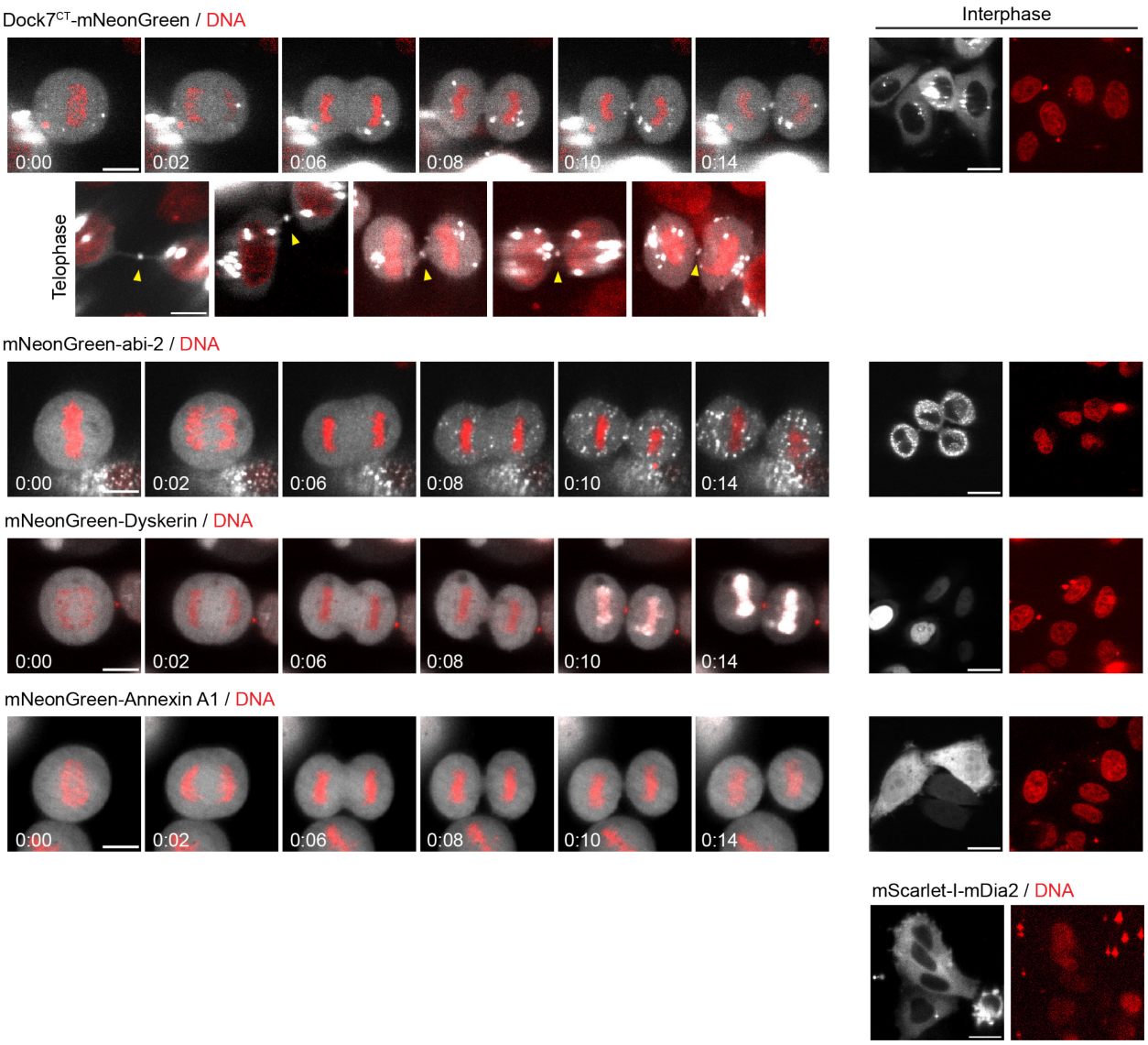

Figure 22. Localization of high-confidence interactors in interphase and dividing cells.

On the left, timelapse images of HeLa cells expressing mNeonGreen-tagged Dock7^{CT}, abi-2, dyskerin or annexin A1 (grayscale), with DNA dye (red, Hoechst). Scale bar is 10 μm, and t = 0 is anaphase onset. Time is in hours:minutes. For Dock7^{CT}, examples of midbody localization are shown below the timelapse in telophase cells. For mDia2, overexpression caused cytokinesis phenotypes which prevented the acquisition of timelapse images. On the right, localization of the constructs in interphase cells as individual channels, with DNA on the right. Scale bar for interphase cells is 20 μm.

caused cell shape phenotypes during mitosis, we were only able to observe its subcellular localization in interphase cells, where it localized to the cytosol (Figure 22).

4.6 Discussion

Multiple pathways coordinate the dynamic events that occur during cell division. This work has identified potential targets for the Ran-importin pathway in regulating cytokinesis. Our TurboID assay to identify importin-β1-interactors has confirmed 13 previously published interactions, and uncovered 11 potential novel interactors (10, if we exclude mDia2). Using pull-down assays to complement the proteomics approach, we found that abi-2, dyskerin and Dock7 can bind to importin-β1. It remains unclear if these proteins bind importin-β1 directly or indirectly via an intermediary like importin-α, and how this binding can regulate their function. Unlike dyskerin, abi-2 and the C-terminus of Dock7 were cytosolic in interphase cells, suggesting that their NLS is inhibited. Similarly, the C-terminal NLS in anillin and Ect2 are auto-inhibited (Liot et al., 2011; Beaudet et al., 2017, 2020). The NLS of abi-2 and Dock7 could be inhibited by intramolecular forces, a different protein, or post-translational modification. For example, phosphorylation of the Ect2 central NLS impairs binding *in vitro* (Suzuki et al., 2015). It is also possible that accessibility of the NLS for importins is temporally regulated. Results from our pull-down assays suggest that this apparent inhibition does not abolish binding, despite blocking nuclear import. Because we were only able to clone the C-terminus of Dock7, the full-length protein may localize differently in interphase and in mitosis.

We showed that the C-terminus of Dock7 localizes to the midbody immediately after ingression, suggesting that it could play a role in abscission, possibly in midbody maturation or intercellular bridge stability. Despite the name (Dedicator of Cytokinesis), no known roles in

cytokinesis have been shown for the DOCK family of proteins. Dock7 is a GEF for the GTPases Rac1 and Rac3, with known roles in axon formation and neuron differentiation (Majewski et al., 2012; Sobczak et al., 2016). Dock7 has been shown to bind to myosin-VI in neurons, but whether it can bind to nonmuscle myosin II is unknown (Sobczak et al., 2016; Menin et al., 2023). Recent work showed that nucleation of branched F-actin by Arp2/3 may act as an actin “cap” to prevent the ESCRT-III complex from expanding past the intercellular bridge during abscission (Advedissian et al., 2024). This suggests that branched F-actin plays an important role in cytokinesis. Since Rac1 is an upstream activator of the Arp2/3 complex, Dock7 could play a role in regulating branched F-actin during abscission.

Abi-2 is another regulator of branched F-actin. abi-2 is a component of the WAVE complex, which is activated by Rac1 to activate Arp2/3 for lamellipodia formation (Chen et al., 2010). Similar to Dock7, abi-2 could also play a role in regulating branched F-actin during cytokinesis. However, we did not detect abi-2 at the midbody or intercellular bridge. Instead, abi-2 localized as bright puncta in interphase and as a diffuse, cytosolic signal during cell division. Strikingly, abi-2 puncta formed immediately following ingression. It is unclear what structures abi-2 puncta localize to, but these could be adherens junctions, or patches of nucleating branched actin.

It is unclear what role dyskerin plays in mitosis. dyskerin is a pseudouridine synthase that is involved in various processes (Alawi and Lin, 2013). Previous work showed that it localizes to the perichromosomal region during mitosis, then to the nucleus and nucleoli. Although we observed nuclear localization in interphase, in our hands, dyskerin did not localize strongly to the nucleoli nor around the chromosomes. Depletion of dyskerin impairs the formation of the mitotic spindle and chromosome segregation (Alawi and Lin, 2013). What role dyskerin plays in regulating the mitotic spindle is unclear, since it appears to be excluded from the mitotic spindle. A splice variant of dyskerin localizes to the cytoplasm and, when overexpressed, appears to

promote cell-adhesion and proliferation, suggesting that dyskerin may play a role in regulating F-actin (Angrisani et al., 2011).

How importin-binding controls protein function remains to be determined. Importin-binding may cause conformational changes, which could alter the protein's accessibility for other proteins or limits, either promoting or inhibiting their function. One outstanding question is whether regulation by importin-α, -β and the α/β heterodimer differ. Importin-α binds cargo via its armadillo repeat domains, whereas importin-β1 binds with its central HEAT repeat regions (Lu et al., 2021). Since their molecular structures are different, regulation by importin-α or -β is likely to hold proteins in different conformations, despite recognizing the same motifs. Recent work showed that importin-α localizes to the cortex upon palmitoylation (Brownlee and Heald, 2019). This finding raises the exciting possibility that importin-α could regulate NLS-containing proteins at the cortex, as a monomer and potentially as a heterodimer with importin-β1.

Using a shRNA-mediated knockdown screen, we also showed that annexin A1 may be weakly required for cytokinesis. However, it is important to note that Ect2 knockdown was weaker than expected. It is unclear what role annexin A1 could play in cell division. Annexin A1 is a calcium- and phospholipid-binding protein We did not observe localized enrichment of annexin A1 during mitosis. Annexin A1 also weakly/did not bind to importin-β1 in our pull-down assay. A different member of the annexin family, annexin A2 (ANXA2) has been shown to be required for both Ect2 and RhoA activation at the equatorial cortex (Benaud et al., 2015). It is possible that annexin A1 plays a similar role, although we detected no cortical enrichment in our hands using over-expression. There could be redundancy that is impeding our ability to study a role for annexin A1, and further studies can answer whether annexin A1 is required for cytokinesis.

Among high-confidence interactors, mDia2 (DIAPH3), Shtn1 and Ckap5 would be interesting to validate further. The actin nucleator mDia2 is activated by RhoA, and localizes to the cleavage furrow (Watanabe et al., 2010; Chen et al., 2017). mDia2 is reported to be nuclear when nuclear export is inhibited (Miki et al., 2009). Ckap5 (ch-TOG) is a microtubule-associated protein required for microtubule polymerization for spindle assembly and plays a role in regulating kinetochore attachments (Gergely et al., 2003; Brouhard et al., 2008; Herman et al., 2020). Although Shtn1 interacts with cytoskeletal proteins, it has no known role in cell division (Kastian et al., 2021). Whether binding to importins regulates the function of mDia2, Ckap5 or Shtn1 during cytokinesis is an exciting question.

By identifying the importin-β1 cytokinesis interactome, this work opens new avenues to investigate the role of the Ran-importin pathway in cytokinesis. Although the role of the Ran pathway for regulating the mitotic spindle is well established, its role in cytokinesis is only beginning to be investigated. Our results suggest that other contractile proteins, such as abi-2, dyskerin, Dock7 and mDia2, among others, could be regulated by importins. Further exploration of this pathway will provide more insight on how cytokinesis is regulated.

Chapter 5

5.1 Overview

During cell division, the mitotic spindle provides the dominant cues to position key cytokinesis regulators at the cortex. The central spindle promotes ring assembly at the equatorial cortex by leading to RhoA activation, whereas asters inhibit contractility at the poles. RhoA then orchestrates cytokinesis by recruiting effectors that assemble the contractile ring and tethers the ring to the plasma membrane. Ultimately, cytokinesis is a cortical event involving complex machinery in a protein-dense and lipid-rich location. Many of these proteins share binding sites with each other, including microtubules, actomyosin filaments and phospholipids. How are these binding events coordinated to form a well-defined contractile ring and drive ingression? Is affinity the main determinant of complex formation? Are these proteins forming different pools, and if so, what provides the cues to form these distinct complexes, and how can they transition from one complex to another?

We propose that the Ran-importin pathway is a mechanism that can regulate these interactions. Active Ran inhibits importins from binding to partners near chromatin. By extension, importins are well-positioned to act as chaperones near or at the cortex, where they can bind to partners and regulate their function. The work described in Chapters 2 and 3 uncover important functions for the importin-binding sites (NLSs) in Ect2. In Chapter 4, we identified new potential targets of the Ran-importin pathway during mitotic exit, some of which could play a role in cytokinesis.

5.2 Ect2 regulation

In Chapter 2, we focused on studying a poorly-understood region of Ect2 called the polybasic cluster (PBC) region. Our interest was piqued by the presence of a cryptic C-terminal NLS. This mirrored anillin, which we identified as a target of the Ran pathway in cytokinesis in previous work (Beaudet et al., 2017; Beaudet et al., 2020). Both anillin and Ect2 have two NLSs, with the C-terminal NLS in each protein being inhibited by intramolecular interactions (Liot et al., 2011; Beaudet et al., 2017; Beaudet et al., 2020). Since the PBC was shown to be required for cytokinesis in concert with the neighbouring PH domain, we sought to determine whether this requirement was due to loss of importin-binding, which would identify Ect2 as a target of the Ran pathway (Su et al., 2011).

Our results identify that lysines and arginines spanning 800-818 define the NLS in the PBC region. Expression of tagged-PBC is sufficient to be nuclear, and mutating residues in this region is sufficient to impair nuclear localization and importin-binding. Notably, we show that the localization of Ect2 at the equatorial cortex can be widened or abolished depending on how the NLS is mutated. To our knowledge, this is the first report that the PBC can control the breadth of Ect2 localization at the cortex. How the PBC regulates this localization is an important question. The PBC may bind to lipids cooperatively with the PH domain. Notably, importin-binding could regulate the C-terminal NLS, similar to anillin. We hypothesize that importin-binding at this NLS could induce a conformational change that alters the affinity of the PBC for lipids (Figure 10, 23). Accessibility to this NLS appears to be limited by the BRCTs, and an attractive model is that binding of the BRCTs to Cyk4 frees inhibition of the PBC. In addition, phosphorylation could also control accessibility of this NLS. Previous studies identified a Cdk1 phosphorylation site in the PBC, and proposed that phosphorylation of this site could repel phospholipid-binding, and binding

would only occur after mitotic exit and Cdk1 activity drops (Su et al., 2011). Our studies support this, however, we found that Cdk1 regulates importin-binding, which in turn could then control lipid binding. Notably, since the NLS is positively charged, phosphorylation would repel this interaction, and prevent binding until after mitotic exit. This was confirmed by assessing changes in the localization of the PBC to the membrane when the site was made to be phosphodeficient vs. phosphomimetic. Since this site is never used for nuclear localization, this control via importin-binding is likely exclusively to control access to the overlying phospholipids.

Post-translational modification sites are often found in disordered regions due to their accessibility to kinases and other modifiers (Bah and Forman-Kay, 2016). Importins and lipids may also leverage this accessibility. This overlap raises important considerations. Do importins and lipids compete for binding to the same regions? If this is the case, how could importins regulate the function of cortical proteins at the cortex? In cells, importin-β1 localizes subcortically, away from chromatin. There, importins may form transient vs. stable interactions with proteins, and promote a conformation that has higher affinity for cortical partners and lipids (Beaudet et al., 2020). Anillin is known to stabilize RhoA, and has been proposed to increase RhoA residence time at the membrane through cyclic binding and dissociation (Budnar et al., 2019). Importins could regulate contractile proteins by a similar mechanism, overcoming the need for membrane association *per se*. Although importin-β1 is not cortically enriched, importin-α associates with the polar cortex during mitosis upon palmitoylation (Brownlee and Heald, 2019; Sutton et al., 2025). It is unclear if this modified importin-α can form complexes with importin-β1 or with NLS-containing proteins. Hyper-palmitoylation of importin-α3 reduced nuclear import of lamin 3B, which suggests that palmitoylation interferes with NLS-importin-α interactions (Brownlee and Heald, 2019). On the other hand, binding to the SAF NuMa appears to be unaffected by palmitoylation. Together,

these findings indicate that palmitoylation may change the binding specificity of importin-α. Localization to the polar cortex rather than the equator suggests that importin-α likely does not play a role in regulating contractility, but possibly limiting it, similar to the astral microtubule pathway. Further research into the interplay between importins and their partners will be necessary for a complete understanding of their role in cytokinesis.

5.3 Nuclear localization as a global mechanism

The nuclear localization of Ect2 is mediated through its NLS in the centrally located S-loop region. Studies have shown that removal of the NLS can cause multinucleation, or confer transforming activity when the BRCT domains are absent (Miki et al., 1993; Saito et al., 2004; Chalamalasetty et al., 2006). In Chapter 3, we studied the requirement of this NLS for cytokinesis. Our results show that this NLS is required to remove Ect2 from the midbody for successful cytokinesis. In cells expressing NLS-mutant Ect2, active RhoA remains at the intercellular bridge, causing instability and membrane regression. We report for the first time a role for nuclear localization to sequester a key regulator of the contractile ring, likely to ensure reduced RhoA activity and to permit the transition to later stages of cytokinesis.

We propose that nuclear sequestration acts as a general mechanism to promote midbody maturation (Figure 18, 23). This mechanism may regulate other contractile proteins with NLSs, like anillin, Cyk4 and Mklp1. In fact, an NLS mutant of Mklp1 appears to inhibit abscission, with cells remaining connected by an intercellular bridge for a significantly longer period of time (Liu and Erikson, 2007). We showed that tagging Ect2 with a SV40NLS sequence leads to a faster

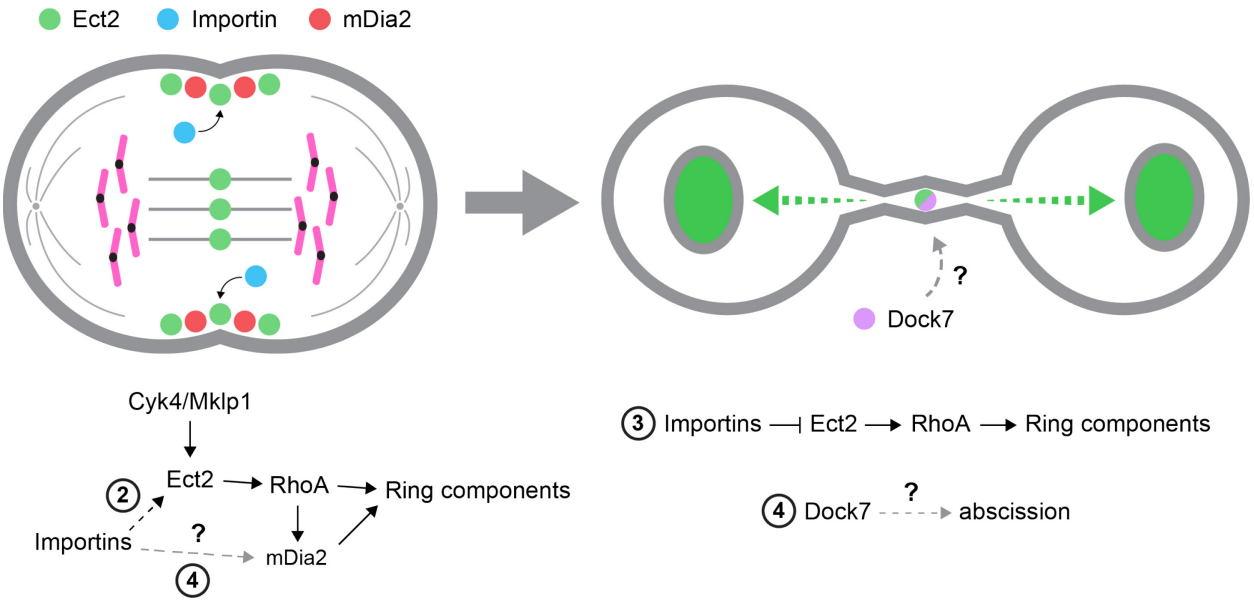

Figure 23. Importins regulate Ect2, and potentially other contractile proteins, for cytokinesis

We showed in Chapter 2 that the C-terminal NLS of Ect2 (green) is required for cytokinesis, and that loss of binding is associated with reduced membrane recruitment of the PBC domain. These results suggest that importins (blue) may facilitate the recruitment of Ect2 to the cortex through the PBC (black dashed line; see circled "2", for Chapter 2). In Chapter 3, we show that the sequestration of Ect2 from the midbody to the nucleus after ingression is required for intercellular bridge stability and preventing cytokinesis failure. Nuclear sequestration acts as a mechanism to inactivate RhoA at the bridge by removing its activator (solid black line; see circled "3", for Chapter 3). This mechanism may also regulate other contractile proteins, such as anillin, Cyk4 and Mklp1. In Chapter 4, we found that mDia2 (red) is a mitotic interactor of importin-β1, and propose that its function could be regulated by importin-binding (gray dashed line; see circled "4", for Chapter 4). We also found that the C-terminus of Dock7 (purple) localizes to the midbody, suggesting that Dock7 may have a function in abscission (gray dashed line).

removal from the midbody, suggesting that the NLS determines the rate of removal, potentially through its affinity to importins. Since anillin, Cyk4 and Mklp1 have distinct functions at the midbody, their sequestration may be temporally controlled by their NLS sequence. Because the midbody is an extremely dense structure, physical accessibility to importins may also factor into this temporal regulation.

We showed that overexpression of the Ect2 NLS mutant leads to cytokinesis failure in both HeLa and HEK293T cells, suggesting that persistent Ect2 can cause failure in multiple cell types. As discussed in Chapter 1, cytokinesis failure has been proposed to contribute to chromosomal instability through the generation of aneuploid cells from tetraploid cell division. As mentioned in Chapter 1, studies in lung cancer suggest that Ect2 promotes tumorigenesis through Rac1 and potentially by promoting cell-adhesion, but the cytokinesis angle has not been explored. As mentioned previously, the presence of Ect2 in the cytoplasm is associated with poor prognosis in patients with breast cancer, colorectal cancer and lung adenocarcinoma (Kosibaty et al. 2019; Cook et al., 2022; Yi et al., 2022). Therefore, cytosolic Ect2 that persists at the midbody could contribute to aneuploidy and tumourigenesis by causing cytokinesis failure. As an oncogene, Ect2 could drive proliferation through Rac1 and chromosomal instability through RhoA (Figure 24).

5.4 Ran and importins regulating cytokinesis proteins

In Chapter 4, we sought to identify new targets of the Ran-importin pathway for cytokinesis using a proteomics approach. Using a proximity-based biotinylation assay, we confirmed 13 previous published interactions and found 11 potentially novel interactors. As expected, several

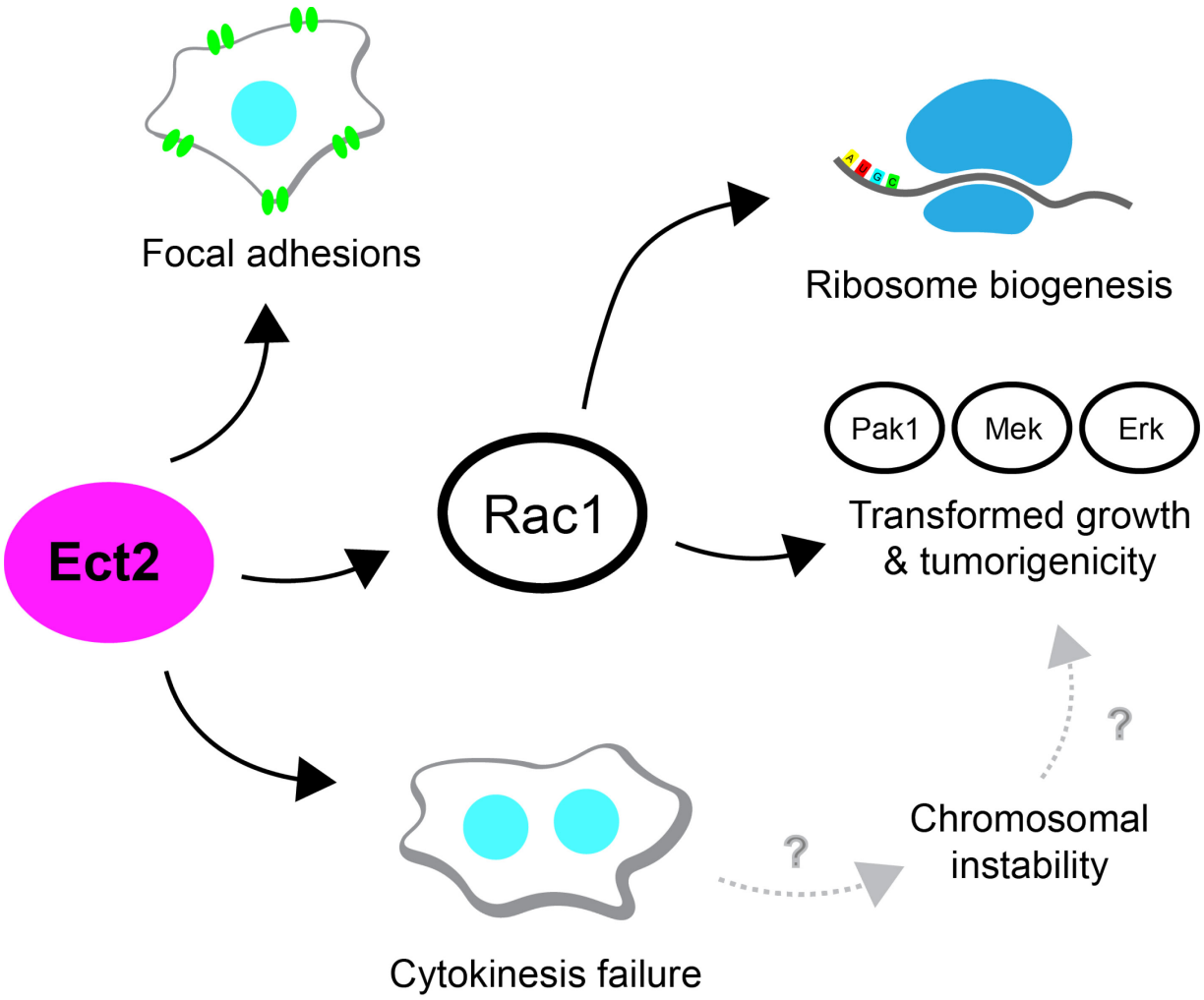

Figure 24. Ect2 could contribute to tumourigenesis through cytokinesis failure.

Ect2 is overexpressed in many cancers, and the presence of cytoplasmic Ect2 is associated with a poor prognosis (Fields and Justilien, 2010; Kosibaty et al., 2019; Cook et al., 2021; Yi et al., 2022). Ect2 is proposed to contribute to tumourigenesis through Rac1 and potentially through focal adhesion kinase (FAK). We propose that cytoplasmic Ect2 could contribute to tumourigenesis through cytokinesis failure. Tetraploid cell division is error-prone, and often leads to aneuploid cells, which are associated with cancer (Lens and Medema, 2019).

interactors on our list were members of the importin-α and nuclear pore complex proteins. We focused on proteins that appeared likely to regulate actin or microtubules. Using a pull-down assay, we confirmed binding for abi-2, dyskerin and Dock7. Our results show that annexin A1 may bind weakly to importin-β1 and is potentially required for cytokinesis. Among high-confidence interactors were also the formin mDia2, sumoylation proteins SUMO-1 and SUMO-5, the microtubule polymerizer CKAP5 (Ch-TOG), and the actin-binding protein Shootin-1. This section will focus on proteins which are more likely to contribute to cytokinesis.

The formin mDia2 is required for cytokinesis and has been shown to interact with importin-β1 (Miki et al., 2009; Shao et al., 2015). Interestingly, mDia2 has both NLSs and NESs, which explains its cytosolic localization in interphase (Miki et al., 2009). During cytokinesis, mDia2 localizes to the equatorial cortex and nucleates actin filaments for the contractile ring (Watanabe et al., 2008, 2010; Chen et al., 2017; Shah et al., 2024). Binding to RhoA activates mDia2 by relieving its auto-inhibition. Similar to both anillin and Ect2, mDia2 has an N-terminal NLS, which is functional, and is reported to also have a cryptic C-terminal NLS (Copeland et al., 2007). This raises the possibility that importins can promote mDia2 function by binding to either or both NLSs, potentially stabilizing the active conformation after RhoA binding (Figure 23).

The role of unbranched actin filaments – a contractile ring component – is well established, but it is less clear whether branched actin filaments are required. They have been proposed to regulate cortical stiffness in the dividing cell (Canman et al., 2008; Zhuravlev et al., 2017). Recently, an actin ‘plug’ made of branched F-actin was shown to be required in abscission to spatially restrict the ESCRT-III complex in the intercellular bridge (Advedissian et al., 2024). One pathway for branched actin nucleation is through the GTPase Rac1, which recruits the WAVE complex to activate the branched actin nucleator Arp2/3 (Gautreau et al., 2022). Interestingly, our

TurboID assay identified Dock7, a GEF for Rac1, and abi-2, a member of the WAVE complex. We found that the C-terminus of Dock7 localizes to the midbody, but not abi-2. The localization of this GEF raises the possibility that it activates Rac1, potentially for this actin plug, and this may be importin-regulated. Since we were not able to clone the entire Dock7 sequence, future work must first validate this midbody localization with full-length Dock7 (Figure 23). Since abi-2 did not localize to any specific structures during mitosis, it is unclear if it has a role in cytokinesis. Abi-2 was shown to localize to adherens junctions, but it is unclear if these were the puncta we observed (Grove et al., 2004). Whether importins can regulate branched actin nucleation during cytokinesis warrants further exploration.

How importins regulate protein function is a fascinating question. They have been proposed to act as chaperones (Patrick Lusk et al., 2002; Padavannil et al., 2019). Our previous findings that importin-binding facilitates anillin's recruitment at the cortex supports this model (Beaudet et al., 2017, 2020). Interestingly, NLSs are often located near or inside disordered regions, and this is the case for the NLSs of both anillin and Ect2. Because disordered regions are highly dynamic, an appealing model is that importin-binding may stabilize these regions, inducing a conformational change that alters the accessibility of the protein for binding partners. In support of this, modeling of the chromatin protein HP1γ showed that its disordered regions are less dynamic in complex with importin-α (Velez et al., 2016). It is unclear whether importins can induce a secondary structure when binding a disordered region, and this is likely to differ depending on the protein partner. For instance, the transcription activator domain (TAD) of p53 is disordered, but becomes helical when bound to MDM2 (Kussie et al., 1996). In docking simulations, the disordered region of the nuclear protein NUP1RL remained disordered even when bound to importin-α3, but binding appeared to shift the region from random coils to a turn-

like structure (Neira et al., 2020a; b). Future research can answer how importins induce structural changes to regulate protein function.

Our TurboID assay did not reproducibility identify anillin, Ect2 and Mklp1, despite experimental evidence of importin-binding or the presence of NLSs. We found one or more of these proteins in one experiment, but not in all three. We also found septins, a binding partner for anillin with low confidence. The reasons for not identifying them more reproducibly may involve differences in protein abundance and affinity. In Chapter 4, we compared our complete list of interactors, indiscriminate of confidence score, with BioGRID, and found that proteins which scored low on our list had been identified as interactors by other groups. This supports the notion that proteomics approaches purify different complexes and can complement one another (Lambert et al., 2015). Affinity purification of the midbody interactome using anillin, Ect2 and Mklp1 as bait proteins did identify importin-β1 as an interactor (Capalbo et al., 2019).

5.5. Future directions

The work described in this thesis opens the door to several different avenues of research. A natural continuation is further investigation of the PBC in the regulation of Ect2 localization, including lipid-binding assays and uncovering how the BRCTs inhibit the PBC. To further explore the role of the Ran-importin pathway in cytokinesis, we recommend studying Cyk4, Mklp1, mDia2 and Dock7 as potential targets. This will involve mapping and/or mutating the NLSs, performing rescue assays and characterizing localization, as was done previously for anillin, and here for Ect2 (Beaudet et al., 2017, 2020).

A complete understanding of how importins regulate proteins will require structural insight into how the monomers differ compared to the heterodimer (α/β). As discussed previously, the disordered regions on which NLSs tend to map are highly dynamic and thus do not adopt a single stable conformation. Because disordered regions cannot be crystallized, using a combination of cryogenic electron microscopy (cryo-EM) and nuclear magnetic resonance (NMR) may be a suitable approach (Musselman and Kutateladze, 2021). Since NMR does not require structural homogeneity, it can be used to sample higher resolution information about the protein or complex. This information could then be combined with structural data from cryo-EM, which already requires a computational framework to construct a 3D structure from multiple images. This approach could determine if importins trigger conformational transitions of these disordered regions or, at the very least, if they become less dynamic.

The work performed in this thesis used HeLa and HEK293T cells, which have hyperploidy. Cells with higher ploidy could have more RCC1, generating a steeper Ran-GTP gradient near chromatin (Hasegawa et al., 2013). This was proposed to promote mitotic spindle assembly in cells with hyperploidy. This raises the possibility that cancer cells may hi-jack the Ran pathway to ensure robust mitosis. It is unclear what consequences this steeper gradient could have on cytokinesis. A steeper gradient would lead to a higher threshold of importins in the equatorial plane to promote the cortical enrichment of contractile proteins there, while importins would fall below a threshold at the poles near chromatin. This could ensure a robust concentration of contractile proteins at the equatorial cortex for cell division. Cytoplasmic Ect2 is associated with poor prognosis in various cancer types, as mentioned previously. We show that cytoplasmic Ect2 can cause cytokinesis failure in both HeLa and HEK293T cells. Whether Ect2 can promote cancer through cytokinesis failure is an important question. The only reports of tetraploid cells becoming aneuploid and forming tumours are in mice (Fujiwara et al., 2005; Lv et al., 2012). Evidence of

the same in human cells is lacking. Determining whether cancer cells rely on the Ran pathway more than healthy cells and if cytokinesis failure can contribute to tumourigenesis could better guide the development of therapeutics.

Finally, the future of cell biology must include the study of healthy cells, beyond diseased models. Most of our knowledge in cytokinesis is from experiments using HeLa cells, including this work. The utility of cancer cell lines cannot be overstated, especially in the context of therapeutics and disease, but they cannot reflect healthy cell biology. Induced pluripotent stem cells (iPSCs) are emerging as a new model for both cell biology research and therapeutics. While still challenging to manipulate and cost-prohibitive, iPSCs enable the study of different cell types in an isogenic background. Recently, our lab engineered an endogenous split-mNeonGreen parental iPSC line to study proteins at endogenous levels (Husser et al., 2024). This tool improves tagging efficiency of proteins of interest, since only the small fragment of mNeonGreen needs to be inserted into the locus. Using this cell line, we tagged anillin, RhoA, tubulin and actin with mNeonGreen, and visualized their localization in dividing iPSCs. Compared to HeLa, we found that anillin localizes to the equatorial cortex earlier in iPSCs, and the breadth of RhoA localization is broader (Husser et al., 2024). In iPSCs, we also observed that the central spindle appears to be weaker, and astral microtubules extend further into the equatorial region. Studying healthy cells will allow us to better discriminate between the proteins and pathways used in cancer cells vs. healthy cells, and may help in the design of therapeutics.

References

Adriaans, I.E., A. Basant, B. Ponsioen, M. Glotzer, and S.M.A. Lens. 2019. PLK1 plays dual roles in centralspindlin regulation during cytokinesis. *J. Cell Biol.* 218:1250–1264. doi:10.1083/jcb.201805036.

Advedissian, T., S. Frémont, and A. Echard. 2024. Cytokinetic abscission requires actin-dependent microtubule severing. *Nat. Commun.* 15:25–28. doi:10.1038/s41467-024-46062-9.

Alawi, F., and P. Lin. 2013. Dyskerin localizes to the mitotic apparatus and is required for orderly mitosis in human cells. *PLoS One*. 8. doi:10.1371/journal.pone.0080805.

Albee, A.J., W. Tao, and C. Wiese. 2006. Phosphorylation of maskin by Aurora-A is regulated by RanGTP and importin β. *J. Biol. Chem.* 281:38293–38301. doi:10.1074/jbc.M607203200.

El Amine, N., A. Kechad, S. Jananji, and G.R.X. Hickson. 2013. Opposing actions of septins and Sticky on Anillin promote the transition from contractile to midbody ring. *J. Cell Biol.* 203:487–504. doi:10.1083/jcb.201305053.

Angrisani, A., M. Turano, L. Paparo, C. Di Mauro, and M. Furia. 2011. A new human dyskerin isoform with cytoplasmic localization. *Biochim. Biophys. Acta - Gen. Subj.* 1810:1361–1368. doi:10.1016/j.bbagen.2011.07.012.

Bah, A., and J.D. Forman-Kay. 2016. Modulation of intrinsically disordered protein function by post-translational modifications. *J. Biol. Chem.* 291:6696–6705. doi:10.1074/jbc.R115.695056.

Basant, A., and M. Glotzer. 2018. Spatiotemporal Regulation of RhoA during Cytokinesis. *Curr. Biol.* 28:R570–R580. doi:10.1016/j.cub.2018.03.045.

Basant, A., S. Lekomtsev, Y.C. Tse, D. Zhang, K.M. Longhini, M. Petronczki, and M. Glotzer. 2015. Aurora B Kinase Promotes Cytokinesis by Inducing Centralspindlin Oligomers that Associate with the Plasma Membrane. *Dev. Cell*. 33:204–215. doi:10.1016/j.devcel.2015.03.015.

Beaudet, D., T. Akhshi, J. Phillipp, C. Law, and A. Piekny. 2017. Active Ran regulates anillin function during cytokinesis. *Mol. Biol. Cell*. 28:3517–3531. doi:10.1091/mbc.E17-04-0253.

Beaudet, D., N. Pham, N. Skaik, and A. Piekny. 2020. Importin binding mediates the intramolecular regulation of anillin during cytokinesis. *Mol. Biol. Cell*. 31:1124–1139. doi:10.1091/mbc.E20-01-0006.

Bement, W.M., H.A. Benink, and G. Von Dassow. 2005. A microtubule-dependent zone of active RhoA during cleavage plane specification. *J. Cell Biol.* 170:91–101. doi:10.1083/jcb.200501131.

Benaud, C., G. Le Dez, S. Mironov, F. Galli, D. Reboutier, and C. Prigent. 2015. Annexin A2 is required for the early steps of cytokinesis. *EMBO Rep.* 16:481–489. doi:10.15252/embr.201440015.

Blower, M.D., M. Nachury, R. Heald, and K. Weis. 2005. A Rae1-containing ribonucleoprotein complex is required for mitotic spindle assembly. *Cell*. 121:223–234. doi:10.1016/j.cell.2005.02.016.

Branon, T.C., J.A. Bosch, A.D. Sanchez, N.D. Udeshi, T. Svinkina, S.A. Carr, J.L. Feldman, N. Perrimon, and A.Y. Ting. 2018. Efficient proximity labeling in living cells and organisms with TurboID. *Nat. Biotechnol.* 36:880–898. doi:10.1038/nbt.4201.

Bringmann, H., and A.A. Hyman. 2005. A cytokinesis furrow is positioned by two consecutive

signals. *Nature*. 436:731–734. doi:10.1038/nature03823.

Brouhard, G.J., J.H. Stear, T.L. Noetzel, J. Al-Bassam, K. Kinoshita, S.C. Harrison, J. Howard, and A.A. Hyman. 2008. XMAP215 Is a Processive Microtubule Polymerase. *Cell*. 132:79–88. doi:10.1016/j.cell.2007.11.043.

Brownlee, C., and R. Heald. 2019. Importin α Partitioning to the Plasma Membrane Regulates Intracellular Scaling. *Cell*. 176:805-815.e8. doi:10.1016/j.cell.2018.12.001.

Budnar, S., K.B. Husain, G.A. Gomez, M. Naghibosadat, A. Varma, S. Verma, N.A. Hamilton, R.G. Morris, and A.S. Yap. 2019. Anillin Promotes Cell Contractility by Cyclic Resetting of RhoA Residence Kinetics. *Dev. Cell*. 49:894-906.e12. doi:10.1016/j.devcel.2019.04.031.

Cabernard, C., K.E. Prehoda, and C.Q. Doe. 2010. A spindle-independent cleavage furrow positioning pathway. *Nature*. 467:91–94. doi:10.1038/nature09334.

Canman, J.C., D.B. Hoffman, and E.D. Salmon. 2000. The role of pre- and post-anaphase microtubules in the cytokinesis phase of the cell cycle. *Curr. Biol.* 10:611–614. doi:10.1016/S0960-9822(00)00490-5.

Canman, J.C., L. Lewellyn, K. Laband, S.J. Smerdon, A. Desai, B. Bowerman, and K. Oegema. 2008. Inhibition of Rac by the GAP Activity of Centralspindlin Is Essential for Cytokinesis. *Science (80-.).* 322:1543–1546. doi:10.1126/science.1163086.

Capalbo, L., Z.I. Bassi, M. Geymonat, S. Todesca, L. Copoiu, A.J. Enright, G. Callaini, M.G. Riparbelli, L. Yu, J.S. Choudhary, E. Ferrero, S. Wheatley, M.E. Douglas, M. Mishima, and P.P. D'Avino. 2019. The midbody interactome reveals unexpected roles for PP1 phosphatases in cytokinesis. *Nat. Commun.* 10:4513. doi:10.1038/s41467-019-12507-9.

Carim, S.C., A. Kechad, and G.R.X. Hickson. 2020. Animal Cell Cytokinesis: The Rho-Dependent

Actomyosin-Anilloseptin Contractile Ring as a Membrane Microdomain Gathering, Compressing, and Sorting Machine. *Front. Cell Dev. Biol.* 8. doi:10.3389/fcell.2020.575226.

Carlton, J.G., M. Agromayor, and J. Martin-Serrano. 2008. Differential requirements for Alix and ESCRT-III in cytokinesis and HIV-1 release. *Proc. Natl. Acad. Sci. U. S. A.* 105:10541–10546. doi:10.1073/pnas.0802008105.

Chalamalasetty, R.B., S. Hümmer, E.A. Nigg, and H.H.W. Silljé. 2006. Influence of human Ect2 depletion and overexpression on cleavage furrow formation and abscission. *J. Cell Sci.* 119:3008–3019. doi:10.1242/jcs.03032.

Chen, A., T.K. Akhshi, B.D. Lavoie, and A. Wilde. 2015. Importin β2 Mediates the Spatio-temporal Regulation of Anillin through a Noncanonical Nuclear Localization Signal. *J. Biol. Chem.* 290:13500–13509. doi:10.1074/jbc.M115.649160.

Chen, A., P.D. Arora, C.A. McCulloch, and A. Wilde. 2017. Cytokinesis requires localized β-actin filament production by an actin isoform specific nucleator. *Nat. Commun.* 8. doi:10.1038/s41467-017-01231-x.

Chen, A., L. Ulloa Severino, T.C. Panagiotou, T.F. Moraes, D.A. Yuen, B.D. Lavoie, and A. Wilde. 2021. Inhibition of polar actin assembly by astral microtubules is required for cytokinesis. *Nat. Commun.* 12:1–13. doi:10.1038/s41467-021-22677-0.

Chen, M., H. Pan, L. Sun, P. Shi, Y. Zhang, L. Li, Y. Huang, J. Chen, P. Jiang, X. Fang, C. Wu, and Z. Chen. 2020. Structure and regulation of human epithelial cell transforming 2 protein. *Proc. Natl. Acad. Sci. U. S. A.* 117:1027–1035. doi:10.1073/pnas.1913054117.

Chen, Z., D. Borek, S.B. Padrick, T.S. Gomez, Z. Metlagel, A.M. Ismail, J. Umetani, D.D. Billadeau, Z. Otwinowski, and M.K. Rosen. 2010. Structure and control of the actin regulatory

WAVE complex. *Nature*. 468:533–538. doi:10.1038/nature09623.

Chircop, M. 2014. Rho GTPases as regulators of mitosis and cytokinesis in mammalian cells. *Small GTPases*. 5. doi:10.4161/sgtp.29770.

Clarke, P.R., and C. Zhang. 2008. Spatial and temporal coordination of mitosis by Ran GTPase. *Nat. Rev. Mol. Cell Biol.* 9:464–477. doi:10.1038/nrm2410.

Clifford, D.M., B.A. Wolfe, R.H. Roberts-Galbraith, W.H. McDonald, J.R. Yates, and K.L. Gould. 2008. The Clp1/Cdc14 phosphatase contributes to the robustness of cytokinesis by association with anillin-related Mid1. *J. Cell Biol.* 181:79–88. doi:10.1083/jcb.200709060.

Connell, J.W., C. Lindon, J.P. Luzio, and E. Reid. 2009. Spastin couples microtubule severing to membrane traffic in completion of cytokinesis and secretion. *Traffic*. 10:42–56. doi:10.1111/j.1600-0854.2008.00847.x.

Cook, D.R., M. Kang, T.D. Martin, J.A. Galanko, G.H. Loeza, D.G. Trembath, V. Justilien, K.A. Pickering, D.F. Vincent, A. Jarosch, P. Jurmeister, A.M. Waters, P.S. Hibshman, A.D. Campbell, C.A. Ford, T.O. Keku, J.J. Yeh, M.S. Lee, A.D. Cox, A.P. Fields, R.S. Sandler, O.J. Sansom, C. Sers, A. Schaefer, and C.J. Der. 2021. Aberrant Expression and Subcellular Localization of ECT2 Drives Colorectal Cancer Progression and Growth. *Cancer Res.* 82:90–104. doi:10.1158/0008-5472.CAN-20-4218.

Copeland, S.J., B.J. Green, S. Burchat, G.A. Papalia, D. Banner, and J.W. Copeland. 2007. The diaphanous inhibitory domain/diaphanous autoregulatory domain interaction is able to mediate heterodimerization between mDia1 and mDia2. *J. Biol. Chem.* 282:30120–30130. doi:10.1074/jbc.M703834200.

Crasta, K., N.J. Ganem, R. Dagher, A.B. Lantermann, E. V. Ivanova, Y. Pan, L. Nezi, A.

Protopopov, D. Chowdhury, and D. Pellman. 2012. DNA breaks and chromosome pulverization from errors in mitosis. *Nature*. 482:53–58. doi:10.1038/nature10802.

Dambournet, D., M. MacHicoane, L. Chesneau, M. Sachse, M. Rocancourt, A. El Marjou, E. Formstecher, R. Salomon, B. Goud, and A. Echard. 2011. Rab35 GTPase and OCRL phosphatase remodel lipids and F-actin for successful cytokinesis. *Nat. Cell Biol.* 13:981–988. doi:10.1038/ncb2279.

Echard, A. 2008. Membrane traffic and polarization of lipid domains during cytokinesis. *Biochem. Soc. Trans.* 36:395–399. doi:10.1042/BST0360395.

Elia, N., G. Fabrikant, M.M. Kozlov, and J. Lippincott-Schwartz. 2012. Computational model of cytokinetic abscission driven by ESCRT-III polymerization and remodeling. *Biophys. J.* 102:2309–2320. doi:10.1016/j.bpj.2012.04.007.

Ems-McClung, S.C., Y. Zheng, and C.E. Walczak. 2004. Importin α/β and Ran-GTP Regulate XCTK2 Microtubule Binding through a Bipartite Nuclear Localization Signal. *Mol. Biol. Cell*. 15:46–57. doi:10.1091/mbc.e03-07-0454.

Engler, C., R. Kandzia, and S. Marillonnet. 2008. A One Pot, One Step, Precision Cloning Method with High Throughput Capability. *PLoS One*. 3:e3647. doi:10.1371/journal.pone.0003647.

Estey, M.P., C. Di Ciano-Oliveira, C.D. Froese, M.T. Bejide, and W.S. Trimble. 2010. Distinct roles of septins in cytokinesis: SEPT9 mediates midbody abscission. *J. Cell Biol.* 191:741–749. doi:10.1083/jcb.201006031.

Field, C.M., and B.M. Alberts. 1995. Anillin, a contractile ring protein that cycles from the nucleus to the cell cortex. *J. Cell Biol.* 131:165–178. doi:10.1083/jcb.131.1.165.

Fields, A.P., and V. Justilien. 2010. The guanine nucleotide exchange factor (GEF) Ect2 is an

oncogene in human cancer. *Adv. Enzyme Regul.* 50:190–200. doi:10.1016/j.advenzreg.2009.10.010.

Forwood, J.K., M.H.C. Lam, and D.A. Jans. 2001. Nuclear import of Creb and AP-1 transcription factors requires importin-β1 and Ran but is independent of importin-α. *Biochemistry*. 40:5208–5217. doi:10.1021/bi002732+.

Frémont, S., and A. Echard. 2018. Membrane Traffic in the Late Steps of Cytokinesis. *Curr. Biol.* 28:R458–R470. doi:10.1016/j.cub.2018.01.019.

Frenette, P., E. Haines, M. Loloyan, M. Kinal, P. Pakarian, and A. Piekny. 2012. An anillin-ect2 complex stabilizes central spindle microtubules at the cortex during cytokinesis. *PLoS One*. 7. doi:10.1371/journal.pone.0034888.

Fujiwara, T., M. Bandi, M. Nitta, E. V. Ivanova, R.T. Bronson, and D. Pellman. 2005. Cytokinesis failure generating tetraploids promotes tumorigenesis in p53-null cells. *Nature*. 437:1043–1047. doi:10.1038/nature04217.

Ganem, N.J., S.A. Godinho, and D. Pellman. 2009. A mechanism linking extra centrosomes to chromosomal instability. *Nature*. 460:278–282. doi:10.1038/nature08136.

Gautreau, A.M., F.E. Fregoso, G. Simanov, and R. Dominguez. 2022. Nucleation, stabilization, and disassembly of branched actin networks. *Trends Cell Biol.* 32:421–432. doi:10.1016/j.tcb.2021.10.006.

Gergely, F., V.M. Draviam, and J.W. Raff. 2003. The ch-TOG/XMAP215 protein is essential for spindle pole organization in human somatic cells. *Genes Dev.* 17:336–341. doi:10.1101/gad.245603.

Glotzer, M. 2013. Cytokinesis: Centralspindlin Moonlights as a Membrane Anchor. *Curr. Biol.*

23:R145–R147. doi:10.1016/j.cub.2013.01.006.

Glotzer, M. 2017. Cytokinesis in metazoa and fungi. *Cold Spring Harb. Perspect. Biol.* 9:1–18. doi:10.1101/cshperspect.a022343.

Gómez-Cavazos, J.S., K.Y. Lee, P. Lara-González, Y. Li, A. Desai, A.K. Shiau, and K. Oegema. 2020. A Non-canonical BRCT-Phosphopeptide Recognition Mechanism Underlies RhoA Activation in Cytokinesis. *Curr. Biol.* 30:3101-3115.e11. doi:10.1016/j.cub.2020.05.090.

Green, R.A., E. Paluch, K. Oegema, and R. Rappaport. 2012. Cytokinesis in Animal Cells. *Annu. Rev. Cell Dev. Biol.* 31:169–214. doi:10.1016/S0074-7696(08)60059-5.

Grove, M., G. Demyanenko, A. Echarri, P.A. Zipfel, M.E. Quiroz, R.M. Rodriguiz, M. Playford, S.A. Martensen, M.R. Robinson, W.C. Wetsel, P.F. Maness, and A.M. Pendergast. 2004. Abi2-Deficient Mice Exhibit Defective Cell Migration, Aberrant Dendritic Spine Morphogenesis, and Deficits in Learning and Memory. *Mol. Cell. Biol.* 24:10905–10922. doi:10.1128/mcb.24.24.10905-10922.2004.

Guizetti, J., L. Schermelleh, J. Mäntler, S. Maar, I. Poser, H. Leonhardt, T. Müller-Reichert, and D.W. Gerlich. 2011. Cortical Constriction During Abscission Involves Helices of ESCRT-III–Dependent Filaments. *Science (80-.).* 331:1616–1620. doi:10.1126/science.1201847.

Hanahan, D., and R.A. Weinberg. 2011. Hallmarks of Cancer: The Next Generation. *Cell*. 144:646–674. doi:10.1016/j.cell.2011.02.013.

Hasegawa, K., S.J. Ryu, and P. Kaláb. 2013. Chromosomal gain promotes formation of a steep RanGTP gradient that drives mitosis in aneuploid cells. *J. Cell Biol.* 200:151–161. doi:10.1083/jcb.201206142.

He, B., N. Gnawali, A.W. Hinman, A.J. Mattingly, A. Osimani, and D. Cimini. 2019. Chromosomes

missegregated into micronuclei contribute to chromosomal instability by missegregating at the next division. *Oncotarget*. 10:2660–2674. doi:10.18632/oncotarget.26853.

Herman, J.A., M.P. Miller, and S. Biggins. 2020. chTOG is a conserved mitotic error correction factor. *Elife*. 9. doi:10.7554/eLife.61773.

Hintzen, D.C., M. Soto, M. Schubert, B. Bakker, D.C.J. Spierings, K. Szuhai, P.M. Lansdorp, R.J.C. Kluin, F. Foijer, R.H. Medema, and J.A. Raaijmakers. 2022. The impact of monosomies, trisomies and segmental aneuploidies on chromosomal stability. *PLoS One*. 17:1–27. doi:10.1371/journal.pone.0268579.

Hirata, D., T. Yamabuki, D. Miki, T. Ito, E. Tsuchiya, M. Fujita, M. Hosokawa, K. Chayama, Y. Nakamura, and Y. Daigo. 2009. Involvement of epithelial cell transforming sequence-2 oncoantigen in lung and esophageal Cancer progression. *Clin. Cancer Res.* 15:256–266. doi:10.1158/1078-0432.CCR-08-1672.

Husser, M.C., N.P. Pham, C. Law, F.R. Araujo, V.J. Martin, and A. Piekny. 2024. Endogenous tagging using split mNeonGreen in human iPSCs for live imaging studies. *Elife*. 12:1–28. doi:10.7554/elife.92819.3.

Jeong, S., J. Ahn, I. Jo, S.M. Kang, B.J. Park, H.S. Cho, Y.H. Kim, and N.C. Ha. 2022. Cyclin-dependent kinase 1 depolymerizes nuclear lamin filaments by disrupting the head-to-tail interaction of the lamin central rod domain. *J. Biol. Chem.* 298:102256. doi:10.1016/j.jbc.2022.102256.

Justilien, V., and A.P. Fields. 2009. Ect2 links the PKC-Par6α complex to Rac1 activation and cellular transformation. *Oncogene*. 28:3597–3607. doi:10.1038/onc.2009.217.

Justilien, V., K.C. Lewis, N.R. Murray, and A.P. Fields. 2019. Oncogenic Ect2 signaling regulates

rRNA synthesis in NSCLC. *Small GTPases*. 10:388–394. doi:10.1080/21541248.2017.1335274.

Kaláb, P., A. Pralle, E.Y. Isacoff, R. Heald, and K. Weis. 2006. Analysis of a RanGTP-regulated gradient in mitotic somatic cells. *Nature*. 440:697–701. doi:10.1038/nature04589.

Kalab, P., K. Weis, and R. Heald. 2002. Visualization of a Ran-GTP gradient in interphase and mitotic Xenopus egg extracts. *Science (80-.).* 295:2452–2456. doi:10.1126/science.1068798.

Kamasaki, T., E. O'Toole, S. Kita, M. Osumi, J. Usukura, R.R. McIntosh, and G. Goshima. 2013. Augmin-dependent microtubule nucleation at microtubule walls in the spindle. *J. Cell Biol.* 202:25–32. doi:10.1083/jcb.201304031.

Kamijo, K., N. Ohara, M. Abe, T. Uchimura, H. Hosoya, J.-S. Lee, and T. Miki. 2006. Dissecting the Role of Rho-mediated Signaling in Contractile Ring Formation. *Mol. Biol. Cell*. 17:43–55. doi:10.1091/mbc.e05-06-0569.

Karg, T., B. Warecki, and W. Sullivan. 2015. Aurora B-mediated localized delays in nuclear envelope formation facilitate inclusion of late-segregating chromosome fragments. *Mol. Biol. Cell*. 26:2227–2241. doi:10.1091/mbc.E15-01-0026.

Kastian, R.F., T. Minegishi, K. Baba, T. Saneyoshi, H. Katsuno-Kambe, S. Saranpal, Y. Hayashi, and N. Inagaki. 2021. Shootin1a-mediated actin-adhesion coupling generates force to trigger structural plasticity of dendritic spines. *Cell Rep.* 35. doi:10.1016/j.celrep.2021.109130.

Kechad, A., S. Jananji, Y. Ruella, and G.R.X. Hickson. 2012. Anillin acts as a bifunctional linker coordinating midbody ring biogenesis during cytokinesis. *Curr. Biol.* 22:197–203. doi:10.1016/j.cub.2011.11.062.

Kim, J.E., D.D. Billadeau, and J. Chen. 2005. The tandem BRCT domains of Ect2 are required for both negative and positive regulation of Ect2 in cytokinesis. *J. Biol. Chem.* 280:5733–5739. doi:10.1074/jbc.M409298200.

Kiyomitsu, T., and I.M. Cheeseman. 2013. Cortical dynein and asymmetric membrane elongation coordinately position the spindle in anaphase. *Cell*. 154:391–402. doi:10.1016/j.cell.2013.06.010.

Koh, S.P., N.P. Pham, and A. Piekny. 2021. Seeing is believing: tools to study the role of Rho GTPases during cytokinesis. *Small GTPases*. 1–14. doi:10.1080/21541248.2021.1957384.

Köhler, M., C. Speck, M. Christiansen, F.R. Bischoff, S. Prehn, H. Haller, D. Görlich, and E. Hartmann. 1999. Evidence for Distinct Substrate Specificities of Importin α Family Members in Nuclear Protein Import. *Mol. Cell. Biol.* 19:7782–7791. doi:10.1128/mcb.19.11.7782.

Kosako, H., T. Yoshida, F. Matsumura, T. Ishizaki, S. Narumiya, and M. Inagaki. 2000. Rho-kinase/ROCK is involved in cytokinesis through the phosphorylation of myosin light chain and not ezrin/radixin/moesin proteins at the cleavage furrow. *Oncogene*. 19:6059–6064. doi:10.1038/sj.onc.1203987.

Kosibaty, Z., Y. Murata, Y. Minami, T. Dai, J. Kano, R. Matsuoka, N. Nakano, and M. Noguchi. 2019. Cytoplasmic expression of epithelial cell transforming sequence 2 in lung adenocarcinoma and its implications for malignant progression. *Lab. Investig.* 99:551–567. doi:10.1038/s41374-018-0142-4.

Kosibaty, Z., Y. Murata, Y. Minami, M. Noguchi, and N. Sakamoto. 2021. ECT2 promotes lung adenocarcinoma progression through extracellular matrix dynamics and focal adhesion signaling. *Cancer Sci.* 112:703–714. doi:10.1111/cas.14743.

Kotadia, S., E. Montembault, W. Sullivan, and A. Royou. 2012. Cell elongation is an adaptive response for clearing long chromatid arms from the cleavage plane. *J. Cell Biol.* 199:745–753. doi:10.1083/jcb.201208041.

Kotera, I., T. Sekimoto, Y. Miyamoto, T. Saiwaki, E. Nagoshi, H. Sakagami, H. Kondo, and Y. Yoneda. 2005. Importin α transports CaMKIV to the nucleus without utilizing importin β. *EMBO J.* 24:942–951. doi:10.1038/sj.emboj.7600587.

Kotýnková, K., K.C. Su, S.C. West, and M. Petronczki. 2016. Plasma Membrane Association but Not Midzone Recruitment of RhoGEF ECT2 Is Essential for Cytokinesis. *Cell Rep.* 17:2672–2686. doi:10.1016/j.celrep.2016.11.029.

Kussie, P.H., S. Gorina, V. Marechal, B. Elenbaas, J. Moreau, A.J. Levine, and N.P. Pavletich. 1996. Structure of the MDM2 oncoprotein bound to the p53 tumor suppressor transactivation domain. *Science (80-.).* 274:948–953. doi:10.1126/science.274.5289.948.

Kuznetsova, A.Y., K. Seget, G.K. Moeller, M.S. de Pagter, J.A.D.M. de Roos, M. Dürrbaum, C. Kuffer, S. Müller, G.J.R. Zaman, W.P. Kloosterman, and Z. Storchová. 2015. Chromosomal instability, tolerance of mitotic errors and multidrug resistance are promoted by tetraploidization in human cells. *Cell Cycle*. 14:2810–2820. doi:10.1080/15384101.2015.1068482.

Lambert, J.P., M. Tucholska, C. Go, J.D.R. Knight, and A.C. Gingras. 2015. Proximity biotinylation and affinity purification are complementary approaches for the interactome mapping of chromatin-associated protein complexes. *J. Proteomics*. 118:81–94. doi:10.1016/j.jprot.2014.09.011.

Lee, M.E., W.C. DeLoache, B. Cervantes, and J.E. Dueber. 2015. A Highly Characterized Yeast

Toolkit for Modular, Multipart Assembly. *ACS Synth. Biol.* 4:975–986. doi:10.1021/sb500366v.

Leite, J., D.S. Osorio, A.F. Sobral, A.M. Silva, and A.X. Carvalho. 2019. Network Contractility during Cytokinesis—From Molecular to Global Views. *Biomolecules*. 9:194. doi:10.3390/biom9050194.

Lekomtsev, S., K.C. Su, V.E. Pye, K. Blight, S. Sundaramoorthy, T. Takaki, L.M. Collinson, P. Cherepanov, N. Divecha, and M. Petronczki. 2012. Centralspindlin links the mitotic spindle to the plasma membrane during cytokinesis. *Nature*. 492:276–279. doi:10.1038/nature11773.

Lens, S.M.A., and R.H. Medema. 2019. Cytokinesis defects and cancer. *Nat. Rev. Cancer*. 19:32–45. doi:10.1038/s41568-018-0084-6.

Lewellyn, L., J. Dumont, A. Desai, and K. Oegema. 2010. Analyzing the Effects of Delaying Aster Separation on Furrow Formation during Cytokinesis in the Caenorhabditis elegans Embryo. *Mol. Biol. Cell*. 21:50–62. doi:10.1091/mbc.e09-01-0089.

Liot, C., L. Seguin, A. Siret, C. Crouin, S. Schmidt, and J. Bertoglio. 2011. APC cdh1 mediates degradation of the oncogenic Rho-GEF Ect2 after mitosis. *PLoS One*. 6. doi:10.1371/journal.pone.0023676.

Liu, H., and J.H. Naismith. 2008. An efficient one-step site-directed deletion, insertion, single and multiple-site plasmid mutagenesis protocol. *BMC Biotechnol.* 8:91. doi:10.1186/1472-6750-8-91.

Liu, J., G.D. Fairn, D.F. Ceccarelli, F. Sicheri, and A. Wilde. 2012. Cleavage furrow organization requires PIP 2-mediated recruitment of anillin. *Curr. Biol.* 22:64–69.

doi:10.1016/j.cub.2011.11.040.

Liu, X., and R.L. Erikson. 2007. The nuclear localization signal of mitotic kinesin-like protein Mklp-1: Effect on Mklp-1 function during cytokinesis. *Biochem. Biophys. Res. Commun.* 353:960–964. doi:10.1016/j.bbrc.2006.12.142.

Lu, J., T. Wu, B. Zhang, S. Liu, W. Song, J. Qiao, and H. Ruan. 2021. Types of nuclear localization signals and mechanisms of protein import into the nucleus. *Cell Commun. Signal.* 19:1–10. doi:10.1186/s12964-021-00741-y.

Luo, Y., S.-L. Qin, Y.-F. Mu, Z.-S. Wang, M. Zhong, and Z.-Q. Bian. 2015. Elevated expression of ECT2 predicts unfavorable prognosis in patients with colorectal cancer. *Biomed. Pharmacother.* 73:135–139. doi:10.1016/j.biopha.2015.06.007.

Lv, L., T. Zhang, Q. Yi, Y. Huang, Z. Wang, H. Hou, H. Zhang, W. Zheng, Q. Hao, Z. Guo, H.J. Cooke, and Q. Shi. 2012. Tetraploid cells from cytokinesis failure induce aneuploidy and spontaneous transformation of mouse ovarian surface epithelial cells. *Cell Cycle*. 11:2864–2875. doi:10.4161/cc.21196.

Mahlandt, E.K., J.J.G. Arts, W.J. van der Meer, F.H. van der Linden, S. Tol, J.D. van Buul, T.W.J. Gadella, and J. Goedhart. 2021. Visualizing endogenous Rho activity with an improved localization-based, genetically encoded biosensor. *J. Cell Sci.* 134. doi:10.1242/jcs.258823.

Majewski, Ł., M. Sobczak, S. Havrylov, J. Jóźwiak, and M.J. Rędowicz. 2012. Dock7: A GEF for Rho-family GTPases and a novel myosin VI-binding partner in neuronal PC12 cells. *Biochem. Cell Biol.* 90:565–574. doi:10.1139/o2012-009.

Mangal, S., J. Sacher, T. Kim, D.S. Osório, F. Motegi, A.X. Carvalho, K. Oegema, and E. Zanin. 2018. TPXL-1 activates Aurora A to clear contractile ring components from the polar cortex

during cytokinesis. *J. Cell Biol.* 217:837–848. doi:10.1083/jcb.201706021.

Mastop, M., D.S. Bindels, N.C. Shaner, M. Postma, T.W.J. Gadella, and J. Goedhart. 2017. Characterization of a spectrally diverse set of fluorescent proteins as FRET acceptors for mTurquoise2. *Sci. Rep.* 7:11999. doi:10.1038/s41598-017-12212-x.

Mehmood, R., N. Yasuhara, M. Fukumoto, S. Oe, T. Tachibana, and Y. Yoneda. 2011. Cross-talk between distinct nuclear import pathways enables efficient nuclear import of E47 in conjunction with its partner transcription factors. *Mol. Biol. Cell*. 22:3715–3724. doi:10.1091/mbc.E10-10-0809.

Menin, L., J. Weber, S. Villa, E. Martini, E. Maspero, C.A. Niño, V. Cancila, A. Poli, P. Maiuri, A. Palamidessi, E. Frittoli, F. Bianchi, C. Tripodo, K.J. Walters, F. Giavazzi, G. Scita, and S. Polo. 2023. A planar polarized MYO6-DOCK7-RAC1 axis promotes tissue fluidification in mammary epithelia. *Cell Rep.* 42. doi:10.1016/j.celrep.2023.113001.

Mierzwa, B., and D.W. Gerlich. 2014. Cytokinetic Abscission: Molecular Mechanisms and Temporal Control. *Dev. Cell*. 31:525–538. doi:10.1016/j.devcel.2014.11.006.

Miki, T., K. Okawa, T. Sekimoto, Y. Yoneda, S. Watanabe, T. Ishizaki, and S. Narumiya. 2009. mDia2 shuttles between the nucleus and the cytoplasm through the importin-α/β- and CRM1-mediated nuclear transport mechanism. *J. Biol. Chem.* 284:5753–5762. doi:10.1074/jbc.M806191200.

Miki, T., C.L. Smith, J.E. Long, A. Eva, and T.P. Fleming. 1993. Oncogene ect2 is related to regulators of small GTP-binding proteins. *Nature*. 362:462–465. doi:10.1038/362462a0.

Mishima, M., S. Kaitna, and M. Glotzer. 2002. Central spindle assembly and cytokinesis require a kinesin-like protein/RhoGAP complex with microtubule bundling activity. *Dev. Cell*. 2:41–

54. doi:10.1016/S1534-5807(01)00110-1.

Miyamoto, Y., M. Hieda, M.T. Harreman, M. Fukumoto, T. Saiwaki, A.E. Hodel, A.H. Corbett, and Y. Yoneda. 2002. Importin α can migrate into the nucleus in an importin β- and Ran-independent manner. *EMBO J.* 21:5833–5842. doi:10.1093/emboj/cdf569.

Morita, E., V. Sandrin, H.Y. Chung, S.G. Morham, S.P. Gygi, C.K. Rodesch, and W.I. Sundquist. 2007. Human ESCRT and ALIX proteins interact with proteins of the midbody and function in cytokinesis. *EMBO J.* 26:4215–4227. doi:10.1038/sj.emboj.7601850.

Murthy, K., and P. Wadsworth. 2008. Dual role for microtubules in regulating cortical contractility during cytokinesis. *J. Cell Sci.* 121:2350–2359. doi:10.1242/jcs.027052.

Musselman, C.A., and T.G. Kutateladze. 2021. Characterization of functional disordered regions within chromatin-associated proteins. *iScience*. 24:1–11. doi:10.1016/j.isci.2021.102070.

Neira, J.L., B. Rizzuti, A. Jiménez-Alesanco, O. Abián, A. Velázquez-Campoy, and J.L. Iovanna. 2020a. The paralogue of the intrinsically disordered nuclear protein 1 has a nuclear localization sequence that binds to human importin α3. *Int. J. Mol. Sci.* 21:1–19. doi:10.3390/ijms21197428.

Neira, J.L., B. Rizzuti, A. Jiménez-Alesanco, M. Palomino-Schätzlein, O. Abián, A. Velázquez-Campoy, and J.L. Iovanna. 2020b. A phosphorylation-induced switch in the nuclear localization sequence of the intrinsically disordered nupr1 hampers binding to importin. *Biomolecules*. 10:1–22. doi:10.3390/biom10091313.

Nicholson, J.M., and D. Cimini. 2013. Cancer karyotypes: Survival of the fittest. *Front. Oncol.* 3 JUN:1–9. doi:10.3389/fonc.2013.00148.

Nishimura, Y., and S. Yonemura. 2006. Centralspindlin regulates ECT2 and RhoA accumulation

at the equatorial cortex during cytokinesis. *J. Cell Sci.* 119:104–114. doi:10.1242/jcs.02737.

van Oostende Triplet, C., M.J. Garcia, H.H. Bik, D. Beaudet, A. Piekny, C. van Oostende Triplet, M. Jaramillo Garcia, H. Haji Bik, D. Beaudet, and A. Piekny. 2014. Anillin interacts with microtubules and is part of the astral pathway that defines cortical domains. *J. Cell Sci.* 127:3699–3710. doi:10.1242/jcs.147504.

Ozugergin, I., K. Mastronardi, C. Law, and A. Piekny. 2022. Diverse mechanisms regulate contractile ring assembly for cytokinesis in the two-cell Caenorhabditis elegans embryo. *J. Cell Sci.* 135. doi:10.1242/jcs.258921.

Pachitariu, M., M. Rariden, and C. Stringer. 2025. Cellpose-SAM: superhuman generalization for cellular segmentation. doi:10.1101/2025.04.28.651001.

Padavannil, A., P. Sarkar, S.J. Kim, T. Cagatay, J. Jiou, C.A. Brautigam, D.R. Tomchick, A. Sali, S. D'Arcy, and Y.M. Chook. 2019. Importin-9 wraps around the H2A-H2B core to act as nuclear importer and histone chaperone. *Elife*. 8:1–24. doi:10.7554/eLife.43630.

Patrick Lusk, C., T. Makhnevych, M. Marelli, J.D. Aitchison, and R.W. Wozniak. 2002. Karyopherins in nuclear pore biogenesis: A role for Kap121p in the assembly of Nup53p into nuclear pore complexes. *J. Cell Biol.* 159:267–278. doi:10.1083/jcb.200203079.

Peter, M., J. Nakagawa, M. Dorée, J.C. Labbé, and E.A. Nigg. 1990. In vitro disassembly of the nuclear lamina and M phase-specific phosphorylation of lamins by cdc2 kinase. *Cell*. 61:591–602. doi:10.1016/0092-8674(90)90471-P.

Peterman, E., P. Gibieža, J. Schafer, V.A. Skeberdis, A. Kaupinis, M. Valius, X. Heiligenstein, I. Hurbain, G. Raposo, and R. Prekeris. 2019. The post-abscission midbody is an intracellular signaling organelle that regulates cell proliferation. *Nat. Commun.* 10. doi:10.1038/s41467-

019-10871-0.

Petronczki, M., M. Glotzer, N. Kraut, and J.M. Peters. 2007. Polo-like Kinase 1 Triggers the Initiation of Cytokinesis in Human Cells by Promoting Recruitment of the RhoGEF Ect2 to the Central Spindle. *Dev. Cell*. 12:713–725. doi:10.1016/j.devcel.2007.03.013.

Piekny, A.J., and M. Glotzer. 2008. Anillin Is a Scaffold Protein That Links RhoA, Actin, and Myosin during Cytokinesis. *Curr. Biol.* 18:30–36. doi:10.1016/j.cub.2007.11.068.

Piekny, A.J., and A.S. Maddox. 2010. The myriad roles of Anillin during cytokinesis. *Semin. Cell Dev. Biol.* 21:881–891. doi:10.1016/j.semcdb.2010.08.002.

Prosser, S.L., and L. Pelletier. 2017. Mitotic spindle assembly in animal cells: a fine balancing act. *Nat. Rev. Mol. Cell Biol.* 18:187–201. doi:10.1038/nrm.2016.162.

Rodrigues, N.T.L., S. Lekomtsev, S. Jananji, J. Kriston-Vizi, G.R.X. Hickson, and B. Baum. 2015. Kinetochore-localized PP1-Sds22 couples chromosome segregation to polar relaxation. *Nature*. 524:489–492. doi:10.1038/nature14496.

Rodriguez-Muñoz, M., T. Anglada, and A. Genescà. 2022. A matter of wrapper: Defects in the nuclear envelope of lagging and bridging chromatin threatens genome integrity. *Semin. Cell Dev. Biol.* 123:124–130. doi:10.1016/j.semcdb.2021.03.004.

Rose, R., M. Weyand, M. Lammers, T. Ishizaki, M.R. Ahmadian, and A. Wittinghofer. 2005. Structural and mechanistic insights into the interaction between Rho and mammalian Dia. *Nature*. 435:513–518. doi:10.1038/nature03604.

Saito, S., X.F. Liu, K. Kamijo, R. Raziuddin, T. Tatsumoto, I. Okamoto, X. Chen, C.C. Lee, M. V. Lorenzi, N. Ohara, and T. Miki. 2004. Deregulation and Mislocalization of the Cytokinesis Regulator ECT2 Activate the Rho Signaling Pathways Leading to Malignant Transformation.

J. Biol. Chem. 279:7169–7179. doi:10.1074/jbc.M306725200.

Salhia, B., N.L. Tran, A. Chan, A. Wolf, M. Nakada, F. Rutka, M. Ennis, W.S. McDonough, M.E. Berens, M. Symons, and J.T. Rutka. 2008. The guanine nucleotide exchange factors Trio, Ect2, and Vav3 mediate the invasive behavior of glioblastoma. *Am. J. Pathol.* 173:1828–1838. doi:10.2353/ajpath.2008.080043.

Sano, M., N. Genkai, N. Yajima, N. Tsuchiya, J. Homma, R. Tanaka, T. Miki, and R. Yamanaka. 2006. Expression level of ECT2 proto-oncogene correlates with prognosis in glioma patients. *Oncol. Rep.* 16:1093–1098. doi:10.3892/or.16.5.1093.

Saurin, A.T., J. Durgan, A.J. Cameron, A. Faisal, M.S. Marber, and P.J. Parker. 2008. The regulated assembly of a PKCe complex controls the completion of cytokinesis. *Nat. Cell Biol.* 10:891–901. doi:10.1038/ncb1749.

Schatz, C.A., R. Santarella, A. Hoenger, E. Karsenti, I.W. Mattaj, O.J. Gruss, and R.E. Carazo-Salas. 2003. Importin α-regulated nucleation of microtubules by TPX2. *EMBO J.* 22:2060–2070. doi:10.1093/emboj/cdg195.

Schiel, J.A., G.C. Simon, C. Zaharris, J. Weisz, D. Castle, C.C. Wu, and R. Prekeris. 2012. FIP3-endosome-dependent formation of the secondary ingression mediates ESCRT-III recruitment during cytokinesis. *Nat. Cell Biol.* 14:1068–1078. doi:10.1038/ncb2577.

Shah, R., T.C. Panagiotou, G.B. Cole, T.F. Moraes, B.D. Lavoie, C.A. McCulloch, and A. Wilde. 2024. The DIAPH3 linker specifies a β-actin network that maintains RhoA and Myosin-II at the cytokinetic furrow. *Nat. Commun.* 15:1–17. doi:10.1038/s41467-024-49427-2.

Shao, X., K. Kawauchi, G. V. Shivashankar, and A.D. Bershadsky. 2015. Novel localization of formin mDia2: importin β-mediated delivery to and retention at the cytoplasmic side of the

nuclear envelope. *Biol. Open*. 4:1569–1575. doi:10.1242/bio.013649.

Simon, G.C., E. Schonteich, C.C. Wu, A. Piekny, D. Ekiert, X. Yu, G.W. Gould, M. Glotzer, and R. Prekeris. 2008. Sequential Cyk-4 binding to ECT2 and FIP3 regulates cleavage furrow ingression and abscission during cytokinesis. *EMBO J.* 27:1791–1803. doi:10.1038/emboj.2008.112.

Skoufias, D.A., S. DeBonis, Y. Saoudi, L. Lebeau, I. Crevel, R. Cross, R.H. Wade, D. Hackney, and F. Kozielski. 2006. S-Trityl-L-cysteine Is a Reversible, Tight Binding Inhibitor of the Human Kinesin Eg5 That Specifically Blocks Mitotic Progression. *J. Biol. Chem.* 281:17559–17569. doi:10.1074/jbc.M511735200.

Sobczak, M., V. Chumak, P. Pomorski, E. Wojtera, Ł. Majewski, J. Nowak, J. Yamauchi, and M.J. Redowicz. 2016. Interaction of myosin VI and its binding partner DOCK7 plays an important role in NGF-stimulated protrusion formation in PC12 cells. *Biochim. Biophys. Acta - Mol. Cell Res.* 1863:1589–1600. doi:10.1016/j.bbamcr.2016.03.020.

Somers, W.G., and R. Saint. 2003. A RhoGEF and Rho family GTPase-activating protein complex links the contractile ring to cortical microtubules at the onset of cytokinesis. *Dev. Cell*. 4:29–39. doi:10.1016/S1534-5807(02)00402-1.

Soto, M., I. García-Santisteban, L. Krenning, R.H. Medema, and J.A. Raaijmakers. 2018. Chromosomes trapped in micronuclei are liable to segregation errors. *J. Cell Sci.* 131. doi:10.1242/jcs.214742.

Spiliotis, E.T., M. Kinoshita, and W.J. Nelson. 2005. A Mitotic Septin Scaffold Required for Mammalian Chromosome Congression and Segregation. *Science (80-.).* 307:1781–1785. doi:10.1126/science.1106823.

Su, K.C., T. Takaki, and M. Petronczki. 2011. Targeting of the RhoGEF Ect2 to the Equatorial Membrane Controls Cleavage Furrow Formation during Cytokinesis. *Dev. Cell*. 21:1104–1115. doi:10.1016/j.devcel.2011.11.003.

Süel, K.E., H. Gu, and Y.M. Chook. 2008. Modular organization and combinatorial energetics of proline-tyrosine nuclear localization signals. *PLoS Biol.* 6:1253–1267. doi:10.1371/journal.pbio.0060137.

Sun, L., R. Guan, I.J. Lee, Y. Liu, M. Chen, J. Wang, J.Q. Wu, and Z. Chen. 2015. Mechanistic Insights into the Anchorage of the Contractile Ring by Anillin and Mid1. *Dev. Cell*. 33:413–426. doi:10.1016/j.devcel.2015.03.003.

Sutton, P.J., N. Mosqueda, and C.W. Brownlee. 2025. Palmitoylated importin α regulates mitotic spindle orientation through interaction with NuMA. *EMBO Rep.* 26:3280–3304. doi:10.1038/s44319-025-00484-8.

Suzuki, K., K. Sako, K. Akiyama, M. Isoda, C. Senoo, N. Nakajo, and N. Sagata. 2015. Identification of non-Ser/Thr-Pro consensus motifs for Cdk1 and their roles in mitotic regulation of C2H2 zinc finger proteins and Ect2. *Sci. Rep.* 5:1–9. doi:10.1038/srep07929.

Tatsumoto, T., X. Xie, R. Blumenthal, I. Okamoto, and T. Miki. 1999. Human Ect2 Is an Exchange Factor for Rho Gtpases, Phosphorylated in G2/M Phases, and Involved in Cytokinesis. *J. Cell Biol.* 147:921–928. doi:10.1083/jcb.147.5.921.

Teo, G., G. Liu, J. Zhang, A.I. Nesvizhskii, A.C. Gingras, and H. Choi. 2014. SAINTexpress: Improvements and additional features in Significance Analysis of INTeractome software. *J. Proteomics*. 100:37–43. doi:10.1016/j.jprot.2013.10.023.

Timney, B.L., B. Raveh, R. Mironska, J.M. Trivedi, S.J. Kim, D. Russel, S.R. Wente, A. Sali, and

M.P. Rout. 2016. Simple rules for passive diffusion through the nuclear pore complex. *J. Cell Biol.* 215:57–76. doi:10.1083/jcb.201601004.

Tsai, M.Y., C. Wiese, K. Cao, O. Martin, P. Donovan, J. Ruderman, C. Prigent, and Y. Zheng. 2003. A Ran signalling pathway mediated by the mitotic kinase Aurora A in spindle assembly. *Nat. Cell Biol.* 5:242–248. doi:10.1038/ncb936.

Tsai, M.Y.M.-Y., S. Wang, J.M. Heidinger, D.K. Shumaker, S.A. Adam, R.D. Goldman, and Y. Zheng. 2006. A mitotic lamin B matrix induced by RanGTP required for spindle assembly. *Science (80-.).* 311:1887–1893. doi:10.1126/science.1122771.

Uehara, R., and G. Goshima. 2010. Functional central spindle assembly requires de novo microtubule generation in the interchromosomal region during anaphase. *J. Cell Biol.* 191:259–267. doi:10.1083/jcb.201004150.

Vassilev, L.T., C. Tovar, S. Chen, D. Knezevic, X. Zhao, H. Sun, D.C. Heimbrook, and L. Chen. 2006. Selective small-molecule inhibitor reveals critical mitotic functions of human CDK1. *Proc. Natl. Acad. Sci.* 103:10660–10665. doi:10.1073/pnas.0600447103.

Velez, G., M. Lin, T. Christensen, W.A. Faubion, G. Lomberk, and R. Urrutia. 2016. Evidence supporting a critical contribution of intrinsically disordered regions to the biochemical behavior of full-length human HP1γ. *J. Mol. Model.* 22:1–17. doi:10.1007/s00894-015-2874-z.

Walczak, C.E., and R. Heald. 2008. Mechanisms of Mitotic Spindle Assembly and Function. *Int. Rev. Cytol.* 265:111–158. doi:10.1016/S0074-7696(07)65003-7.

Watanabe, S., Y. Ando, S. Yasuda, H. Hosoya, N. Watanabe, T. Ishizaki, and S. Narumiya. 2008. mDia2 Induces the Actin Scaffold for the Contractile Ring and Stabilizes Its Position during

Cytokinesis in NIH 3T3 Cells. *Mol. Biol. Cell*. 19:2328–2338. doi:10.1091/mbc.e07-10-1086.

Watanabe, S., K. Okawa, T. Miki, S. Sakamoto, T. Morinaga, K. Segawa, T. Arakawa, M. Kinoshita, T. Ishizaki, and S. Narumiya. 2010. Rho and Anillin-dependent Control of mDia2 Localization and Function in Cytokinesis. *Mol. Biol. Cell*. 21:3193–3204. doi:10.1091/mbc.e10-04-0324.

Weaver, L.N., S.C. Ems-Mcclung, S.H.R. Chen, G. Yang, S.L. Shaw, and C.E. Walczak. 2015. The Ran-GTP gradient spatially regulates XCTK2 in the spindle. *Curr. Biol.* 25:1509–1514. doi:10.1016/j.cub.2015.04.015.

Werner, M., E. Munro, and M. Glotzer. 2007. Astral Signals Spatially Bias Cortical Myosin Recruitment to Break Symmetry and Promote Cytokinesis. *Curr. Biol.* 17:1286–1297. doi:10.1016/j.cub.2007.06.070.

Wilson, G.M., A.B. Fielding, G.C. Simon, X. Yu, P.D. Andrews, R.S. Haines, A.M. Frey, A.A. Peden, G.W. Gould, and R. Prekeris. 2005. The FIP3-Rab11 protein complex regulates recycling endosome targeting to the cleavage furrow during late cytokinesis. *Mol. Biol. Cell*. 16:849–860. doi:10.1091/mbc.E04-10-0927.

Winogradoff, D., H.Y. Chou, C. Maffeo, and A. Aksimentiev. 2022. Percolation transition prescribes protein size-specific barrier to passive transport through the nuclear pore complex. *Nat. Commun.* 13. doi:10.1038/s41467-022-32857-1.

Wolfe, B.A., T. Takaki, M. Petronczki, and M. Glotzer. 2009. Polo-like kinase 1 directs assembly of the HsCyk-4 RhoGAP/Ect2 RhoGEF complex to initiate cleavage furrow formation. *PLoS Biol.* 7. doi:10.1371/journal.pbio.1000110.

Yamada, A., K. Wake, S. Imaoka, M. Motoyoshi, T. Yamamoto, and M. Asano. 2024. Analysis of

the effects of importin α1 on the nuclear translocation of IL-1α in HeLa cells. *Sci. Rep.* 14:1–12. doi:10.1038/s41598-024-51521-w.

Yi, M., D. Zhang, B. Song, B. Zhao, M. Niu, Y. Wu, Z. Dai, and K. Wu. 2022. Increased expression of ECT2 predicts the poor prognosis of breast cancer patients. *Exp. Hematol. Oncol.* 11:1–14. doi:10.1186/s40164-022-00361-3.

Yüce, Ö., A. Piekny, and M. Glotzer. 2005. An ECT2-centralspindlin complex regulates the localization and function of RhoA. *J. Cell Biol.* 170:571–582. doi:10.1083/jcb.200501097.

Zanin, E., A. Desai, I. Poser, Y. Toyoda, C. Andree, C. Moebius, M. Bickle, B. Conradt, A. Piekny, and K. Oegema. 2013. A conserved RhoGAP limits M phase contractility and coordinates with microtubule asters to confine RhoA during Cytokinesis. *Dev. Cell*. 26:496–510. doi:10.1016/j.devcel.2013.08.005.

Zhang, D., and M. Glotzer. 2015. Cytokinesis: Placing the Furrow in Context. *Curr. Biol.* 25:R1183–R1185. doi:10.1016/j.cub.2015.10.042.

Zhuravlev, Y., S.M. Hirsch, S.N. Jordan, J. Dumont, M. Shirasu-Hiza, and J.C. Canman. 2017. CYK-4 regulates Rac, but not Rho, during cytokinesis. *Mol. Biol. Cell*. 28:1258–1270. doi:10.1091/mbc.E17-01-0020.

Zou, Y., Z. Shao, J. Peng, F. Li, D. Gong, C. Wang, X. Zuo, Z. Zhang, J. Wu, Y. Shi, and Q. Gong. 2014. Crystal structure of triple-BRCT-domain of ECT2 and insights into the binding characteristics to CYK-4. *FEBS Lett.* 588:2911–2920. doi:10.1016/j.febslet.2014.07.019.

Supplemental Figures

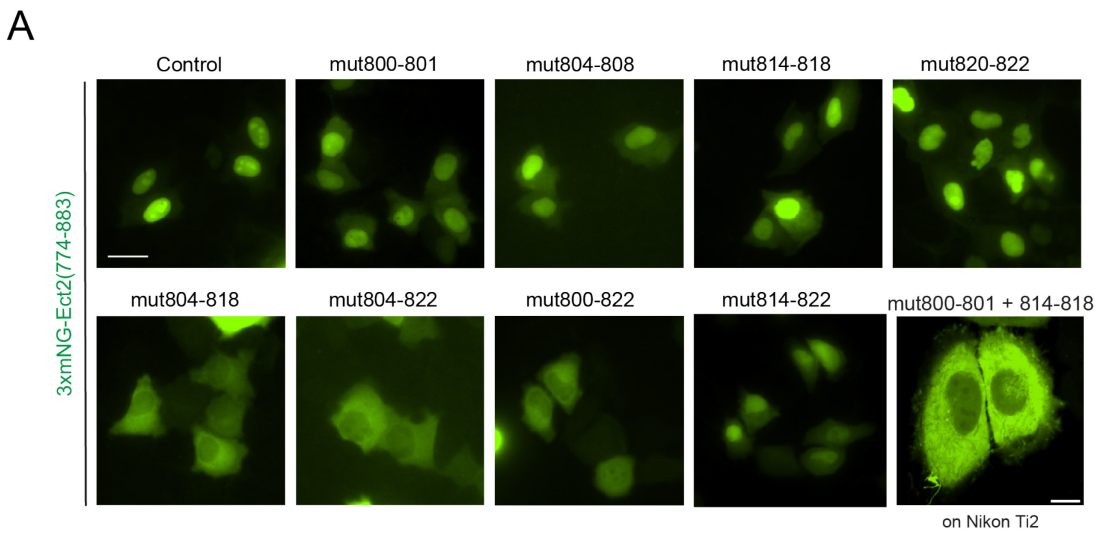
A
Control
mut800-801
mut804-808
mut814-818
mut820-822
3xmNG-Ect2(774-883)
mut804-818
mut804-822
mut800-822
mut814-822
mut800-801 + 814-818
on Nikon Ti2

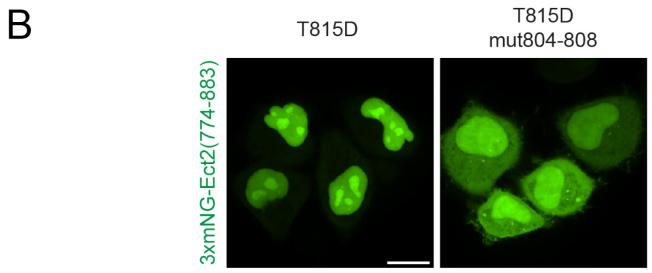
B
T815D
T815D
mut804-808
3xmNG-Ect2(774-883)

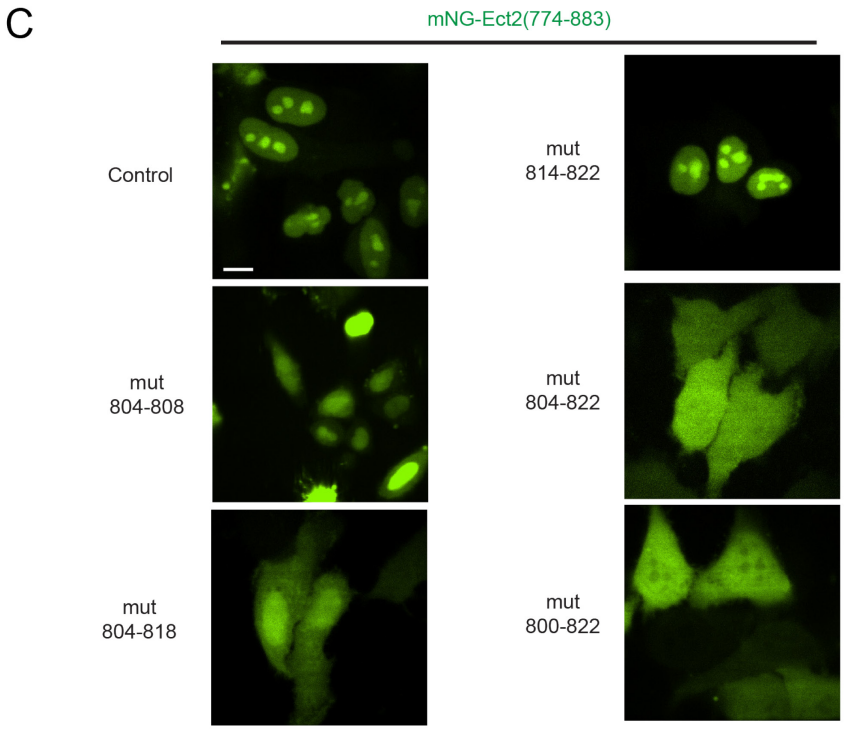
C
mNG-Ect2(774-883)
Control
mut
814-822
mut
804-808
mut
804-822
mut
804-818
mut
800-822

Supplemental Figure 1. Characterizing the C-terminal NLS and the effect of phosphorylation on nuclear import.

(A-B) HeLa cells expressing 3xmNG-Ect2 (774-883) in interphase. Scale bar is 30 μm, except mut800-801 + 814-818, where it is 10 μm. Bottom right panel was acquired on a different microscope and objective (Ti2) and labeled for clarity. (A) shows mutations targeting the C-terminal NLS, and (B) the phosphomimetic mutation (T815D) alone and combined with part of the NLS mutation. (C) HeLa cells expressing mNG-Ect2 (774-883) in interphase. Scale bar is 20 μm.

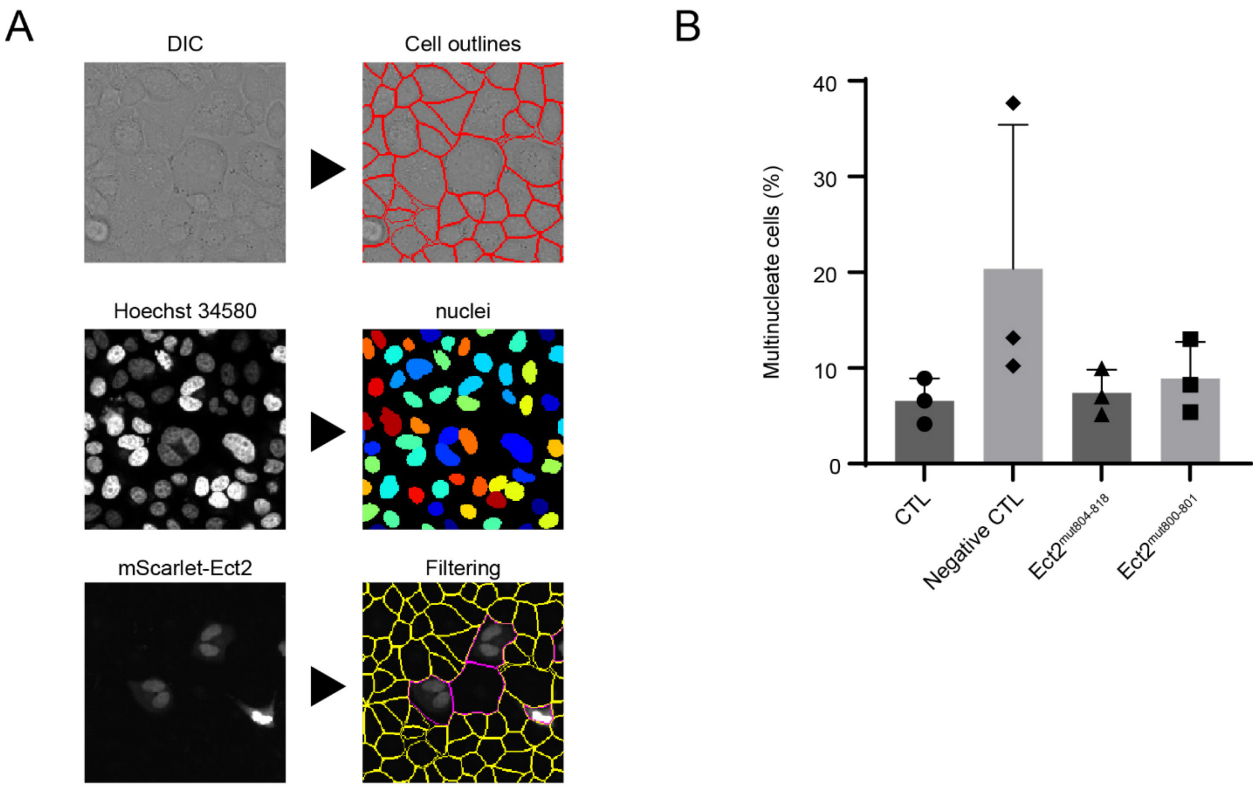

Supplemental Figure 2. Cell segmentaion pipeline to count binucleate cells using CellProfiler and Cellpose-SAM.

(A) Images of HeLa cells segmented in CellProfiler, using Cellpose-SAM to segment cell outlines using differential interference contrast (DIC) and nuclei using Hoechst, and filtering based on expression of mScarlet-Ect2 signal inside a cell. (B) Proportion of multinucleate cells in HeLa cells expressing mScarlet-I:Ect2 (control and NLS mutants) analyzed using the cell segmentation pipeline (n = 3).

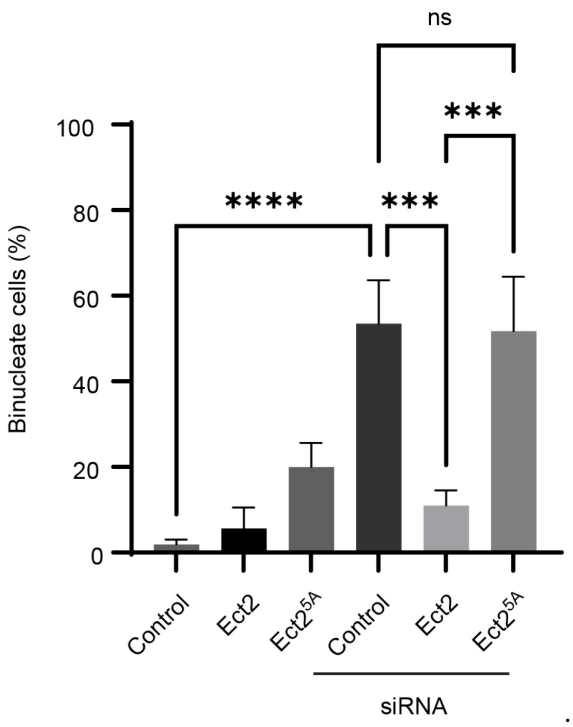

Supplemental Figure 3. The nuclear localization of Ect2 is required for cytokinesis with the 5A NLS mutant.

A bar graph shows the percentage of binucleate cells as a measure of failed cytokinesis in HeLa cells expressing RNAi-resistant myc:Ect2 (Ect2 or Ect2^{5A}) and treated with Ect2 siRNA or untreated. Error bars show standard deviation (N = 3, with n = 21-175 cells per replicate). Statistical analyses were done using ANOVA and Tukey post-hoc test (ns, not significant; ***, $p<0.0002$; ****, $p<0.0001$).

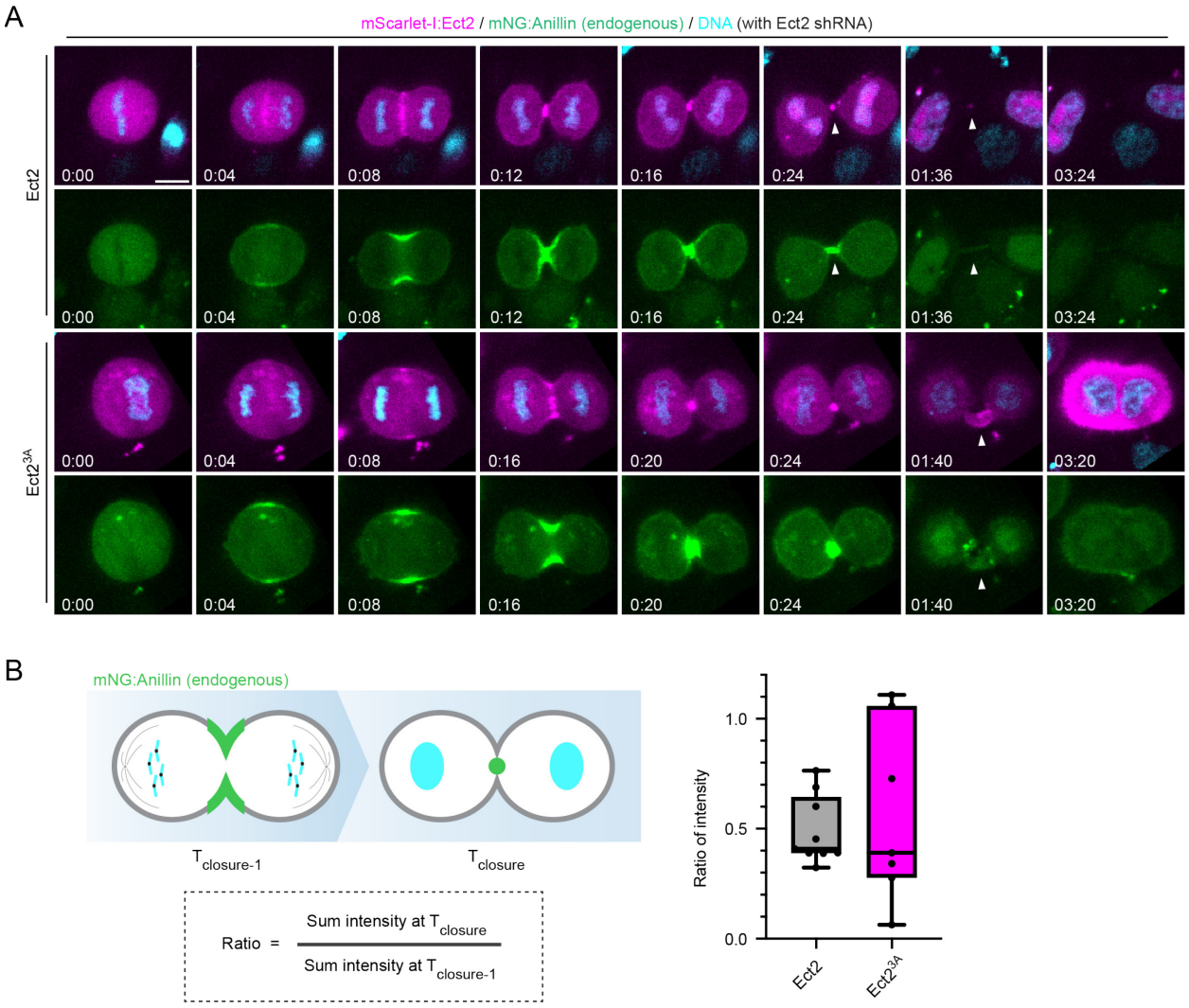

Supplemental Figure 4. Removal of Ect2 from the midbody is required for its formation.

(A) Timelapse images show endogenous mNeonGreen:anillin (green) in HeLa cells co-expressing RNAi-resistant mScarlet-I-Ect2 (magenta; Ect2 or Ect2^{3A}), depleted of endogenous Ect2 using shRNA and co-stained for DNA (cyan, Hoechst). The scale bar is 10 μm (t = 0 is anaphase onset). Time is in hours:minutes. White arrowheads point to the intercellular bridge. (B) On the left, cartoon cells indicate how the ratio of sum anillin intensity at the midbody was measured at ring closure ($T_{closure}$) vs. just before closure ($T_{closure-1}$). On the right, a box-and-whiskers plot shows the ratio of anillin intensities (y-axis) in cells rescued with mScarlet-I:Ect2 (grey, n = 9) and Ect2^{3A} (pink, n = 7) as imaged in (A). Bars indicate standard deviation, and the black line shows the mean.

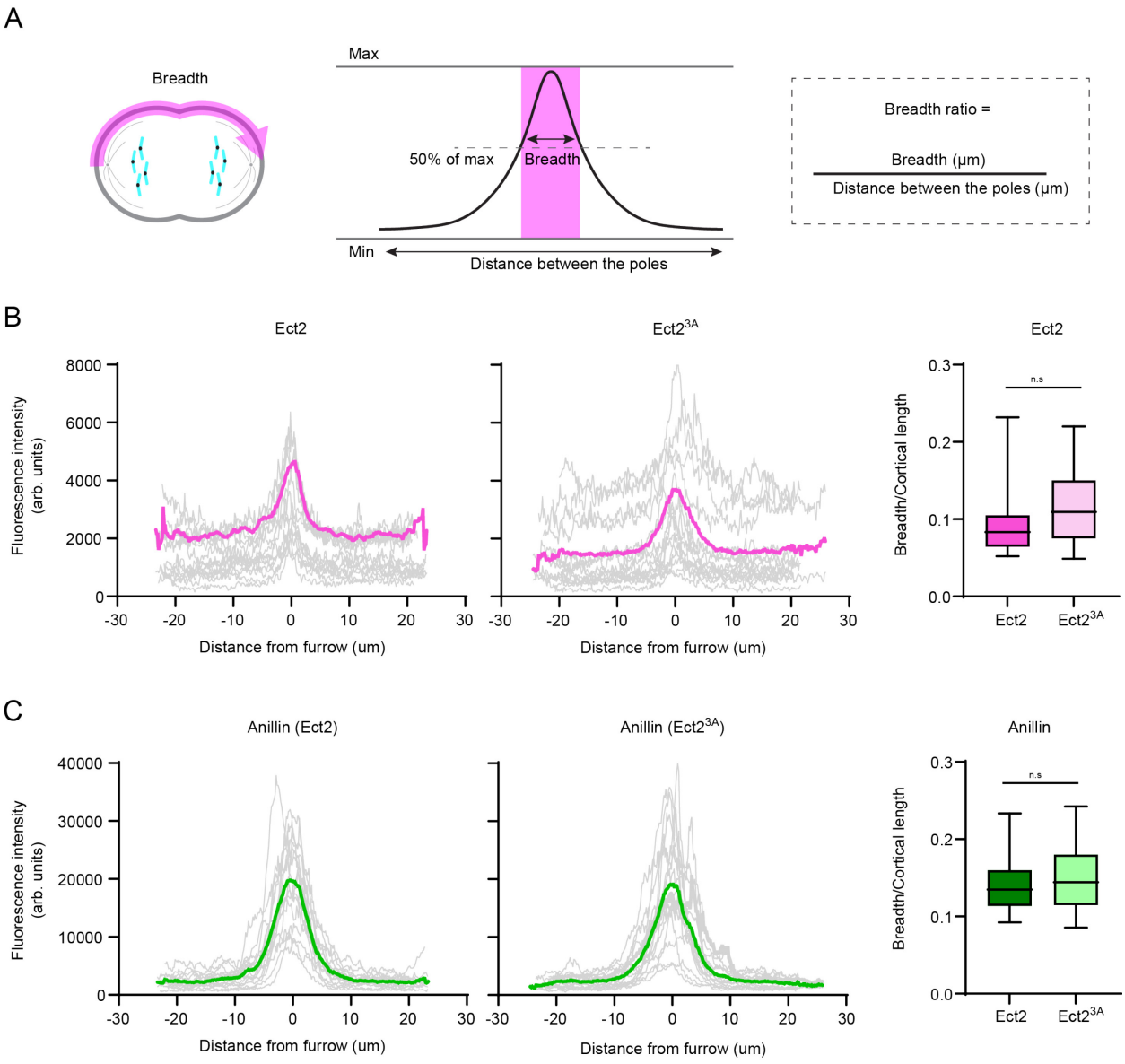

Supplemental Figure 5. The NLS of Ect2 is not required for the localization of Ect2 or anillin at the equatorial cortex.

(A) A schematic shows how breadth of accumulated Ect2 or anillin the equatorial cortex was measured using line scans. A line was drawn along half of the perimeter of a cell in early ingression to measure the intensity of pixels along the line. The breadth was defined as the number of pixels >50% of the normalized maximum intensity, which was converted into mm. To control for cell size, the breadth was divided by the length. (B-C) Graphs (left) show fluorescence intensity (y-axis, a.u.) over distance from the ingressing cortex (x-axis, point of ingression is 0, mm) for (B) mScarlet-I:Ect2 or Ect2^{3A} co-depleted for Ect2 with shRNAs in HeLa cells with (C) endogenous mNeonGreen:anillin (n = 17 for Ect2 and Ect^{3A}). To the right, box-and-whiskers plots show the ratio of the breadth divided by the cortical length. Statistical analysis was performed

using a Student’s T-test for mNeonGreen:anillin and non-parametic test for mScarlet-I:Ect2, and no statistically significant differences between the means were detected.

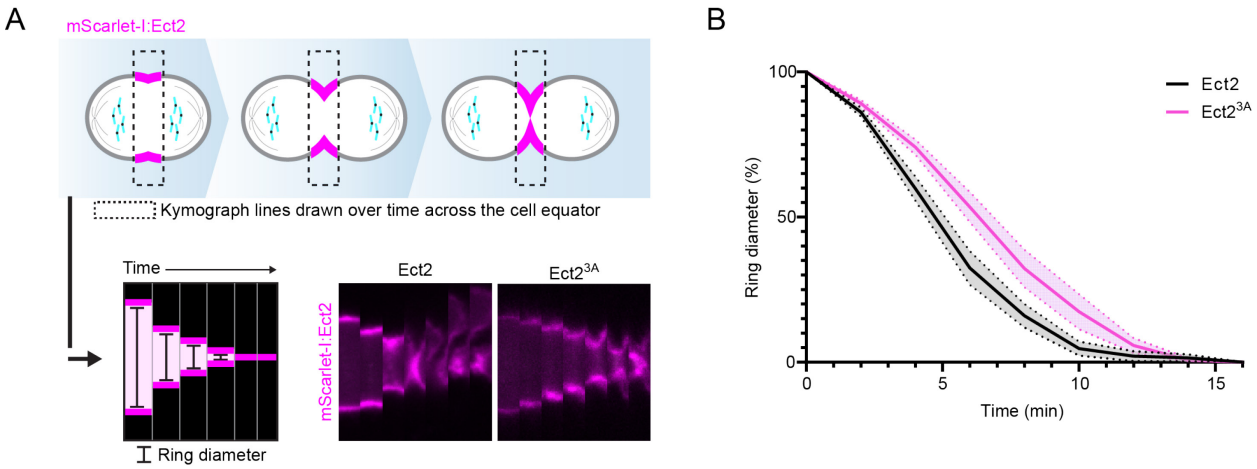

Supplemental Figure 6. The NLS of Ect2 plays a minor role in ring ingression.

(A) Cartoon cells shows the region that was used to generate kymographs for cells expressing mScarlet-I:Ect2 or Ect2^{3A} (magenta) as shown. (B) The line graph shows % change in ring diameter over time in cells expressing mScarlet-I:Ect2 (black, n = 24) or Ect2^{3A} (pink, n = 13) depleted for endogenous Ect2 with shRNA. The bars show standard error of the mean (SEM).

The colors for log scale:

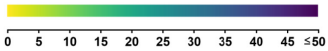

GO:BP

Term name	Term ID	stats p_{adj}	$-\log_{10}(p_{adj})$ (0 – ≤16)
protein localization to nucleus	GO:0034504	2.120×10^{-13}	
nuclear transport	GO:0051169	3.830×10^{-13}	
nucleocytoplasmic transport	GO:0006913	3.830×10^{-13}	
RNA localization	GO:0006403	7.763×10^{-12}	
nucleic acid transport	GO:0050657	7.947×10^{-11}	
RNA transport	GO:0050658	7.947×10^{-11}	
establishment of RNA localization	GO:0051236	9.417×10^{-11}	
protein import into nucleus	GO:0006606	1.112×10^{-10}	
import into nucleus	GO:0051170	1.458×10^{-10}	
mRNA transport	GO:0051028	1.217×10^{-9}	
nucleobase-containing compound transport	GO:0015931	2.808×10^{-9}	
intracellular transport	GO:0046907	1.900×10^{-8}	
establishment of localization in cell	GO:0051649	1.765×10^{-7}	
protein localization to organelle	GO:0033365	1.448×10^{-6}	
intracellular protein transport	GO:0006886	1.559×10^{-6}	
nitrogen compound transport	GO:0071705	1.580×10^{-6}	
cellular localization	GO:0051641	6.508×10^{-6}	
NLS-bearing protein import into nucleus	GO:0006607	6.516×10^{-6}	
macromolecule localization	GO:0033036	1.194×10^{-5}	
establishment of protein localization to organelle	GO:0072594	2.445×10^{-5}	
nuclear export	GO:0051168	3.474×10^{-5}	
localization	GO:0051179	4.445×10^{-5}	
RNA export from nucleus	GO:0006405	6.717×10^{-5}	
establishment of localization	GO:0051234	6.743×10^{-4}	
transport	GO:0006810	1.127×10^{-3}	
protein transport	GO:0015031	1.768×10^{-3}	
negative regulation of nucleocytoplasmic transport	GO:0046823	3.119×10^{-3}	
viral penetration into host nucleus	GO:0075732	1.072×10^{-2}	
regulation of nucleocytoplasmic transport	GO:0046822	1.122×10^{-2}	
protein localization	GO:0008104	1.375×10^{-2}	
cellular macromolecule localization	GO:0070727	1.439×10^{-2}	
establishment of protein localization	GO:0045184	2.499×10^{-2}	
regulation of cellular component organization	GO:0051128	2.718×10^{-2}	
cytoskeleton organization	GO:0007010	2.781×10^{-2}	
negative regulation of intracellular transport	GO:0032387	3.185×10^{-2}	
organelle organization	GO:0006996	3.362×10^{-2}	
regulation of microtubule cytoskeleton organization	GO:0070507	4.397×10^{-2}	
microtubule cytoskeleton organization involved in mitosis	GO:1902850	4.946×10^{-2}	

1 to 38 of 38 Page 1 of 1

The colors for different evidence codes in the table:

Gene Ontology

- Inferred from experiment [IDA, IPI, IMP, IGI, IEP]
- Direct assay [IDA], Mutant phenotype [IMP]
- Genetic interaction [IGI], Physical interaction [IPI]
- Inferred from High Throughput Experiment [HDA, HMP, HGI, HEP]
- High Throughput Direct Assay [HDA], High Throughput Mutant Phenotype [HMP]
- High Throughput Genetic interaction [HGI], High Throughput Expression pattern [HEP]
- Traceable author [TAS], Non-traceable author [NAS], Inferred by curator [IC]
- Expression pattern [IEP], Sequence or structural similarity [ISS], Genomic context [IGC]
- Sequence Model [ISM], Sequence Alignment [ISA], Sequence Orthology [ISO]
- Biological aspect of ancestor [IBA], Rapid divergence [IRD]
- Reviewed computational analysis [RCA], Electronic annotation [IEA]
- No biological data [ND], Not annotated or not in background [NA]

Supplemental Figure 7. g:Profiler enrichment analysis of the TurboID of importin-β1.

Enrichment analysis of biological process using g:Profiler, showing log transformed adjusted p-value and individual genes belonging to a biological process by type of evidence.

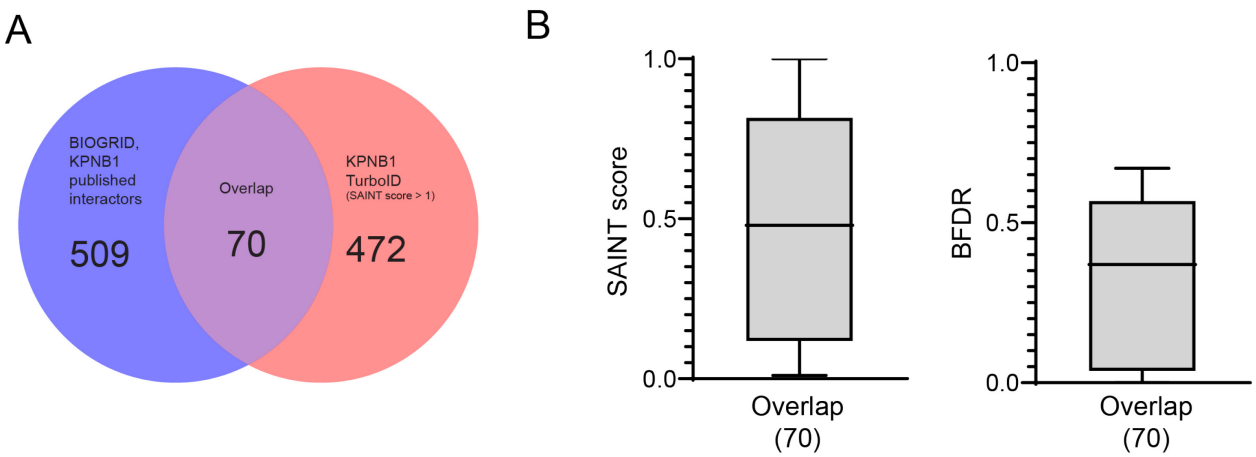

Supplemental Figure 8. Comparison of interactors with a positive SAINT score and BIoGRID.

(A) Comparison between interactors in our TurboID assay with a positive SAINT score (>0.01) and BioGRID. (B) Box-and-whisker plots of the SAINT score and Bayesian false discovery rate (BFDR) of the 70 interactors overlapping with BioGRID in our TurboID assay.

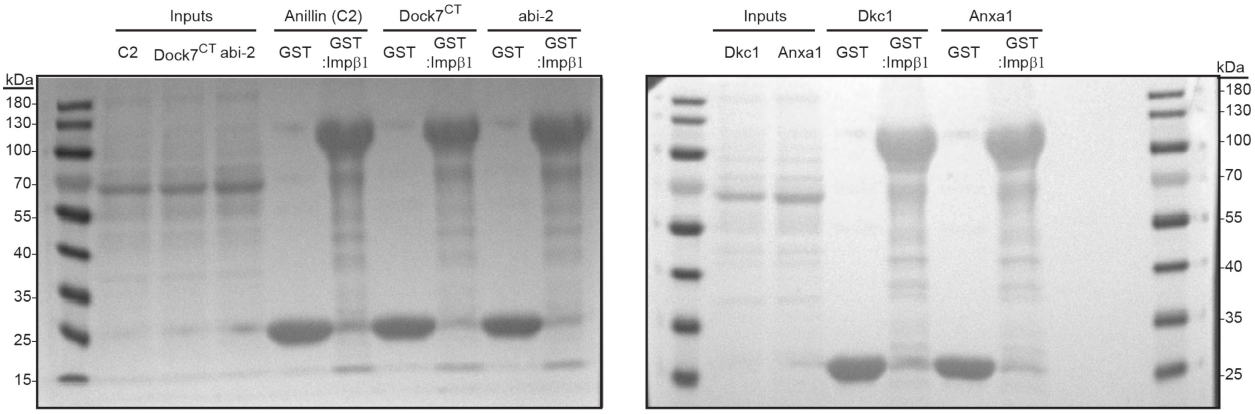

Supplemental Figure 9. Ponceau blot of the pull-downs for Dock7, abi-2, Dkc1 and annexin A1.

Ponceau-stained blots of the immunoblots in Figure 20. Large bands on the top show GST:importin-β1 (100kDa) and bands on the bottom show GST (26kDa).

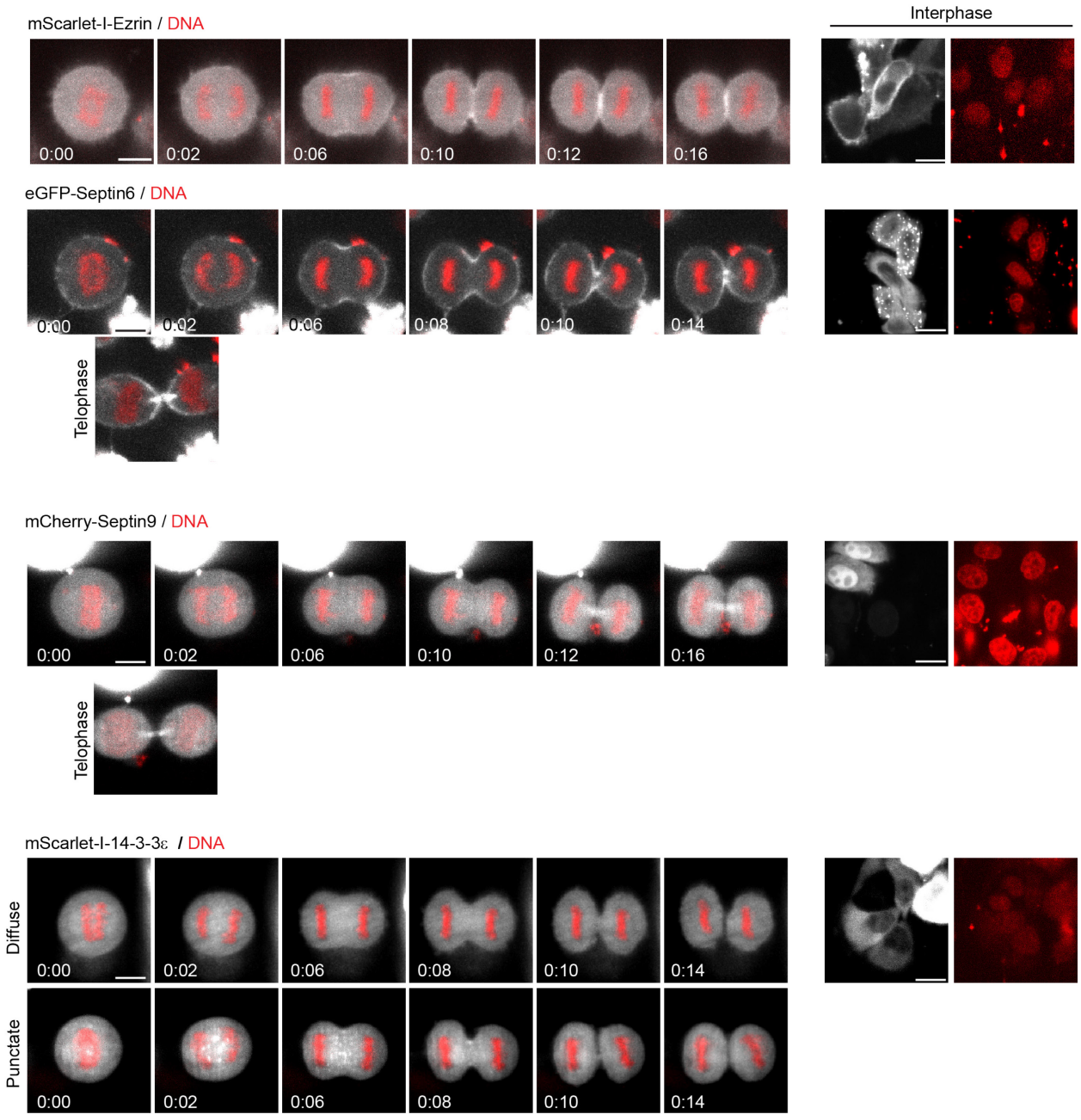

Supplemental Figure 10. Localization of low-confidence interactors with known or suspected roles in regulating the cytoskeleton.

On the left, timelapse images of HeLa cells expressing fluorescent protein-tagged ezrin, septin 6, septin 9, and 14-3-3ε (grayscale) and DNA (red, Hoechst). Scale bar is 10 μm and t = 0 is anaphase onset. Time is in hours:minutes. For septin 6 and septin 9, an example of a telophase cell is shown below the timelapse. On the right, interphase cells show subcellular localization in interphase cells as individual channels, with DNA on the right. Scale bar for interphase cells is 20 μm.